

AN ABSTRACT OF THE THESIS OF

STEPHEN HANS JOHNSON for the DOCTOR OF PHILOSOPHY  
(Name of student) (Degree)

in GEOPHYSICS presented on 13 October 1971  
(Major) (Date)

Title: CRUSTAL STRUCTURES AND TECTONISM IN SOUTH-  
EASTERN ALASKA AND WESTERN BRITISH COLUMBIA  
FROM SEISMIC REFRACTION, SEISMIC REFLECTION,  
GRAVITY, MAGNETIC, AND MICROEARTHQUAKE  
MEASUREMENTS

Abstract approved: Redacted for Privacy

Seismic refraction measurements along two unreversed lines indicate that the earth's crust is 26 km thick in southeastern Alaska and 30 km thick along the Inside Passage of British Columbia. The crust in southeastern Alaska, north of Dixon Entrance, consists of a layer 9 km thick with a seismic velocity of 5.90 km/sec, a layer 7 km thick with a seismic velocity of 6.30 km/sec, and a layer 10 km thick with a seismic velocity of 6.96 km/sec. The crust along the Inside Passage of British Columbia, south of Dixon Entrance, consists of a layer 13 km thick with a seismic velocity of 6.03 km/sec, a layer 5 km thick with a seismic velocity of 6.41 km/sec, and a layer 12 km thick with a seismic velocity of 6.70 km/sec. The velocity of the mantle below the M discontinuity is 7.86 km/sec in southeastern Alaska and 8.11 km/sec in British Columbia.

A compilation of Bouguer gravity data along the Inside Passage from northern Vancouver Island to northern southeastern Alaska indicates near-zero anomalies between steep gradients offshore and near the western margin of the Coast Mountains. A two-dimensional gravity model, constrained by seismic refraction measurements, suggests that the thickness of the crust is constant beneath the region of near-zero gravity anomalies and indicates a step-like transition between oceanic and continental structure.

Seismic reflection, gravity, and magnetic measurements, obtained during a 1970 cruise of the R/V Yaquina, help to determine upper crustal structures in Dixon Entrance. Gravity models, constructed to agree with these data and the measurements of previous investigators, indicate sediment thicknesses of nearly 3 km east of Learmonth Bank and west of Celestial Reef. Magnetic models suggest large lateral changes in basement susceptibility. Either highly metamorphosed rock or basaltic intrusions can account for these changes in susceptibility. Folded sediments suggest post-depositional distortion due either to regional compression or to major local intrusions. Several linear gravity features, observed in northern Dixon Entrance, disappear north of Graham Island. Either the structures responsible for the gravity features end or thick layers of basalt, extending northward from Graham Island, obscure the effect of the structures.

A single-station survey detected microearthquakes at nine locations in western British Columbia and southeastern Alaska. The majority of the observed distant microearthquakes probably originated in the Queen Charlotte Islands fault zone. However, observed nearby microearthquakes indicate a microearthquake seismicity of several events per day along the mainland coast of British Columbia.

Temporary seismic arrays located at a site along the central portion of Chatham Strait near the Chatham Strait fault and at a site in Glacier Bay recorded few nearby microearthquakes. Arrivals at the arrays permitted the location of distant microearthquakes, however, with epicenters in the vicinity of northern Lynn Canal and along the Fairweather fault.

Crustal Structures and Tectonism in Southeastern Alaska  
and Western British Columbia from Seismic Refraction,  
Seismic Reflection, Gravity, Magnetic, and  
Microearthquake Measurements

by

Stephen Hans Johnson

A THESIS

submitted to

Oregon State University

in partial fulfillment of  
the requirements for the  
degree of

Doctor of Philosophy

June 1972

APPROVED:

Redacted for Privacy

\_\_\_\_\_  
Assistant Professor of Geophysics  
in charge of major

Redacted for Privacy

\_\_\_\_\_  
Chairman of the Department of Oceanography

Redacted for Privacy

\_\_\_\_\_  
Dean of the Graduate School

Date thesis is presented October 13, 1971

Typed by Opal Grossnicklaus for Stephen Hans Johnson

## ACKNOWLEDGEMENTS

This research was initiated and guided by Dr. Richard W. Couch. I am grateful for his advice and encouragement during the field work, the analysis of the data, and the editing of the manuscript.

The suggestions, skillful assistance, and companionship of Michael Gemperle and E. Robey Banks were invaluable during the field work. The successful completion of this experiment, often under difficult circumstances, depended many times on their knowledge and experience.

Sincere thanks go to Ray Pearl for the design and construction of the electronic equipment used in the OSU seismic recording system and to Steve Wilcox for the design and construction of the crystal-controlled clock.

Appreciation is extended to the ship's officers and crew for their assistance in obtaining data on the R. V. Yaquina and to my student associates for their assistance at sea and in the laboratory.

The understanding and encouragement shown me by my wife, Joan, and my family during the course of this endeavor is gratefully acknowledged.

Drs. Donald Heinrichs, Gunnar Bodvarsson, Victor Neal, and Fritz Oberhettinger reviewed the thesis and made many helpful comments.

This research was supported by the National Science Foundation, grant GA-26411, and the Office of Naval Research, project N00014-67-A-0369-0007. Computer time was made available by the O. S. U. Computer Center.

## TABLE OF CONTENTS

INTRODUCTION	1
Location and Physiography	1
Previous Geophysical Work	5
Purpose of this Research	9
INSTRUMENTATION	10
Purpose and Requirements of a Seismic Recording System	10
Oregon State University Recording System	13
Recording System Response	17
SEISMIC REFRACTION STUDY	24
Introduction	24
Recording Techniques	26
Geology, Structural Trends, and Gravity	27
Reduction of Refraction Data	34
Bird Lake Refraction Line	38
Ripley Bay Refraction Line	42
Structural Interpretation	43
Attenuation	51
STRUCTURE OF THE UPPER CRUST IN DIXON ENTRANCE FROM GEOPHYSICAL MEASUREMENTS	54
Introduction	54
Gravity Measurements	56
Seismic Measurements	59
Gravity Crustal Cross Section	65
Magnetic Measurements and Crustal Cross Section	71
Summary	75
MICROEARTHQUAKE SURVEY OF WESTERN BRITISH COLUMBIA AND SOUTHEASTERN ALASKA	78
Introduction	78
Field Methods	81
Data Analysis	83
Interpretation	83

MICROEARTHQUAKE MEASUREMENTS WITH ARRAYS AT TWO SITES IN SOUTHEASTERN ALASKA	88
Introduction	88
Field Methods	90
Data Analysis	92
Interpretation	95
SUMMARY AND CONCLUSIONS	100
BIBLIOGRAPHY	104
APPENDICES	114
Appendix 1. Reduction of Survey Data to Obtain Array Dimensions	114
Appendix 2. Hypocenter Location from Seismic Array Data	119

## LIST OF FIGURES

<u>Figure</u>	<u>Page</u>
1. Index map of western British Columbia and southeastern Alaska.	4
2. Earthquake epicenters adjacent to the region of this study: 1912-1970.	6
3. Block diagram of the Oregon State University seismic recording system.	14
4. Maxwell bridge circuit for seismograph calibration.	18
5. Displacement magnification and phase response for direct strip chart recording of Channel 7.	20
6. Displacement magnification and phase response for Channel 7 using tape recorder, tape speed compensator, and high-cut filter with a four-channel chart recorder.	22
7. Views of the Oregon State University seismic recording system: A, array station; B, unattended station; C, during playback.	23
8. Location of shot points and recording stations.	25
9. Generalized geology, location of seismic refraction surveys and position of Dixon Entrance cross section.	30
10. Bouguer gravity anomaly map of southeastern Alaska and western British Columbia.	33
11. Reduced travel-time graphs and computed structure.	36
12. Comparison of a field seismogram with synthetic seismograms at $\Delta = 202$ km.	39
13. Dixon Entrance crustal and subcrustal cross section.	49
14. Observed peak-to-peak amplitude of ground motion, in millimicrons, due to $P_n$ phases from Bird Lake.	52

<u>Figure</u>		<u>Page</u>
15.	Dixon Entrance bathymetry, track lines YA31 and YALOC 70 from cruises of the R/V Yaquina, and seismic refraction lines MK23A and MK23B.	55
16.	Free-air gravity anomaly map of Dixon Entrance and vicinity.	58
17.	Line drawings of seismic profile records made in Dixon Entrance from the Alaskan Abyssal Plain to Celestial Reef.	60
18.	Wave-front solution to reversed seismic refraction profile MK 23.	64
19.	Crustal cross section of Dixon Entrance from seismic and gravity data. Model 1: upper layers determined from the wave front solution of Figure 18.	66
20.	Relation between density and compressional wave velocity used to construct gravity models.	67
21.	Crustal cross section of Dixon Entrance from seismic and gravity data. Model 2: upper layers determined from trial and error fit to observed gravity data.	70
22.	Crustal model developed to fit magnetic anomalies observed in Dixon Entrance.	73
23.	Location of microearthquake recording stations and major mapped and inferred faults.	80
24.	Positions and geometry of the recording arrays, epicenter locations, and mapped and inferred faults.	91
25.	Diagram illustrating equation parameters for the direction of approach of a ray and the geometry of a tripartite array.	119
26.	Straight line ray paths assumed and quantities used in locating hypocenters.	121

## LIST OF TABLES

<u>Table</u>		<u>Page</u>
1.	Standard IRIG frequency channels used in the Oregon State University seismic recording system.	16
2.	Station location, epicentral distance, and arrival times.	37
3.	Time-distance equations and computed thicknesses.	44
4.	Measured frequencies and amplitudes of $P_n$ phases from Bird Lake.	51
5.	Microearthquake survey station location, recording interval, and instrument attenuation.	82
6.	Arrival times and S-P times of events observed in the microearthquake survey.	84
7.	Crustal models used in the computation of hypocenters.	94
8.	Epicenter solutions obtained from array data.	96

CRUSTAL STRUCTURES AND TECTONISM IN SOUTHEASTERN  
ALASKA AND WESTERN BRITISH COLUMBIA FROM  
SEISMIC REFRACTION, SEISMIC REFLECTION,  
GRAVITY, MAGNETIC AND  
MICROEARTHQUAKE  
MEASUREMENTS

INTRODUCTION

Location and Physiography

The continental margin of North America between Queen Charlotte Sound, British Columbia, and Yakutat Bay, Alaska, is an area increasingly studied by geologists and geophysicists because of its location with respect to major crustal features. The number of observations and studies of this portion of North America have increased markedly during the past decade.

On the basis of structure and geology, the margin is dominantly continental in character in spite of being largely water-covered. It contains many islands with moderate topographic relief separated by straits and channels, some having depths in excess of 600 meters. Hecate Strait and the Queen Charlotte Islands, which make up westernmost British Columbia, form the Canadian part of the continental margin. The American portion of the continental margin is known as the Alexander Archipelago and forms the main part of southeastern Alaska. The protected waterway from Seattle to Juneau is known as the Inside Passage. A steep continental slope and narrow continental

shelf characterize the transition from abyssal ocean to continent.

Summaries of geological investigations by Brew, Loney, and Muffler (1966) for southeastern Alaska, by Brown (1966) for the Queen Charlotte Islands, and by Roddick (1966) for the mainland coast of British Columbia reveal a complex geological history. These areas lie within the tectonic belt that rims the northern Pacific Ocean. The Queen Charlotte Islands lie within the Insular Tectonic belt and are characterized by northwest-trending structural highs and thick sequences of basic volcanic rocks and varied sediments. Northwest-trending structural highs and lows continue into southeastern Alaska but complex paleosedimentation pattern, Mesozoic and Tertiary intrusion and metamorphism, and Cenozoic faulting complicate geological interpretation. Mesozoic and Tertiary plutonic and metamorphic rocks are the dominant constituents of the Coast Mountains which form the eastern boundary of the region described in this study.

Current theories of large scale tectonic movements and processes within the earth help to explain the relation of this region to the circumpacific orogenic belt. Hess (1962) and Dietz (1961), in an effort to explain large amounts of geological and geophysical data on a world-wide scale, proposed that the sea floor is spreading apart at ocean ridges. Ocean trenches take up the extension of the crust and consume older crust at depth in the earth's mantle. Morgan (1968)

and Le Pichon (1968) suggest the basic patterns of motion may be described by a set of interactions between huge blocks of lithosphere. Lateral movement of these blocks, or crustal plates, requires a separate class of faults, called transform faults (Wilson, 1965). A large transform fault separating the Pacific plate from the North American plate probably forms the western boundary of the area of this study.

St. Amand (1957), Benioff (1962), Milne (1963), Wilson (1965b), and McManus (1967) proposed, primarily on the basis of earthquake epicenter information, that the region west of British Columbia is bounded on the west by a large fault zone termed the Queen Charlotte Islands fault. This fault extends from the area adjacent to Vancouver Island and the Queen Charlotte Islands into southeastern Alaska where it is known as the Fairweather fault (Figure 1). According to current theories of plate tectonics, the Queen Charlotte Islands fault and the Fairweather fault connect the spreading ridges off Washington and Oregon to the northeastern end of the Aleutian trench in southern Alaska.

The presence of a major transform fault forming the boundary between oceanic and continental crust provides a unique opportunity to study the results of the interaction between two major crustal plates. Shipboard methods of geophysical investigation are available in water covered areas in addition to the advantage of the direct

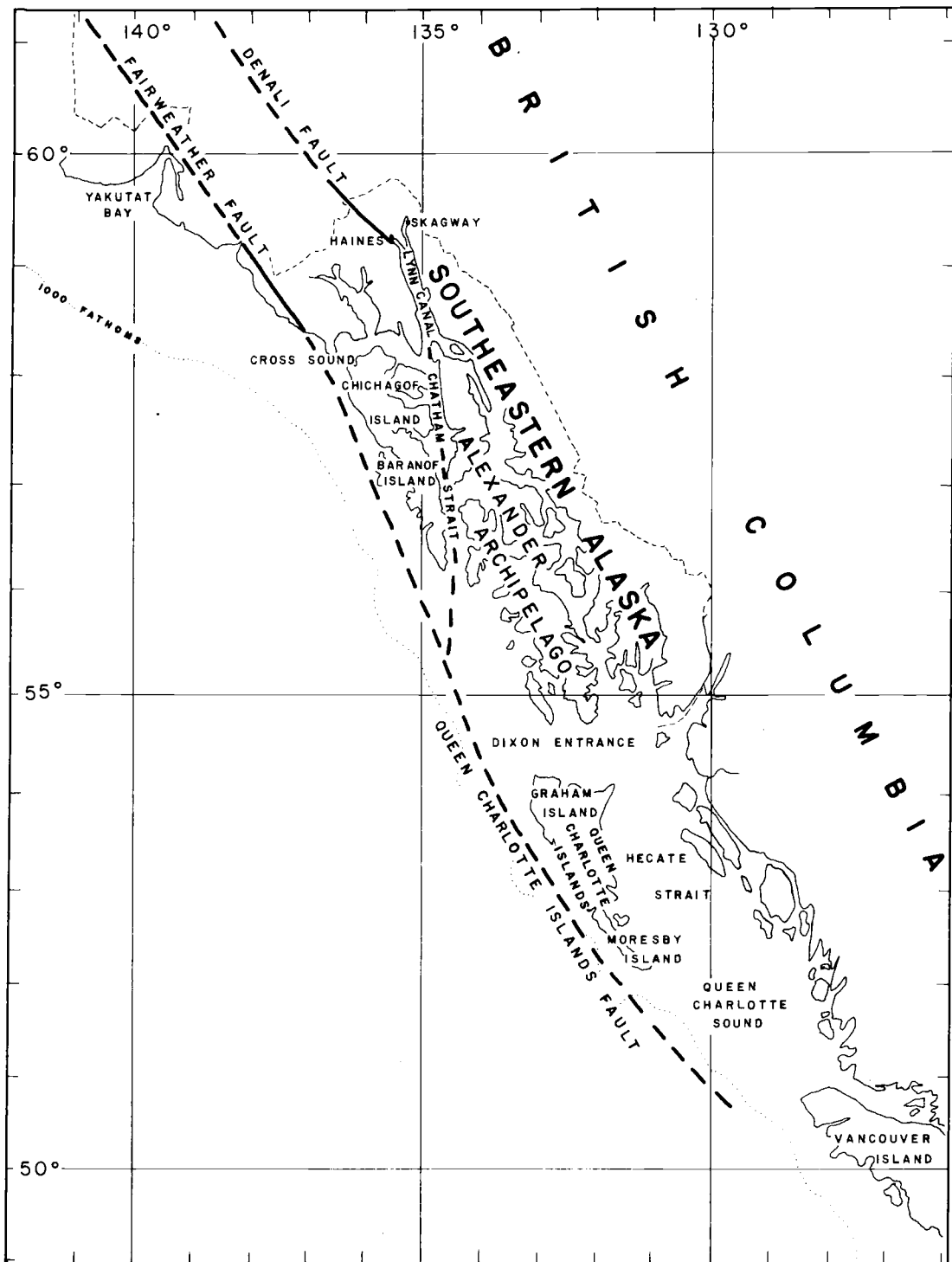


Figure 1. Index map of western British Columbia and southeastern Alaska.

observation of features on land.

An advantage of working in this area is that geophysical measurements are rapidly and efficiently carried out from a ship in water-covered areas. However, it is difficult to land on and travel about on the islands. To make observations, travel is restricted to plane or boat. Geological work is further hampered by rugged topography and heavy forest cover concealing rock outcrops.

Prior to the present study, the majority of geophysical work in the region was accomplished from ships or near centers of population where problems of access and logistics are fewer.

#### Previous Geophysical Work

Early geophysical studies of the region include the earthquake epicenters presented by Gutenberg and Richter (1954) and the U. S. Coast and Geodetic Survey (Murphy, 1950; Murphy and Cloud, 1953; Murphy and Ulrich, 1951a; 1951b; 1952). These data delineate the Queen Charlotte Islands fault and its landward extension, the Fair-weather fault. Figure 2 shows the epicenters which have been instrumentally located in the region of this study between 1912 and 1970 (compiled from Milne and Lombardo, 1952; Milne, 1954a, 1954b, 1956a, 1956b, 1961; Gutenberg and Richter, 1954; Rothe, 1959; U. S. Coast and Geodetic Survey, United States Earthquakes 1955-1962; U. S. Department of Commerce, PDE cards, 1963-1970; and Tobin

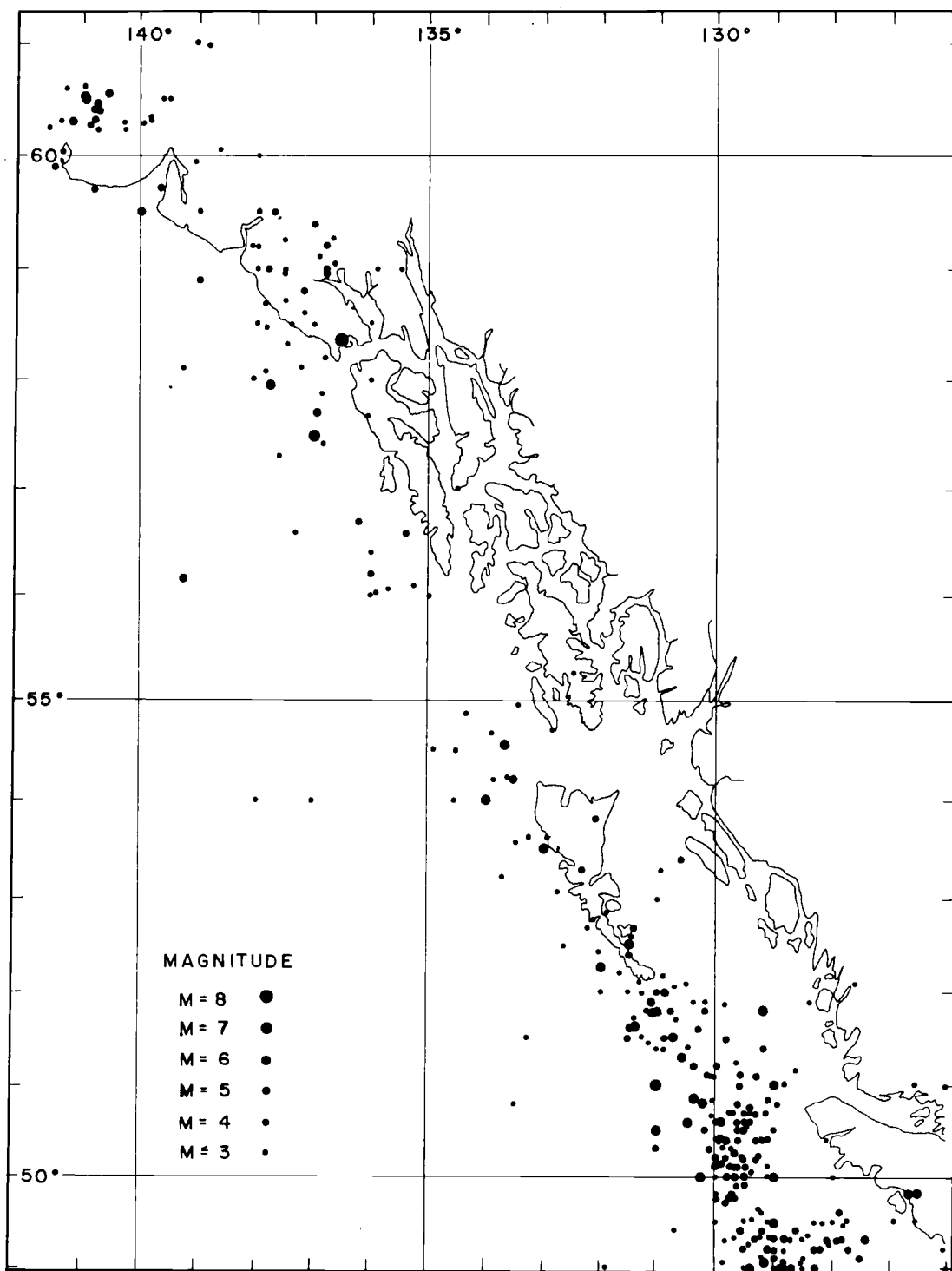


Figure 2. Earthquake epicenters adjacent to the region of this study: 1912-1970 (compiled from Milne and Lombardo, 1952; Milne, 1954a, 1954b, 1956a, 1956b, 1961; Gutenberg and Richter, 1954; Rothe, 1959; U. S. Coast and Geodetic Survey, U. S. Earthquakes 1955-1962; U. S. Department of Commerce, PDE cards, 1963-1970; Tobin and Sykes, 1968).

Sykes, 1968). Hodgson and Milne (1951), Stauder (1959, 1960), Benioff (1962), and Tobin and Sykes (1968) describe the faulting on the Queen Charlotte Islands and the Fairweather faults as predominantly right-lateral strike-slip motion on a steeply dipping plane. Tocher (1960) made field observations which revealed right-lateral movements on the Fairweather fault as large as six meters following the 1958 earthquake. Wilson (1965b) suggested that the fault system is a right-lateral transform fault. Tobin and Sykes (1968) gave evidence from fault plane solutions which supports this idea. Very few epicenters lie east of the fault zone and none between 55 N. and 56 N.

Shor (1962) and Milne (1964) made seismic refraction studies in the area and Tatel and Tuve (1955) and White and Savage (1965) made similar studies in adjacent areas. The reversed refraction lines of Shor (1962) gave crustal velocities and thicknesses in Dixon Entrance and the adjacent ocean. Milne (1964) made a reverse refraction line on the edge of the shelf outside Dixon Entrance but did not observe mantle arrivals. White and Savage (1965) performed refraction work extending to the northern end of Vancouver Island. Tatel and Tuve (1955) made several unreversed refraction measurements north of Skagway, Alaska.

Woolard et al. (1960) made early land gravity measurements in southeastern Alaska. Dehlinger et al. (1966) made shipboard

gravity measurements along the Inside Passage from Skagway to Seattle. Gemperle and Couch (1970) added to this data in southeastern Alaska and extended the study seaward. Stacey et al. (1969) and Stacey and Stephens (1969) reported on detailed gravity measurements made in coastal waters of British Columbia. Couch (1969) and Dehlinger et al. (1971) made free-air gravity measurements in the northeastern Pacific Ocean west of British Columbia.

Shipboard magnetic measurements made outside Queen Charlotte Sound and off Moresby Island by Raff and Mason (1961) and off Graham Island by Couch (1969) show the linear pattern associated with oceanic spreading centers. A high-altitude magnetic survey reported by Haines, Hanaford, and Riddihough (1971) includes long lines over the margin area which show magnetic lineations parallel to the coast line.

Gemperle and Couch (1970) reported the results of an air-gun survey in the vicinity of Chichagof and Baranof Islands.

Boucher and Fitch (1969) observed microearthquakes along the Denali fault as far south as Haines, Alaska. Similar measurements reported by Tobin and Sykes (1968) near Sitka, Alaska, showed a few microearthquakes originating offshore. Milne, Smith, and Rogers (1970), recording with high-gain seismographs in the Coast Mountains of British Columbia, observed microearthquakes originating in the eastern portion of southeastern Alaska.

### Purpose of this Research

This study presents additional geophysical measurements made in southeastern Alaska and western British Columbia and relates these data to possible structures in the earth's crust. The initial portion of this study describes a seismic refraction experiment performed on the continental margin to determine the thickness and velocity of layers in the crust. The second part is an analysis of air-gun, magnetic, and gravity measurements in Dixon Entrance. These data, in conjunction with additional geophysical measurements made by others, form the basis for two-dimensional structural models of the crust in Dixon Entrance. The final portion of this study relates microearthquake measurements to tectonic processes in southeastern Alaska and western British Columbia.

## INSTRUMENTATION

Purpose and Requirements of a Seismic Recording System

The seismic refraction and microearthquake measurements were made with a high-frequency, high-gain, portable seismic recording system recently constructed at Oregon State University. Built primarily for recording microearthquakes at a small array, the flexibility of the recording system allowed its use as a refraction seismograph and as a microearthquake monitor. The following paragraphs discuss the requirements for a microearthquake recording system and describe the Oregon State University (OSU) system.

The measurement of seismic waves from very small earthquakes, called microearthquakes, is a relatively recent development in seismology. Asada (1957) first designed equipment to record low-amplitude, high-frequency waves from small earthquakes. The objective of his research was to place seismic recorders as near as possible to areas of natural seismic activity. Gutenberg and Richter (1954) showed that the frequency of occurrence of earthquakes increases as the magnitude decreases according to the relation

$$\text{Log}_{10} N = a - bM$$

where  $a$  and  $b$  are constants,  $N$  is the number, and  $M$  the magnitude of earthquakes which occur in a region over a given interval of time. For the world at large, this logarithmic relationship between earthquake magnitude and frequency indicates that the frequency of earthquakes at any given magnitude level is approximately eight to ten times higher than that at one magnitude higher (Richter, 1958). If it were possible to record all earthquakes equally well, a much larger number of small earthquakes than large earthquakes would be observed. However, as a result of strong attenuation with distance of high frequency seismic waves, seismic stations distant from epicenters only record large earthquakes (which produce more low frequency components). Thus, in an active region, a seismograph will record a large number of small earthquakes only if it is placed close enough to the epicenters.

Permanent seismic stations are usually installed in seismically quiet regions so that small local shocks do not interfere with the registration of teleseisms. The temporary placement of several such instruments near a tectonically active region to measure seismicity is time consuming, expensive, and often impractical. However small, portable, high-frequency instruments are ideal for measuring the seismicity of a small region because they selectively record nearby earthquakes in preference to more distant earthquakes. With portable seismographs, it is possible to estimate the seismic

activity of a region in a few days or weeks compared to the years that might be required using permanent but more distant seismograph stations.

Portable microearthquake recording systems built by other investigators (e. g. Lehner and Press, 1966; Oliver et al., 1966) share common features but differ in some details. The sensor is usually a small lightweight geophone having a natural frequency of 1 Hz or higher and capable of being buried in the ground to reduce wind-generated noise. Stabilized electronic amplifiers provide high magnification. Mechanical and electronic clocks, crystal controlled timers, and radio time-standard receivers provide precision time. Typically, records are made on paper with revolving drums, strip chart recorders, or magnetic tape recorders. A dust and waterproof container or trailer usually encloses the electronic equipment for field use. Storage batteries or a thermal-electric generator supplies power. Desired recording times range from hours to weeks depending on the rate of microearthquakes. Low power consumption is necessary to avoid frequent visits to the recording site for servicing power sources. Physical size and weight are kept to a minimum and portability is a prime requisite in rugged or roadless areas.

### Oregon State University Recording System

The design of the OSU microearthquake system provides maximum flexibility at low cost. Four channels can be used either together for recording an array of seismometers at one location or each seismometer by itself at widely separated locations. Figure 3 shows the system assembled for use in an array configuration.

Four amplifier modules (one for each channel), a reference signal and calibration module, and a tape speed compensation module form the main electronic components of the system. Each of the four amplifier modules contains an amplifier, filter, modulator, and demodulator. The amplifier section is a single operational amplifier operated in the common rejection mode. A center-tapped Mark Products Model L-4 2 Hz geophone with a 5500 ohm coil operates at 0.67 critical damping. Diode clippers shunt each input to protect against excessively large input signals. The amplifier voltage gain is adjustable in 6 db steps over a range of 60 db to a maximum of 20,000. One output from the amplifier goes to a voltage to frequency converter while a parallel output feeds the signal simultaneously to a hot-wire strip chart recorder (Mechanics For Electronics, Model 20C-AHA). The amplifier passes signals from DC to 200 Hz and the strip chart recorder records linearly from DC to 100 Hz at half chart paper width (half width is 2.5 cm). Low frequency microseisms below

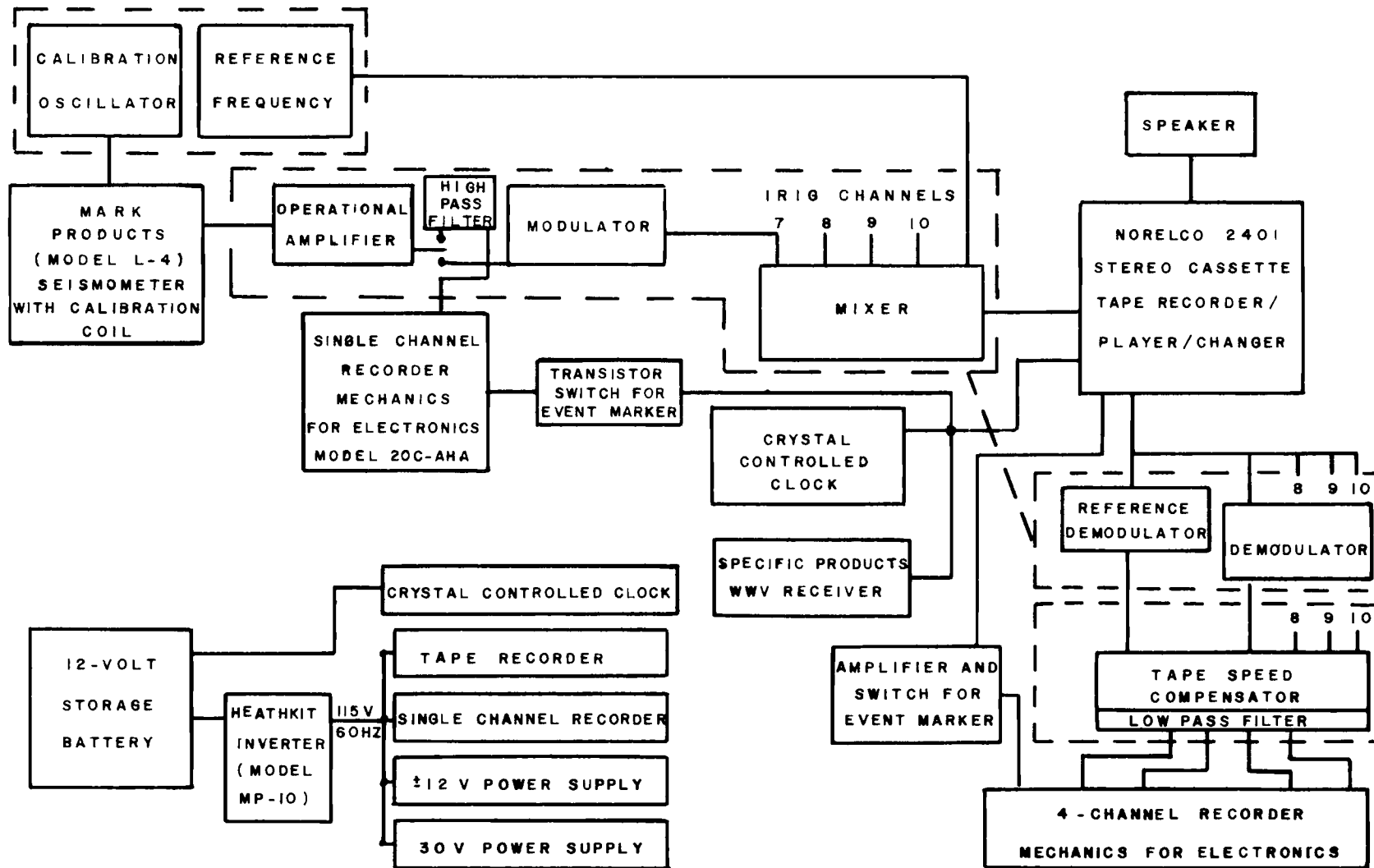


Figure 3. Block diagram of the Oregon State University seismic system. Dashed lines enclose modules described in text.

1 Hz are a problem in coastal areas so a high pass filter which attenuates signals below 1.4 Hz is included in the circuit as an option to the user. The filter, in combination with the rapid fall-off of geophone response below 2 Hz, helps to reduce the recorded amplitude of ocean generated microseismic noise. Long term amplifier drift due to temperature and moisture variations causes excessive recorder drift only at maximum gain. The use of the capacitor-coupled high pass filter eliminates recorder drift. From the amplifier, or the filter if it is in use, a mixer combines signals from one or more channels together with a 1700 Hz reference signal. A magnetic tape recorder records the output from the mixer. On playback, filters separate the frequency modulated signals and a frequency to voltage converter demodulates the signal from each channel. Variations in the demodulated reference signal compensate the seismic signal on each channel to correct for any wow and flutter present on the played-back signal.

Table 1 gives the IRIG frequency channels used in this system together with their center frequencies and the frequency responses. The voltage controlled oscillator is linear for frequencies from DC to the value given in the table.

A built-in signal generator permits calibration of the system in the field. The signal generator drives the seismometer mass through a calibration coil wound on top of the main seismometer coil.

The signal generator supplies sine, triangle, and square wave signals at ten frequencies from 0.2 to 40 Hz. The wide selection of wave shapes and frequencies permits the system to be calibrated using both continuous and transient techniques under field conditions.

Table 1. Standard Inter-Range Instrumentation Group (IRIG) frequency channels used in the Oregon State University seismic recording system.

IRIG Channel	Center Frequency, Hz	Frequency Response from DC, Hz
6 (reference)	1700	25
7	2300	35
8	3000	45
9	3900	59
10	5400	81

A crystal-controlled pulse generator designed and constructed at Oregon State University generates accurate time pulses synchronizable with a radio time signal. Frequency division of the signal from a crystal oscillating at 983,040 Hz generates seconds, minutes, and hours pulses. The pulses pass through a transistor switch to drive an event channel on the strip chart recorder; they can also go directly onto a second channel of a tape recorder. On playback, the pulse passes through an amplifier which operates an event channel on a strip chart recorder. The U. S. Bureau of Commerce, National Bureau of Standards, operates a shortwave radio station WWV which broadcasts an accurate time standard. WWV radio signals, recorded periodically on the timing channel, provide absolute time.

Presently, a Norelco 2401 stereo cassette recorder, player, and changer records the seismic and time signals. Using six C-120 cassettes, the unit records unattended for 12 hours at a speed of  $4.77 \text{ cm sec}^{-1}$  ( $1 \frac{7}{8} \text{ in sec}^{-1}$ ).

Storage batteries supply 12 volt power to the clock and to an inverter which supplies 115 v 60 Hz power for the remaining components of the system. Two medium-sized automobile batteries operate the system for approximately 12 hours.

#### Recording System Response

The amplitude and phase response of each channel of the recording system must be known in order to relate signal amplitude to ground displacement. A Maxwell bridge calibration technique determined the response of the Oregon State University system. The method of Willmore (1959) formed the basis for the calibration procedure. In this method, the seismometer main coil forms one arm of a Maxwell bridge (Figure 4). Resistor  $R_R$  is much smaller than the seismometer coil resistance  $R_C$ , and  $R_B$  is much larger than  $R_C$ . Varying resistor  $R_D$  balances the bridge and  $C_B$  compensates for inductance in the seismometer coil. With the L-4 seismometers,  $C_B$  was unnecessary to obtain a balanced bridge and the calibration used an entirely resistive bridge. The seismometer mass is first clamped by laying it on its side (to prevent the driving signal from moving the

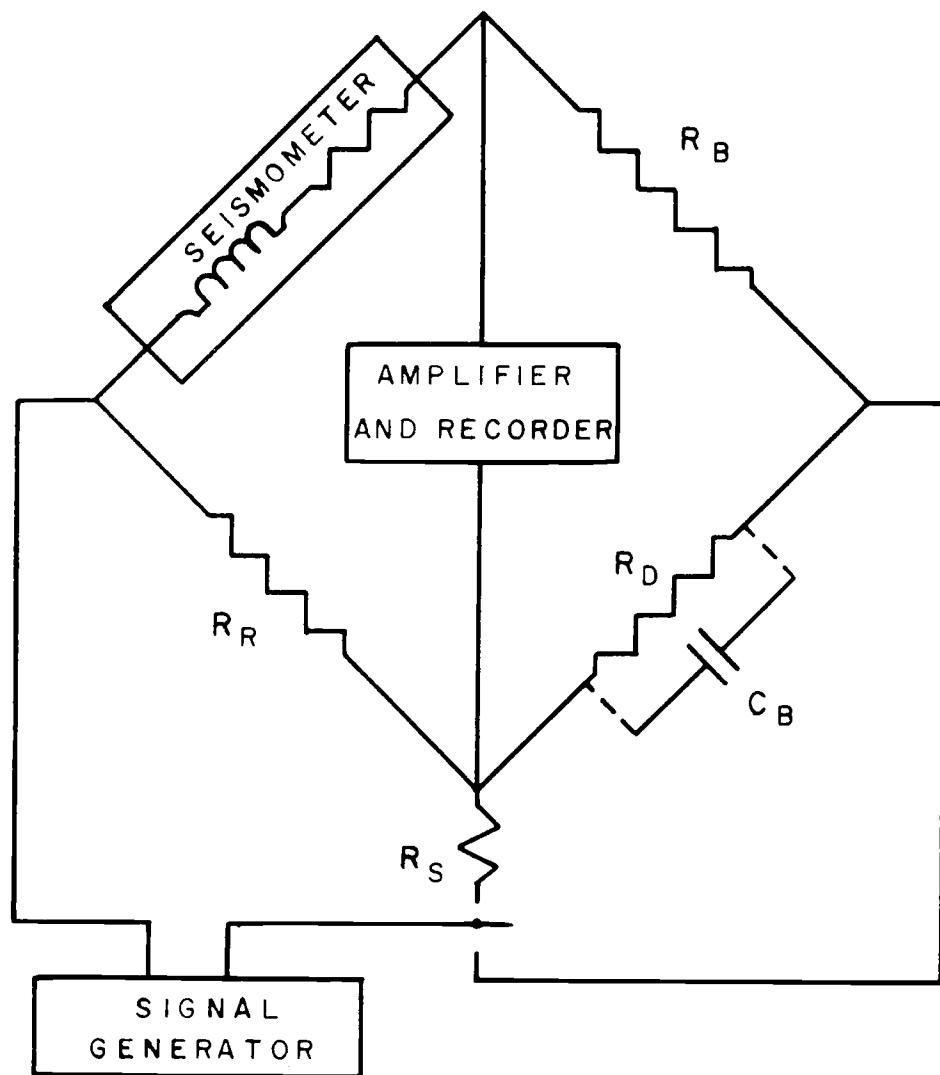


Figure 4. Maxwell bridge circuit for seismograph calibration (after Willmore, 1959)

main coil) and the bridge is balanced. The seismometer is then unclamped and observations are made of the output signal produced by driving the bridge with a known emf at several frequencies. Comparison of the observed amplitude and phase of the resulting output with the driving signal allows computation of the amplitude and phase response of the seismic system. For computational purposes, the mass of the seismometer was considered to be 500 grams (manufacturer's data). The computed transduction is  $2.68 \text{ volts cm}^{-1} \text{ sec}^{-1}$ , a value which compares closely with the manufacturer's stated value of  $2.72 \text{ volts cm}^{-1} \text{ sec}^{-1}$ .

The amplitude response of the system was also obtained by driving the calibration coil with a current of a known size and frequency and observing the system output. Comparison of these results with the results from the bridge calibration allows computation of the amplitude response from later calibrations made during each use of the system in the field.

During playback of seismic signals, high frequency noise (predominantly 60 Hz) originating in the tape recorder interfered with the seismic signal. An active low-pass filter, especially constructed to filter out this noise, effectively attenuated unwanted noise above 20 Hz.

Figure 5 shows amplitude and response curves for direct strip chart recording of Channel 7. This configuration recorded the

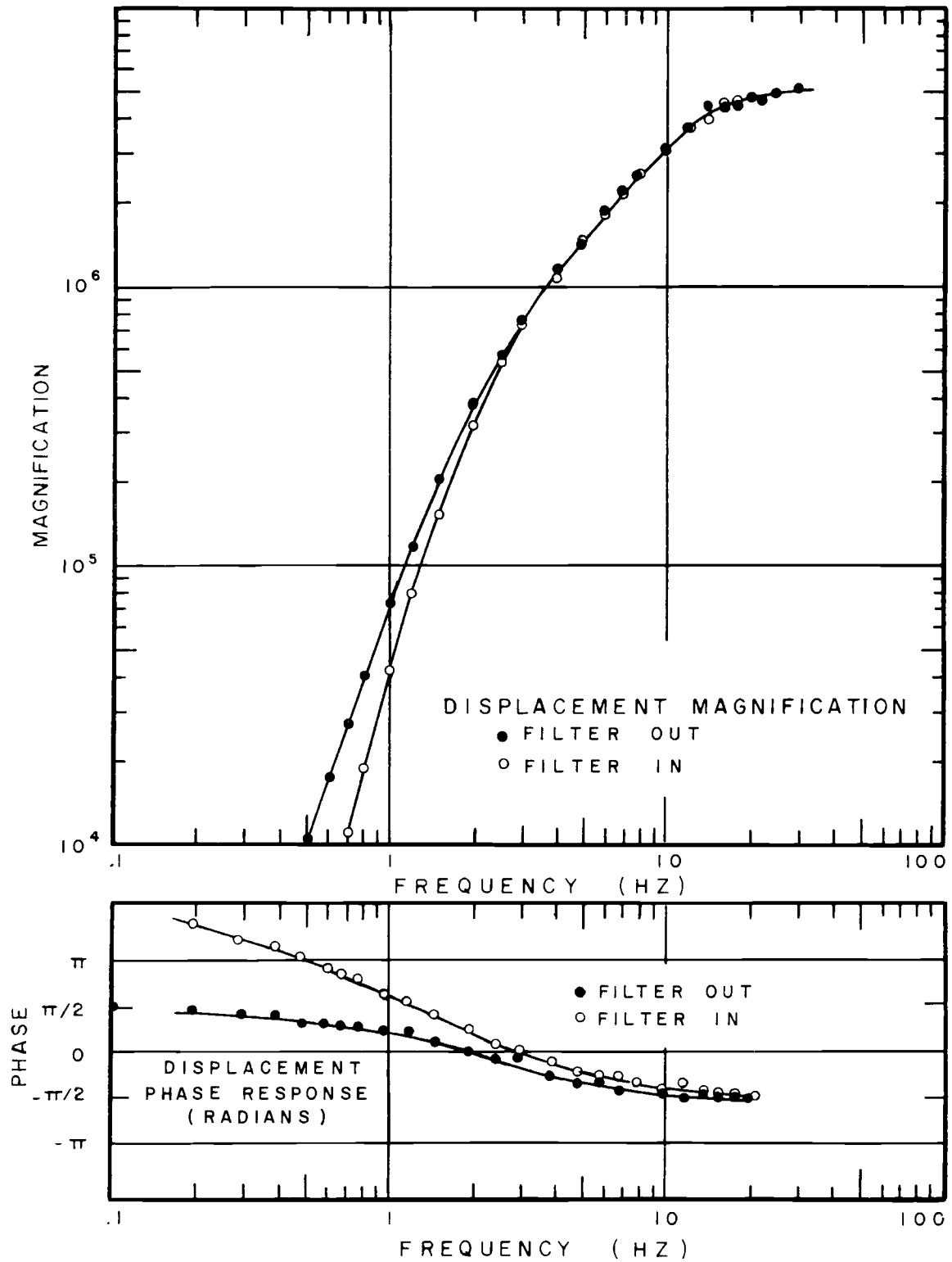


Figure 5. Displacement magnification and phase response for direct strip chart recording of Channel 7.

seismic data at individual microearthquake stations and at the seismic refraction stations. Figure 6 shows displacement magnification and phase response for Channel 7 using the tape recorder, tape speed compensator, and high-cut filter writing on a four-channel recorder. This configuration recorded the data at microearthquake array stations.

Boxes made from 1.27 cm plywood mounted on pack frames protect the instruments. They provide protection from dust and moisture while affording a convenient method of transporting the instruments in rugged terrain. Figure 7 shows views of the seismic system in operation and during playback.

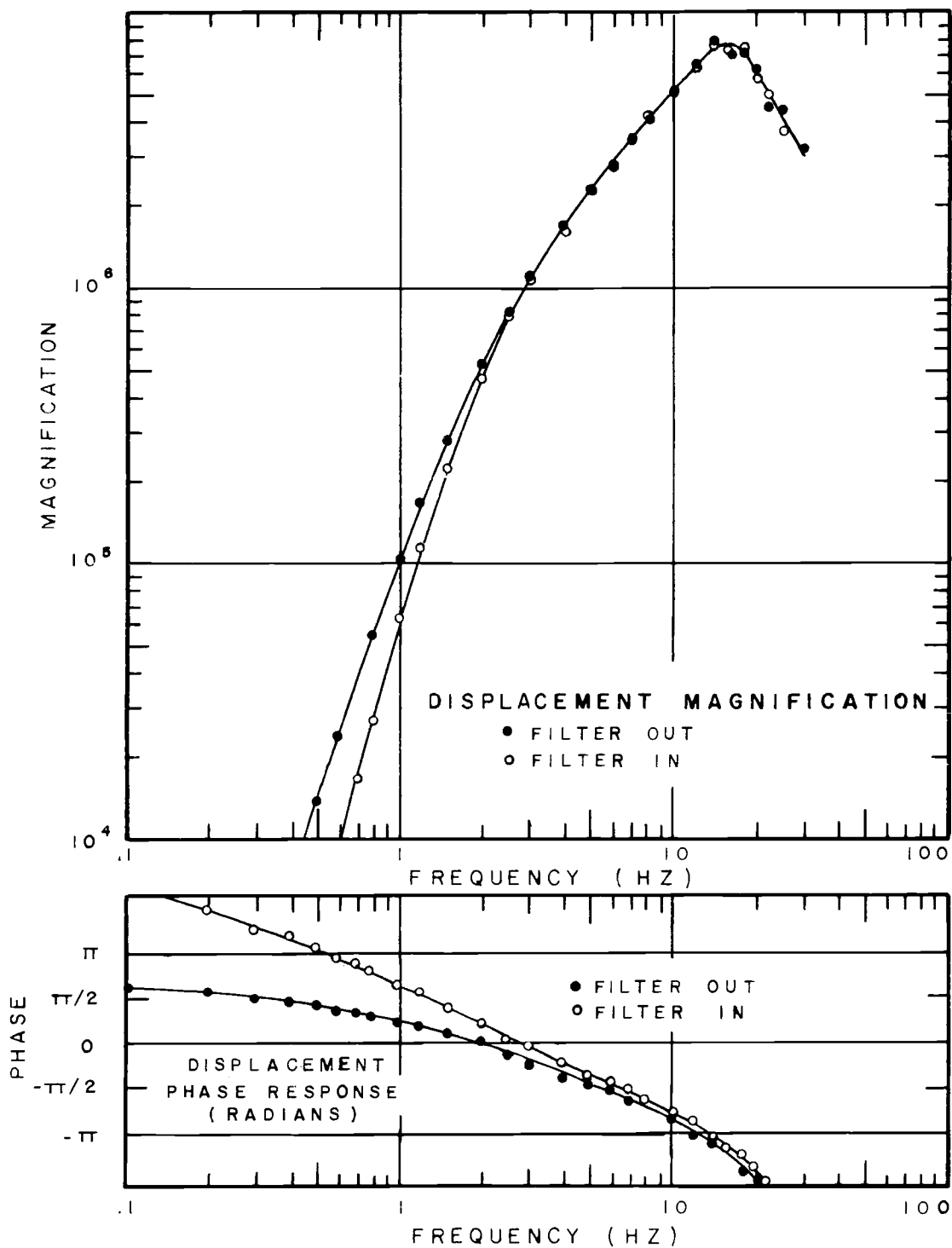


Figure 6. Displacement magnification and phase response for Channel 7 using tape recorder, tape speed compensator, and high-cut filter with a four-channel chart recorder.

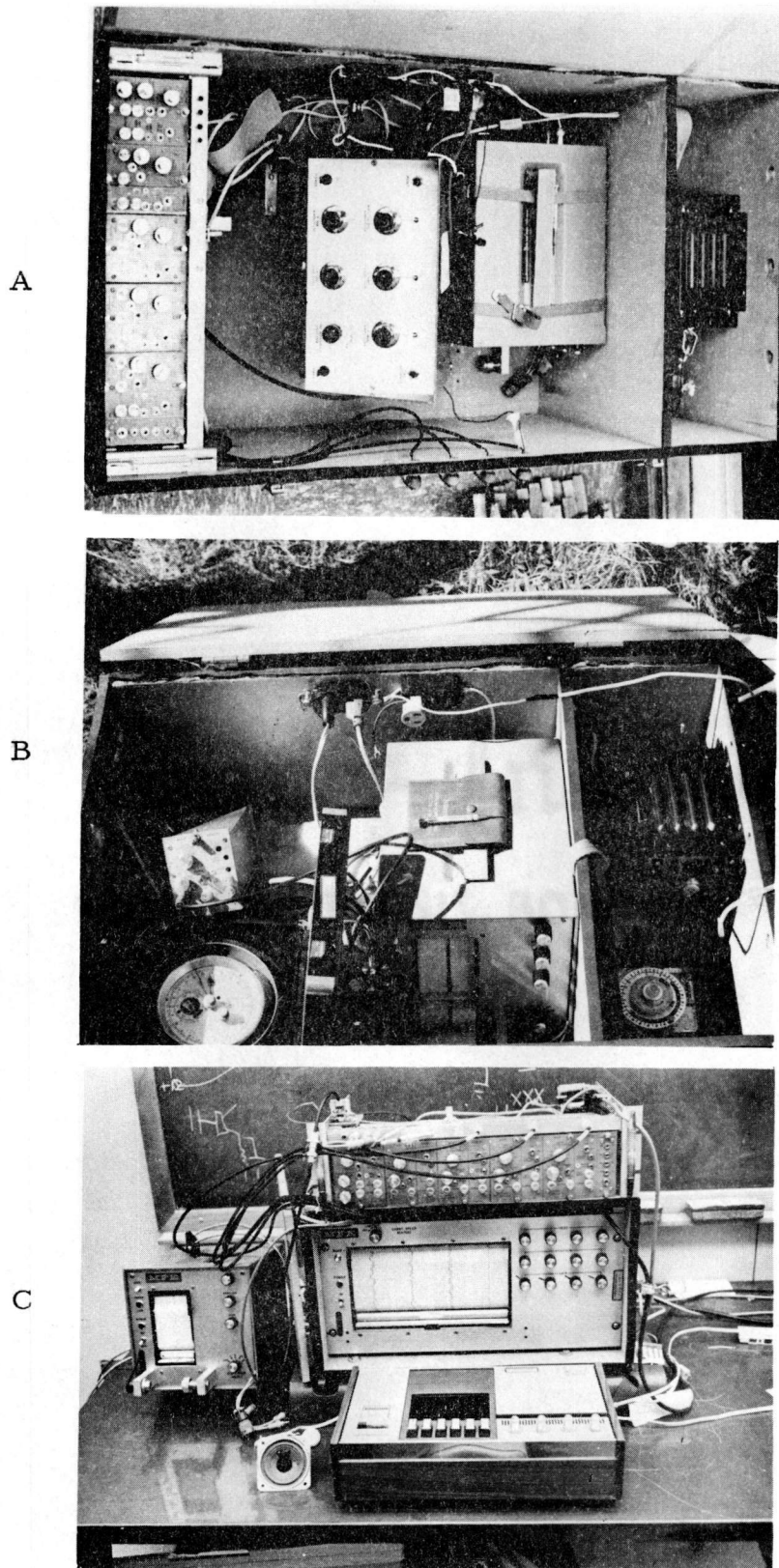


Figure 7. Views of the Oregon State University seismic recording system: A, array station; B, unattended station; C, during playback.

## SEISMIC REFRACTION STUDY

Introduction

During August of 1970, Oregon State University personnel made recordings of ten large chemical explosions at 11 locations in western British Columbia and southeastern Alaska. Figure 8 shows the station locations along two recording lines. Six of the stations lie along a line which extends northwest from the shot point at Ripley Bay ( $52^{\circ} 25.30' N.$ ,  $127^{\circ} 53.25' W.$ ) out to a distance of 290 km. The remaining five stations lie along a line which extends north-northwest from the shot point at Bird Lake ( $53^{\circ} 35.83' N.$ ,  $132^{\circ} 23.92' W.$ ) out to a distance of 384 km.

Personnel from the Dominion Observatory of Canada recorded the shots along lines extending toward the east to determine seismic information on crustal structures in western British Columbia. The three-member team from Oregon State University independently recorded toward the northwest. The charges, detonated by personnel of the Dominion Observatory, ranged in size from 910 to 3630 kg each of Nitrone SM and were exploded in 24 meters and 40 meters of water at Bird Lake and Ripley Bay respectively.

The SEA-ESTA, a 30 foot inboard cruiser, provided the means of transportation for the OSU field team during the experiment. OSU personnel carried the portable seismic recording equipment ashore

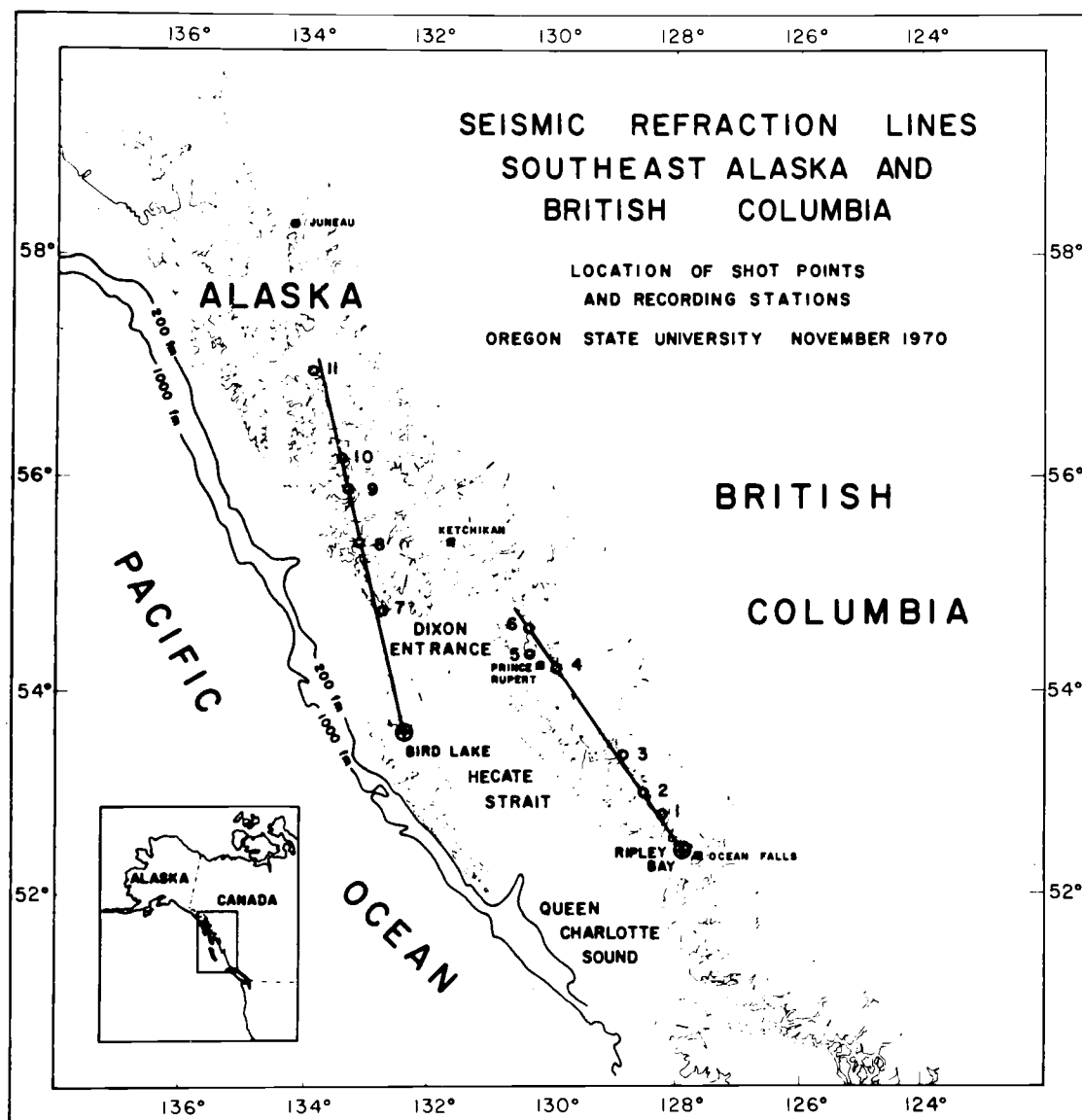


Figure 8. Location of shot points and recording stations.

in a seven foot dingy and placed it in a quiet protected area above high tide at each station. A single geophone recorded the seismic information at each location. The field party placed two systems, one unattended and the other attended, approximately 30 km apart for each shot. Chart scales on the maps used to determine station locations range from 1:10,000 to 1:73,000. The maps were obtained from the Canadian Hydrographic Service, the U. S. Naval Oceanographic Service, the U. S. Navy Hydrographic Office, and the U. S. Coast and Geodetic Survey. Station and shot point locations were read to the nearest 0.01 minute. A computer program written in FORTRAN IV by Chiburis (1965) and modified for use on a CDC 3300 digital computer determined distances and azimuths between the shot point and the seismic recording locations. The calculations employ Rudoe's formula (Bomford, 1958) which uses spherical trigonometry and geocentric coordinates to approximate the geodesic distance between two points on the earth's surface.

#### Recording Techniques

A four-channel recorder recorded simultaneous signals from the geophone, the crystal-controlled clock, and the WWV radio receiver at the attended station. A single vertical geophone, an amplifier module from the OSU seismic system, a chronometer, a clock switch, and a single-channel recorder comprised the equipment

of the unattended station. The recorder operated at a speed of 1 mm/sec until the shot time when a clock-controlled relay switched the recording speed to 25 mm/sec. Linear interpolation between comparisons of chronometer and WWV radio time at the beginning and end of each record provided accurate timing at the unattended station. An interval of approximately 12 hours occurred between placement and retrieval of the unattended station. During this time, personnel traveled to a different location, set up the attended station, recorded the seismic signal, and returned. The placement of the geophone on rock outcrops or in shallow holes dug to bedrock helped to form a good coupling between the geophone and the earth. Low background noise, made possible by low population density and low wind conditions, permitted recordings to be made at gain settings within 12 db of the maximum gain of  $3.5 \times 10^6$  at 10 Hz.

#### Geology, Structural Trends, and Gravity

The refraction lines lie west of the Coast Mountains, a major geologic and topographic feature which extends from northern Washington State to the north-trending part of the Alaska-Yukon boundary. Roddick (1966) outlines the geology of the region as follows. Mesozoic and Tertiary metasedimentary and plutonic rocks comprise the Coast Crystalline belt along the mainland coast of British Columbia in the vicinity of the stations along the Ripley Bay refraction line.

Occurrences of Paleozoic rocks bordering the crystalline complex, and highly metamorphosed roof pendants within the belt, indicate that at the end of Paleozoic time most of the region lay beneath the sea. Isotope age determinations give evidence that intrusion of the main body of plutonic rock occurred during late Cretaceous time. Major uplift took place in the early Tertiary and subsequent erosion resulted in the present pattern of exposed rock. The composition of the granitic rock in the western Coast Mountains is mainly diorite and quartz diorite.

The area seaward from the mainland coast to the continental slope is geologically complex and varied. Brown (1966) summarizes the geology and tectonic history as follows. The Queen Charlotte Islands region has been subjected to a uniform history of deposition, deformation, and plutonism. In this region, folds are gentle and less important than faulting. Major crustal fractures, trending northwest, appear to have been responsible for controlling volcanism, sedimentation, and intrusion. The geologic history of the area is one of episodes of great effusive volcanism alternating with long periods of sedimentation. In the vicinity of Bird Lake, the hot point on Graham Island, the most recent (early Tertiary) volcanic period resulted in the eruption of an extensive sequence of plateau-like basalt flows and breccias and rhyolitic ash flows. The sequence has a maximum thickness of 5500 meters. Late Tertiary

sedimentation resulted in the deposition of a formation of marine and non-marine sandstone, shale, and conglomerate on northeastern Graham Island where it attains a thickness of 1800 meters.

The geologic history of southeastern Alaska, whose southern tip lies only 62 km across Dixon Entrance from Graham Island, is considerably different and more complex. Brew, Loney, and Muffler (1966) outline the geologic history as follows. Dominantly eugosynclinal deposition in troughs trending north-northwest occurred during Paleozoic and Mesozoic time. Widespread plutonic activity, regional metamorphism, and complex deformation affected these marine clastic, volcanic, and carbonate rocks during late Jurassic and Cretaceous time. Two northwest-trending belts of Mesozoic rocks, one adjacent to the Coast Mountains and one along the ocean side of the Alexander Archipelago, dominate the pattern of rock outcrops (Figure 9). A central belt of metamorphosed Paleozoic rocks, intruded by granodiorite and diorite, separate the Mesozoic belts. The recording stations for the Bird Lake refraction line lie in the southern portion of this central Paleozoic region. Deposition of a thick sequence of locally derived continental Tertiary sediments in the central portion followed uplift and erosion in the Cretaceous. Large-scale faults, trending northwest and north and thought to be dominantly strike-slip, formed during the Tertiary and occur within both the eastern and western Mesozoic and Paleozoic belts. Jointing

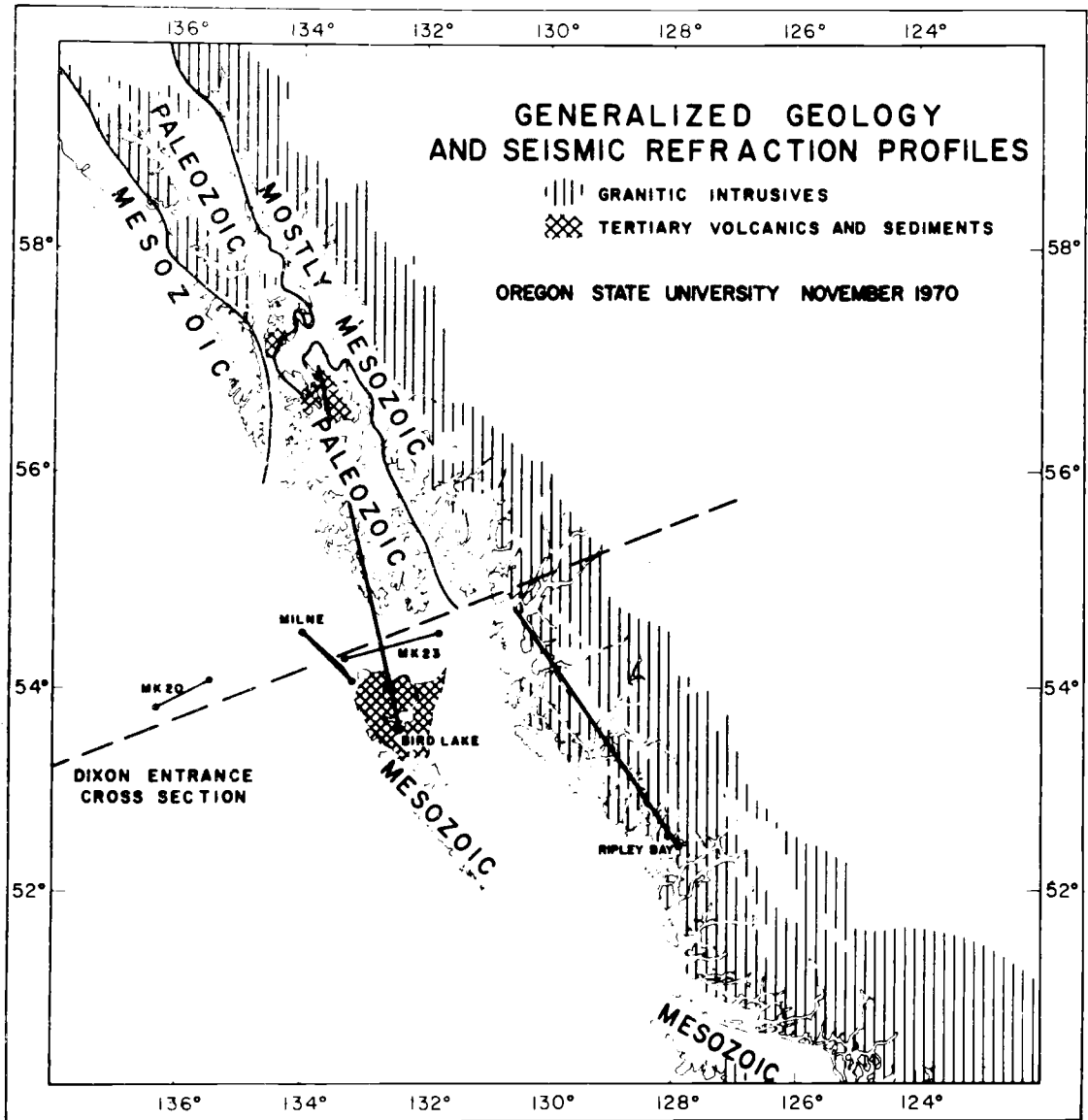


Figure 9. Generalized geology, location of seismic refraction surveys, and position of Dixon Entrance cross section.

and faulting are suggested as being responsible for many of the fiords and channels in southeastern Alaska.

Gravity measurement along the continental margin of southeastern Alaska and western British Columbia began in 1939 and continue today. Heiskanen (1939) occupied 19 pendulum stations along the Inside Passage from just south of Skagway, Alaska, to Seattle, Washington. Later personnel of the University of Wisconsin, transporting gravity meters by airplane, made a gravity survey in southeastern Alaska (Woollard et al., 1960) which showed Bouguer anomaly contours roughly parallel to the continental margin and decreasing inland from 50 mgl at the ocean coast line to less than -20 mgl at the mainland coast. Dehlinger et al. (1966), who made shipboard gravity measurements along the Inside Passage, showed that free-air anomalies become progressively negative inland with a steep gradient east of Hecate Strait. Free-air anomalies reported by Couch (1969) and Dehlinger et al. (1971) and Bouguer anomalies published by Stacey and Stephens (1969) along the west coast of Canada indicate gravity anomalies of low amplitude in Hecate Strait and Queen Charlotte Sound. Along the western edge of the area, positive Bouguer anomalies mark the change from oceanic to continental crust while a negative anomaly along the Coast Mountains may be due to a thickening of the crust beneath these mountains (Stacey and Stephens, 1969). Gemperle and Couch (1970) presented

free-air and Bouguer anomaly maps in southeastern Alaska north of  $56^{\circ}$  N. which also showed near-zero anomalies between the continental margin and the Coast Mountains. Data compiled from Theil et al. (1958), Worzel (1965), Couch (1969), Banks (1969), Stacey and Stephens (1969), and Gemperle and Couch (1970) formed the basis for the construction of the Bouguer gravity map of the region shown in Figure 10. An elongated band of near-zero anomalies lies between the steep gravity gradients associated with the continental slope and the Coast Mountains and extends from Vancouver Island to Cross Sound. The near-zero anomalies indicate an area where little or no change in crustal thickness is expected.

The Bird Lake refraction line, located in the region of low gravity relief, and the Ripley Bay refraction line, oriented along the anomaly trends parallel to the Coast Mountains, are unreversed lines and hence do not permit the determination of dipping layers, should they exist. On the basis of gravity anomaly gradients, however, changes in crustal thickness are not expected along the Bird Lake line nor along the Ripley Bay line. This gravity information is the basis for the assumption of horizontal layering in the interpretation of the refraction data. It is reasonable, however, to expect changes in crustal thickness across the continental margin in the vicinity of the pronounced gravity gradients along the continental shelf and beneath the Coast Mountains.

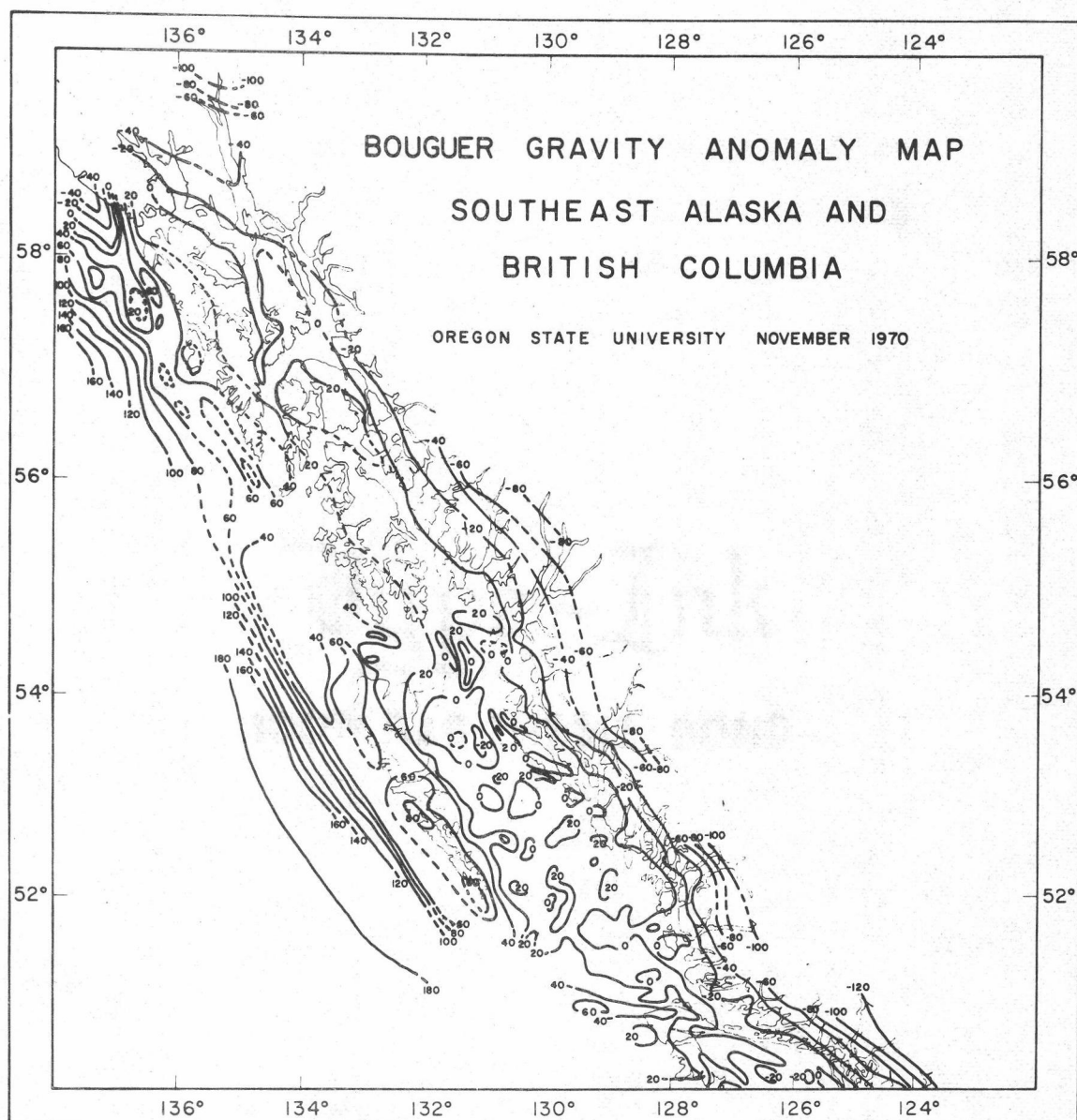


Figure 10. Bouguer gravity anomaly map of southeastern Alaska and western British Columbia (compiled from Theil *et al.*, 1958; Worzel, 1965; Couch, 1969; Banks, 1969; Stacey and Stephens, 1969; Gemperle and Couch, 1970).

### Reduction of Refraction Data

In the analysis of the seismograms, the first motions and the more prominent arrivals in the following wave train formed the basis for the interpretation. Timing, based on WWV radio signals, is accurate to one-hundredth of a second. Except at stations close to the shot points where arrivals are impulsive, the greatest error (on the order of 0.1 sec) in reading arrival times occurs with emergent arrivals which begin very gradually. The arrival times, reduced by subtracting the value  $\Delta/6.0$  where  $\Delta$  is the epicentral distance and plotted as a function of distance in kilometers from the shot point, form a reduced travel time graph. Changes in amplitude or period and character of the waves were used to identify possible arrivals. The background noise level was very low on all but one seismogram. The frequency of the arriving waves ranged from 4.5 to 8.3 Hz, conveniently higher than observed microseisms and lower than noise from local sources such as wind. Such a bracketing of the frequencies was fortunate, because the amplitude of the  $P_n$  phase for the most distant shots was approximately equal to the background noise. This frequency characteristic of the waves allowed  $P_n$  arrival times to be picked with confidence. A composite record section, constructed by tracing each seismogram at its proportionate epicentral distance on a single sheet of paper, aided in the interpretation. In the absence

of apparent velocities at each station, this procedure was a useful visual aid in correlating phases from seismogram to seismogram. The correlation of arrivals depended on the similarity of wave shape and the line-up of arrivals on the travel-time plot.

Once the arrival times were selected, a least squares fit to the arrival times by a line described by the equation  $T = I + \Delta/V$  where  $\Delta$  is the distance,  $V$  is the velocity, and  $I$  is the intercept time, determined apparent velocities and intercept times. Computation of the standard error of  $I$  and  $V$  resulted in an estimate of the variation in the intercept times and velocities. For the P-wave in the crust traveling as  $P_g$ , the intercepts were slightly negative on both lines. Subsequently, a least squares line through the origin of the form  $T = \Delta/V$  determined the  $P_g$  velocities on both lines. This restriction changed the velocity determined for the  $P_g$  phase by less than .03 km/sec.

A program written in FORTRAN IV by Mooney et al. (1969) from the dipping plane layer formulation of Adachi (1954) computed layer thicknesses assuming, in this case, that the layers were plane but without dip. Figure 11 shows the observed data, the interpreted sections, and the arrival times computed for reflected and refracted waves. Table 2 gives station locations, epicentral distances, and arrival times.

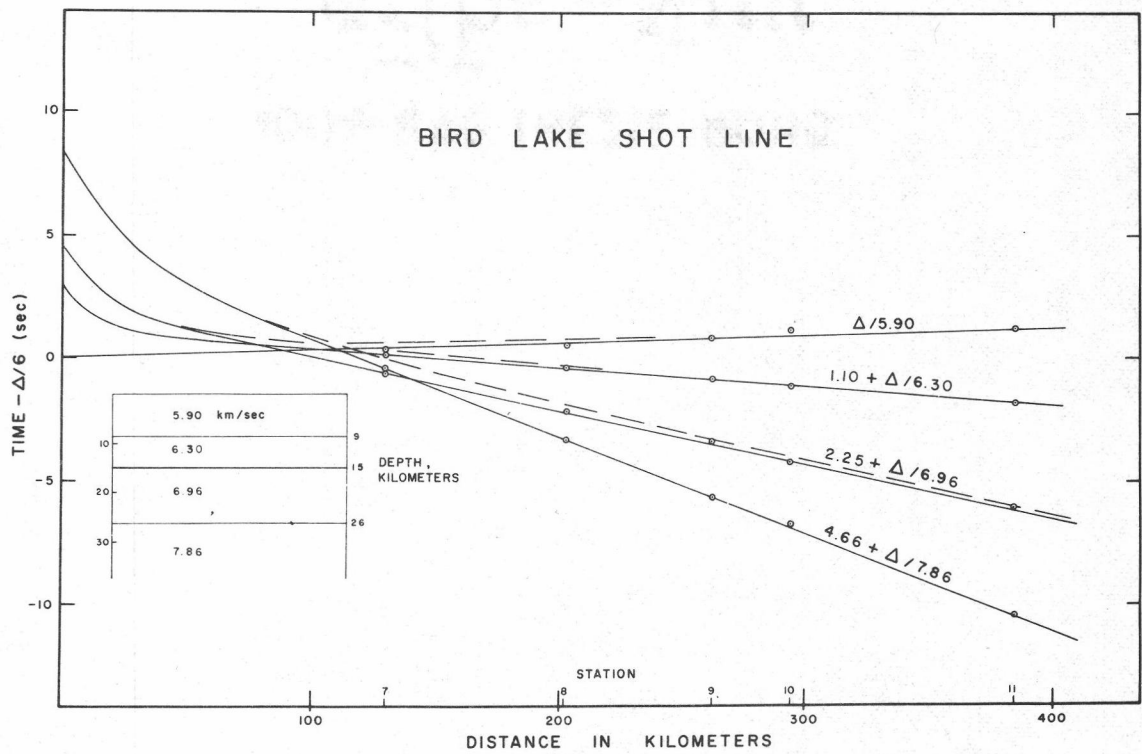
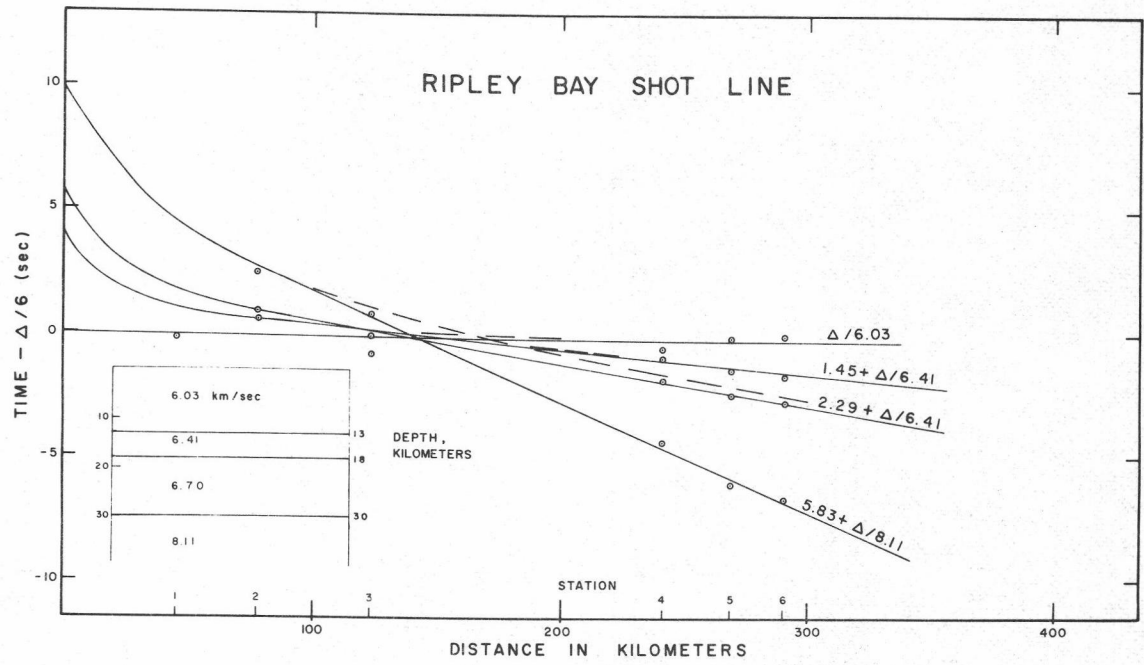


Figure 11. Reduced travel-time graphs and computed structure.

Table 2. Station location, epicentral distance and arrival times.

Station	Distance, km	Latitude, deg.	Longitude, deg.	P <sub>g</sub> sec	P <sub>a</sub> sec	P* sec	P <sub>n</sub> sec
Ripley Bay Line							
1	45.1	52°46.60'	128°12.55'	7.03			
2	77.1	53°00.66'	128°30.24'	13.71	13.55	13.89	15.38
3	123.3	53°21.79'	128°50.80'	19.70		20.40	21.33
4	241.8	54°12.58'	129°55.73'	39.59	39.22	38.32	35.81
5	268.8	54°19.44'	130°22.55'	44.64	43.37	42.39	38.69
6	290.3	54°33.84'	133°23.04'	48.36	46.69	45.66	41.70
Bird Lake Line							
7	129.6	54°44.52'	132°45.60'	21.85	21.63	20.90	21.17
8	202.8	55°21.83'	133°09.70'	34.22	33.39	31.60	30.40
9	261.1	55°53.21'	133°16.74'	44.24	42.61	40.05	37.78
10	293.3	56°10.01'	133°24.34'	49.95	47.65	44.57	42.05
11	384.3	56°56.50'	133°53.67'	65.15	62.13	57.91	53.51

### Bird Lake Refraction Line

Five stations recorded arrivals at distances from 130 km to 384 km from Bird Lake. In this range, only  $P^*$  and  $P_n$  appear as first arrivals. In standard notation,  $P_g$  refers to a compressional wave which travels entirely in the upper layer of the earth's crust,  $P^*$  refers to a compressional wave which is refracted in the lower or 'intermediate' layer of the crust, and  $P_n$  refers to a compressional wave which is critically refracted at the base of the crust. The discontinuity in velocity at the base of the crust is referred to as the M discontinuity or Moho after its discoverer, seismologist Andrija Mohorovicic.

An interpretation of two phases identified on the seismograms suggests that they come from layers in the upper 15 km of the crust (Figure 12). The largest arrival on all the seismograms is the wave which travels entirely in the upper layer of the crust,  $P_g$ . These arrivals give an apparent velocity of 5.90 km/sec. An arrival, labeled  $P_a$ , appears slightly earlier but with an amplitude nearly as large as  $P_g$ . The  $P_a$  phase arrives between the  $P^*$  and  $P_g$  phases and is the first of a series of disturbances which, on the basis of large amplitude, are probably more related to  $P_g$  than to  $P^*$ .

A phase with an apparent velocity of 6.96 km/sec, labeled  $P^*$ , the head wave arrival from the intermediate layer, appears at

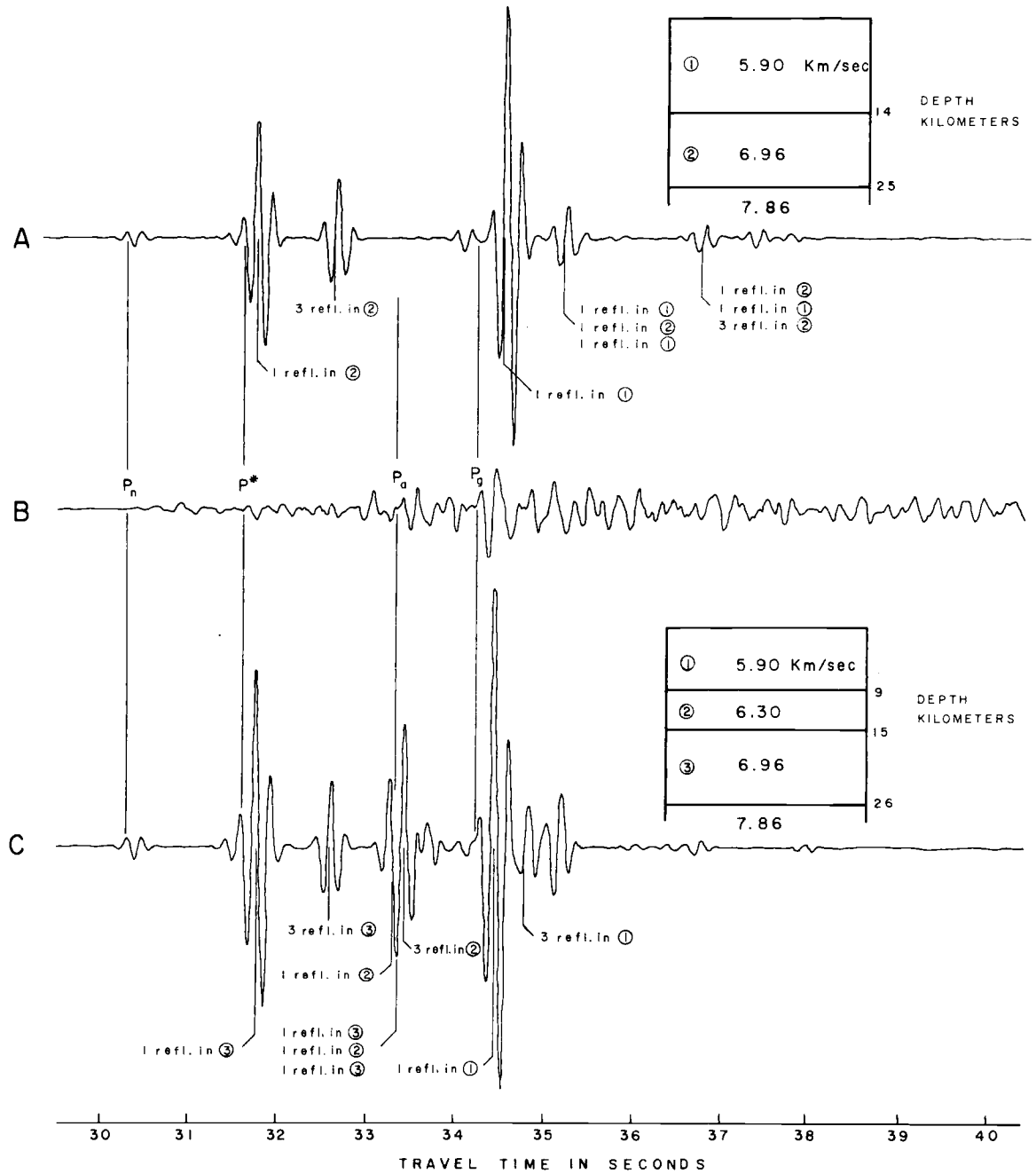


Figure 12. Comparison of a field seismogram with synthetic seismograms at  $\Delta = 202$  km.

Station 7 as a clear first arrival. On the remaining seismograms, the phase starts abruptly and is followed by a wave train containing characteristically three or four cycles.

Clearly identified as a first arrival at Stations 8, 9, and 10 is  $P_n$ , the refracted wave from the M discontinuity. At Station 7,  $P_n$  registers as an abrupt change in the direction of the recorded signal immediately following the  $P^*$  arrival while at Station 11 a change in frequency of the background noise indicates the  $P_n$  arrival.

On the basis of field studies by Ryall and Stuart (1963) and Roller (1965) and a theoretical study by Berry and West (1966) of wave amplitudes in crustal refraction,  $P_g$  wave amplitudes should not be greater than  $P^*$  or  $P_n$  wave amplitudes at distances between approximately 50 km and 250 km from the shot point. Ryall and Stuart (1963) suggested that the continuation of the  $P_g$  branch may be due to guided crustal waves. Consequently, the  $P_g$  and  $P_a$  phases seen in this study are probably most likely waves reflected one or more times in the two upper layers of the crust.

Comparison of a field seismogram obtained at a distance of 202 km from Bird Lake and theoretical seismograms computed at the same distance by Hron (1971) using methods developed by Kanesewich and Hron (1970) and Hron (1970) gives additional support to the interpretation that  $P_g$  and  $P_a$  are reflected waves in the crust. Two earth structures formed the models for the seismogram

computations. The first, a three layer model computed using  $P_g$ ,  $P^*$ , and  $P_n$  arrivals, and the second, a four layer model determined from  $P_g$ ,  $P_a$ ,  $P^*$ , and  $P_n$  arrivals, resulted in the theoretical seismograms shown in Figure 12.

The synthetic seismograms illustrate two important points. First, the largest deflections found on the synthetic seismograms are due to waves reflected one or more times in the upper crust. The energy from refracted waves is approximately an order of magnitude less than multiply-reflected or guided waves. Second, the more times a wave is reflected or the deeper the layer from which it reflects, the more the wave is attenuated. The explanation for these observations is that energy is lost with each refraction and reflection; accordingly the largest amplitude wave in Figure 12 is the wave which reflected once in layer 1.

On the field records, reflected waves are still relatively larger than refracted waves but the ratio of reflected to refracted waves is much reduced in comparison to the synthetic seismograms. This difference may be due to the simplifications used in computing the synthetic seismograms or to topographic irregularities in the reflecting boundaries which can lead to loss of energy by scattering. Finally, there is an important difference in the wave arrivals present on the seismograms. The disturbance attributed to the  $P_a$  phase in the field record appears to be due to the 6.3 km/sec layer which is present in the four layer model (trace C) but which is not present in the three layer model (trace A). This evidence, in addition to

the travel time data, supports the interpretation of a four layer model. The total depth to the M discontinuity computed from these two models differs by less than 0.5 km, however the difference in layering is important in the relation between crustal structure and other observable geophysical parameters, especially gravity as shown below.

#### Ripley Bay Refraction Line

Six stations recorded arrivals at distances of 45 km to 290 km along a line extending northwest from Ripley Bay. Three stations recorded direct  $P_g$  waves as first arrivals and three stations recorded  $P_g$  waves as later arrivals. The first motions had low amplitudes at Stations 2 and 3. Either a wrong choice of the times of first arrivals or large lateral variations in crustal velocity caused large scatter in the first arrivals at these distances (Figure 11). Arrivals which appear along the extension of the line drawn through  $P_g$  arrivals at Stations 4, 5, and 6 are probably guided waves in the crust as discussed earlier. The three most distant stations recorded a second crustal phase, denoted here as  $P_a$ , with a large amplitude arriving before the  $P_g$  waves. The  $P_a$  arrival has large amplitude at Stations 2 and 3 which are close to the distance where refracted and reflected waves arrive nearly simultaneously (critical distance). The large amplitudes support the prediction of many investigators (e. g. Berry and West, 1965) that large arrivals should appear at the

critical distance. A strong arrival with an apparent velocity of 6.70 km/sec follows the relatively quiet period after the  $P_n$  arrival at Stations 4, 5, and 6. It is identified as  $P^*$ , the wave refracted from the intermediate layer. The ratio of the amplitudes of  $P^*$  and  $P_n$  is greater on the Ripley Bay line than on the Bird Lake line.

Waves refracted from the M discontinuity are quite weak; they are distinguishable on some records mainly on the basis of frequency differences. For example, at Station 6, the ratio of the signal amplitude to noise amplitude for  $P_n$  is approximately unity while the ratio of signal frequency to background noise frequency is about seven. The frequency ratio allows picking the  $P_n$  arrival to the nearest one-half cycle, or to an accuracy of 0.07 second. Large secondary arrivals at Stations 2 and 3 may be waves from the M discontinuity arriving at distances near the critical point.

### Structural Interpretation

The coefficients of the time-distance equations computed from the least squares fit to the data permit calculation of the crustal thicknesses. Assuming that the apparent velocities are true velocities and thus that the structure is formed of plane horizontal layers, the calculated depth to the M discontinuity is 25.9 km for the Bird Lake line and 29.9 km for the Ripley Bay line. Table 3 gives the time-distance equations and the results of the depth computations.

Table 3. Time distance equations and computed thicknesses

## Bird Lake line

$$P_g: T = \Delta / (5.90 \pm .02)$$

$$P_a: T = (1.10 \pm .09) + \Delta / (6.30 \pm .01)$$

$$P^*: T = (2.25 \pm .18) + \Delta / (6.96 \pm .03)$$

$$P_n: T = (4.66 \pm .11) + \Delta / (7.86 \pm .03)$$

	Velocity, km/sec	Thickness, km	Depth to interface, km
Layer 1	5.90	9.25	9.25 ± .23
Layer 2	6.30	6.49	15.75 ± .37
Layer 3	6.96	10.15	25.89 ± .54
Layer 4	7.86		

## Ripley Bay line

$$P_g: T = \Delta / (6.03 \pm .05)$$

$$P_a: T = (1.45 \pm .17) + \Delta / (6.41 \pm .03)$$

$$P^*: T = (2.29 \pm .06) + \Delta / (6.70 \pm .01)$$

$$P_n: T = (5.83 \pm .39) + \Delta / (8.11 \pm .11)$$

	Velocity, km/sec	Thickness, km	Depth to interface, km
Layer 1	6.03	12.89	12.89 ± .31
Layer 2	6.41	4.70	17.59 ± .41
Layer 3	6.70	12.33	29.91 ± .63
Layer 4	8.11		

Estimation of uncertainties in calculated values is difficult in seismic refraction work. In this study, the estimated uncertainty assigned to a given depth was calculated by adding or subtracting, as appropriate, the standard error in the time-distance equation and recomputing the depth. The difference between the recomputed depth and the mean depth gives an estimate of the possible uncertainty in computed depth. The uncertainty should be regarded as a minimum uncertainty inasmuch as dip may be present.

The orientation of the refraction lines minimizes the effects of changes in structure. Geologic and gravity data which support this assumption include the facts that the refraction lines lie parallel to geologic trends, the small scatter in the data points imply nearly plane layers, and the observed gravity field suggests little or no dip in structure in the direction of the refraction lines. Therefore, the assumption of plane horizontal layers made in computing the structural thickness is reasonably valid.

Shor (1962) reported a crustal thickness of 25 km in Dixon Entrance on the basis of possible second arrivals from the mantle with an apparent velocity of 8.49 km/sec. He also reported an upper layer with a velocity of 5.78 km/sec which probably corresponds to the layer with the velocity of 5.90 km/sec determined in this study. However, the depth to the top of the intermediate layer computed by Shor is more than 8 km shallower than reported here.

The shallow and relatively high velocity layer measured by Shor (6.80 km/sec) may be a local effect associated with the large quantity of basaltic rock noted on Graham Island near his refraction line. The high velocities may originate from crustal layers intruded by high velocity rock from the lower crust or upper mantle. Available gravity data does not support the probability of a rapid change in upper crustal layering across Dixon Entrance.

Milne (1964) completed a reversed profile at the edge of the continental shelf outside Dixon Entrance where he observed a layer 3.5 km thick having a velocity of 4.45-4.88 km/sec. He suggested that volcanic or sedimentary rocks comprise this layer. Beneath this layer he observed a crustal velocity of 6.16 km/sec which he attributed to the granitic layer of the continental crust. He did not observe higher velocity layers.

White and Savage (1965) obtained information on velocities in the upper crust of northern Vancouver Island, south of the area studied in this report. From explosions in Queen Charlotte Strait and Johnstone Strait, they obtained an average upper crustal velocity of 6.4 km/sec and an average lower crustal velocity of 6.8 km/sec. They calculated the depth to the top of the intermediate layer as 11 km. They did not find  $P_n$  arrivals. Brown (1966) considered Vancouver Island to be a part of the Insular Tectonic belt on the basis of geology, so it is not surprising that velocities and depths

obtained there correspond rather closely to those obtained from the Bird Lake explosions.

Tatel and Tuve (1955) made additional refraction studies north of the Bird Lake-Ripley Bay lines near Skagway, Alaska. Tatel and Tuve (1956), Woollard et al. (1960), and Hales and Asada (1966) interpreted these records. The seismic lines near Skagway traverse a rapidly changing Bouguer anomaly field suggestive of abrupt changes in crustal structure. The crust as computed is 36-42 km thick northwest of Skagway but north of Skagway it is 35 km thick. Three layers with velocities of 5.7, 6.0, and 6.7 km/sec comprise the crust and the mantle has a velocity of 7.7 to 8.0 km/sec. In comparison, the velocities north of Skagway are similar to those obtained from the Ripley Bay line.

Considerable evidence, presented earlier, shows that changes in major crustal structure occur normal to the continental margin. The structure, the geology, and the Bouguer anomalies are all aligned parallel to the margin. An attempt to determine the character of the transition from oceanic to continental structure uses a two-dimensional gravity model to fit the gravity profile of Couch (1969) which strikes N 69° E and intersects the coast at Dixon Entrance. The seismic refraction studies of Shor (1962), Milne (1964), and this study provided the depths to the layers in the cross section. Figure 9 shows the position of the two-dimensional model

together with the position of the seismic surveys. The gravity profile uses the free air anomaly values at sea and complete Bouguer on land. The cross section extends to 50 km in depth and 400 km in length from the Alaskan Abyssal Plain to the Coast Mountains. The line integral method as applied by Talwani, Worzel, and Landisman (1959) enabled computation of the vertical component of the gravitational acceleration at points on the earth's surface. In this method, a series of joined polygons of appropriate density approximates the crust and the gravity at any point is the combined attraction of these two-dimensional polygons. The results of the seismic refraction surveys were restraints on the layering. The empirical relation established by Ludwig, Nafe, and Drake (1971) permitted a systematic conversion from crustal velocities to densities. Bathymetric and seismic refraction boundaries, plotted on a working cross section, formed the basis for the construction of polygons to approximate the structure and iterative adjustments to densities and polygons followed until the computed and observed gravity agreed. A standard crustal and subcrustal section at the ocean end of the profile given by Couch (1969) ties this section to his.

The resulting cross section, shown in Figure 13, is a reinterpretation of the Dixon Entrance cross section given by Couch (1969) and the structure is identical to his model west of the

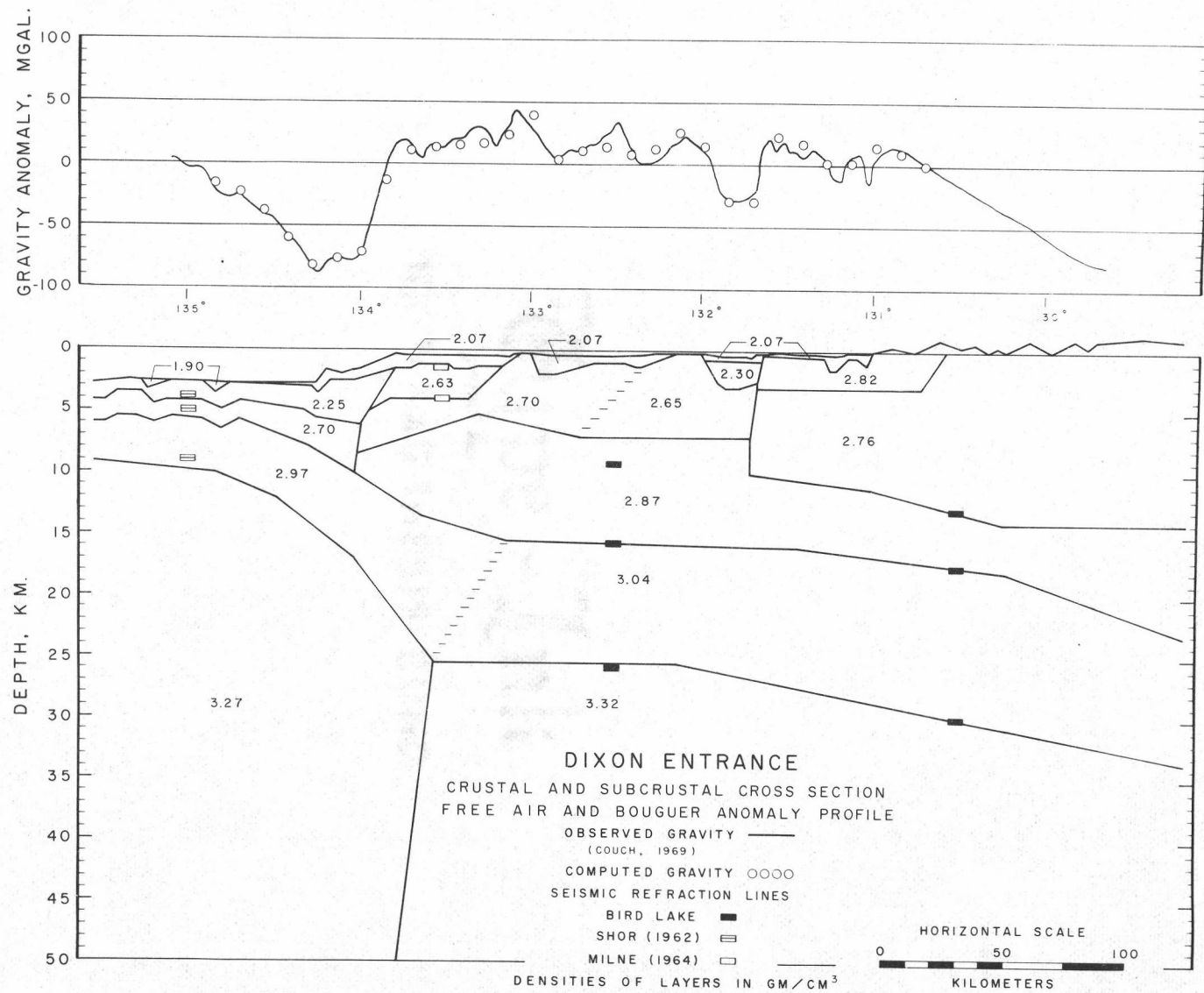


Figure 13. Dixon Entrance crustal and subcrustal cross section.

continental shelf. The large negative free-air anomaly over the continental slope is due to shoaling of the sea bottom and the steep dip of the M discontinuity. Three layers overlain by sediments comprise the continental crust. Short wavelength gravity anomalies in Dixon Entrance are due to variations in the thickness of the upper layers. The upper portion of the cross section will be discussed more completely below. The depth to the intermediate or oceanic layer increases from 6 km offshore to 15 km under Dixon Entrance. At the continental slope the structure of the upper crust changes to the thick upper crustal layer typical of continental areas. The plateau in the gravity anomaly suggests little change in crustal thickness under Dixon Entrance and the model indicates a crust of constant thickness. The decrease in the Bouguer anomaly at the mainland coast is due to a second increase in crustal thickness. The M discontinuity is 30 km deep under the Ripley Bay line and is assumed to increase in depth to 40 km beneath the Coast Mountains.

The seismic results from the Bird Lake and Ripley Bay lines and the character of the changes in crustal thickness at the edge of the continent in western British Columbia agree with the estimates of Couch (1969).

### Attenuation

Attenuation measurements of the  $P_n$  arrivals on the Ripley Bay line were not possible because of the short distance over which clear amplitudes were observed. The calibration curves in Figure 5 allowed peak-to-peak amplitudes of the first full cycle of the  $P_n$  phase, measured on the Bird Lake seismograms, to be converted to vertical displacement in millimicrons. Linear factors adjusted the amplitudes to the size of the largest explosion (3630 kg). Table 4 lists adjusted ground amplitudes for Stations 7 through 11 together with the estimated frequencies of the waves, and Figure 14 shows the plotted values.

Table 4. Measured frequencies and amplitudes of  $P_n$  phases from Bird Lake.

Station	Shot size, lbs Nitron SM	Frequency, Hz	Amplitudes millimicrons
7	2000	7.4	25.9
8	6000	4.5	4.19
9	7000	5.9	2.28
10	7000	5.0	5.11
11	8000	6.7	.38

An estimate of the  $Q$  value, a measure of energy dissipated per cycle, of the mantle results by fitting the equation

$$A = A_0 \Delta^{-\frac{1}{2}} (\Delta - D)^{-2/3} e^{-k\Delta} \quad (\text{where } D \text{ is the point of first emergence}$$

of the critically refracted  $P_n$  wave) to the data. The factor

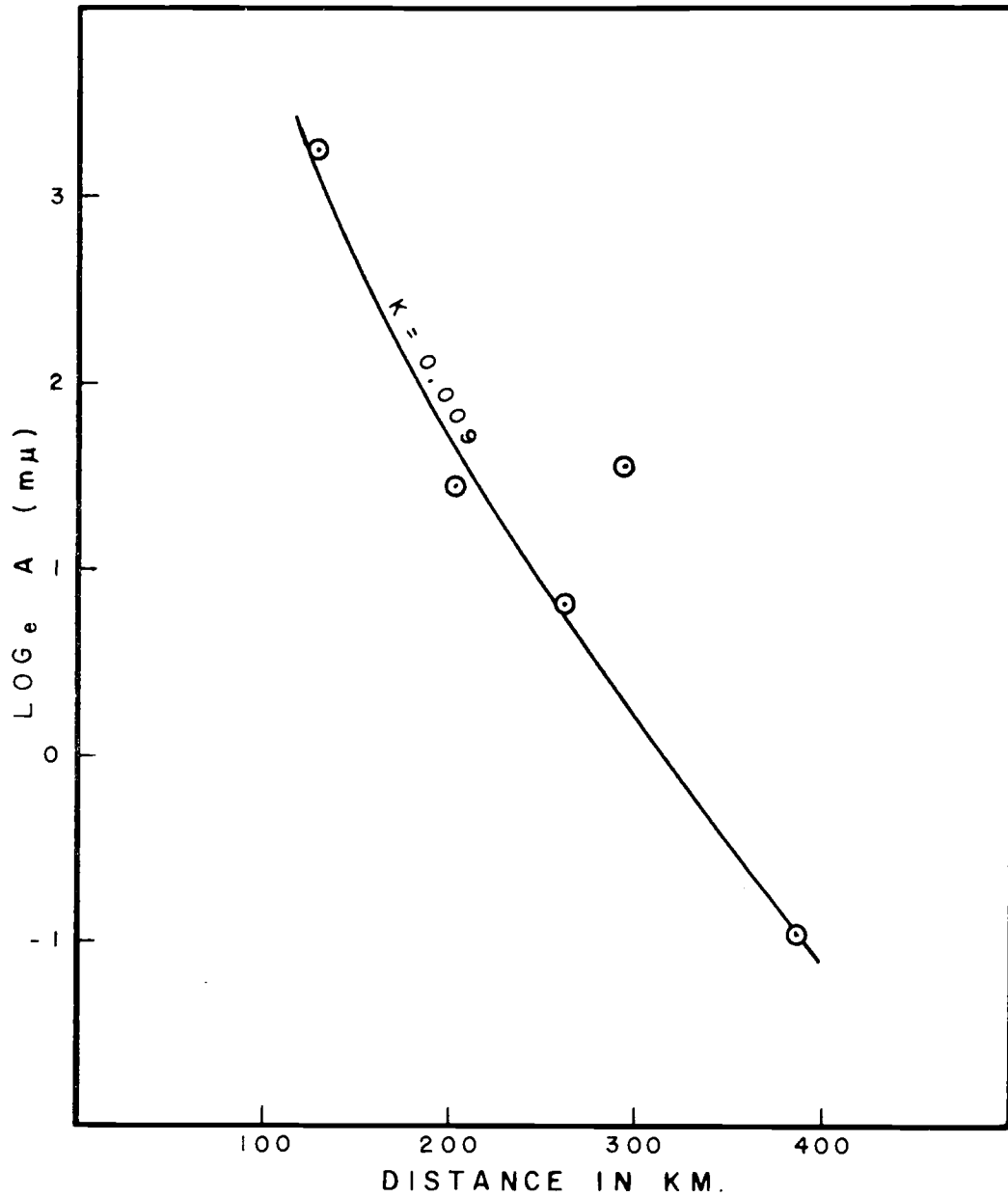


Figure 14. Observed peak-to-peak amplitude of ground motion, in millimicrons, due to  $P_n$  phases from Bird Lake.

$\Delta^{-\frac{1}{2}} (\Delta-D)^{-2/3}$  represents a geometrical spreading factor for head waves as derived by Heelan (1953). The term  $e^{-k\Delta}$  expresses scattering and absorption in the mantle. Attributing the point at 292 km to experimental error, an absorption coefficient of  $k = .009$  gave a good fit of the equation to the remaining data. Using the relation  $Q = \pi f/kV$  (Knopoff, 1956) and the values  $k = .009$ ,  $V(P_n) = 7.86$  km/sec, and  $f = 5.9 \pm 1.1$  Hz, the apparent  $Q$  of the upper mantle is  $260 \pm 50$ . The value obtained here is lower than those obtained from measurements in Nevada, California, Arizona, and New Mexico by Werth, Herbst, and Springer (1962) ( $Q = 300-400$ ), in Nevada, Utah, and Colorado by Ryall and Stuart (1963) ( $Q=520$ ), and in British Columbia and Washington by Johnson and Couch (1969) ( $Q=384$ ) but similar to the value determined in Nevada, Arizona, and New Mexico by Wright, Carpenter, and Saville (1962) ( $Q=240$ ).

## STRUCTURE OF THE UPPER CRUST IN DIXON ENTRANCE FROM GEOPHYSICAL MEASUREMENTS

### Introduction

Important changes in structure and geology between Graham Island and southeastern Alaska lie underwater in Dixon Entrance. Shor (1962), Milne (1964), Stacey and Stephens (1969), Couch (1969), Dehlinger et al. (1971), and Haines, Hannaford, and Riddihough (1971), among others, obtained geophysical data in Dixon Entrance as parts of gravity, magnetic, or seismic studies. There are differences between the results of Shor (1962) and the Bird Lake line of this study in the upper crustal layers near Dixon Entrance. In October, 1970, the R/V Yaquina made a traverse (YALOC -70, Figure 15) in Dixon Entrance in an effort to gather additional geophysical data to reconcile these differences. The continuous seismic reflection, bathymetric, magnetic, and gravity measurements made, in combination with the geophysical measurements of others, permitted the construction of structural models of Dixon Entrance.

This study is a compilation of geophysical measurements made in Dixon Entrance from the base of the continental slope on the west to the mainland coast on the east. The bathymetry shown in Figure 15 suggests a shallow depression north of Graham Island which is nearly closed off from the ocean by Learmonth Bank. A second

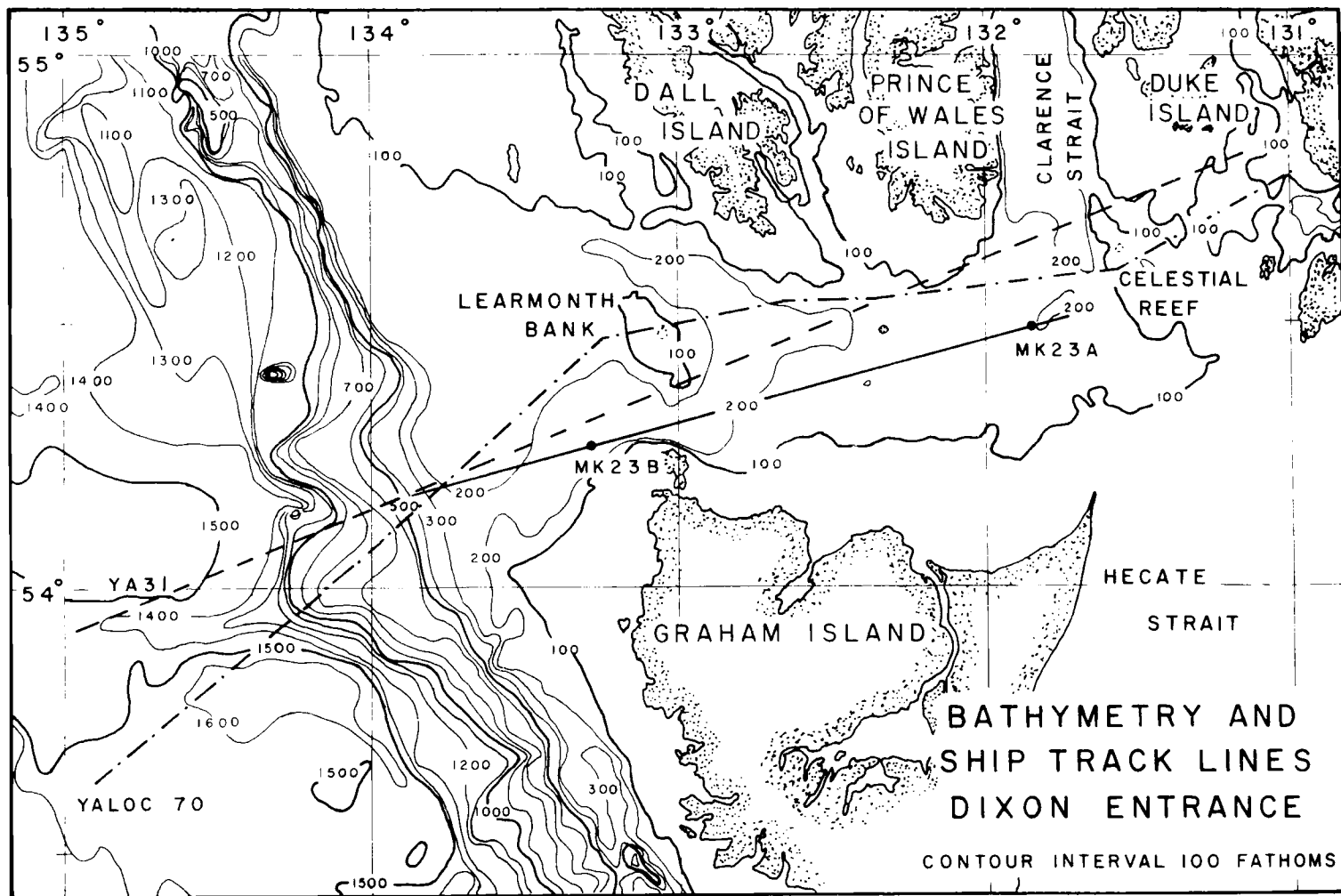


Figure 15. Dixon Entrance bathymetry (from Hydrographic Office map BC 1411N, 1952), track lines YA31 and YALOC 70 from cruises of the R/V Yaquina, and seismic refraction lines MK23A and MK23B (Shor, 1962).

depression in Clarence Strait ends just west of Celestial Reef. Two bathymetric highs which protrude seaward from the base of the continental slope west of Dixon Entrance interrupt the linearity of the slope contours.

### Gravity Measurements

The following equation describes the free-air anomaly:

$$F. A. = g_o + fc - g_t$$

where F. A. is the free-air anomaly,  $g_o$  is the observed gravity,  $fc$  is the free-air correction (zero at sea level), and  $g_t$  is the theoretical gravity computed from the 1930 International Gravity Formula (e. g. Heiskanen and Vening Meinesz, 1958). Free-air gravity anomalies result from horizontal and vertical variations of mass, topographical effects, or a combination of the two.

The Lacoste and Romberg gimbal-suspended surface skip gravity meter S-9 measured 60 values of gravity in Dixon Entrance on cruise YALOC 70. Computer programs written by Gemperle and Keeling (1970) were used to make instrument and Eötvös corrections, to calculate the free-air anomaly, and to merge the gravity data with the bathymetric and navigational data. These values, when added to the 290 pre-existing free-air anomaly measurements gave a station density of one station per  $34 \text{ km}^2$ . The previous measurements

available in the area include sea gravity meter values of Couch (1969) and Dehlinger et al. (1966), pendulum stations of Worzel (1965), and the land and underwater gravimeter measurements by personnel of the Dominion Observatory of Canada (Stacey, 1967).

The free-air anomaly map of Dixon Entrance by Couch (1969), was adjusted where necessary to agree with data from YALOC-70 (Figure 16). Dominant anomaly trends run northwest-southeast along the eastern and western edges of Dixon Entrance. The steep gradient over the continental slope is due to changes in thickness and composition of the crust arising from the oceanic-continental transition, the effect of the shoaling sea bottom, and the effect of a sediment wedge at the base of the slope (Couch, 1969).

The linear northwest-southeast anomaly passing through G in Figure 16 is due to topographical effects and a thick sediments basin which extends southeast from Clarence Strait in southeastern Alaska. Topographic effects and large contrasts in densities of near-surface rocks probably cause the +80 mgl free-air anomalies at Learmonth Bank and Celestial Reef. Basalt flows near the surface may cause the anomaly over northwestern Graham Island. Discussion of other features of Figure 16 follows the presentation of additional data.



### Seismic Measurements

Seismic information, compiled in Dixon Entrance, provides initial constraints for construction of two-dimensional gravity models. Seismic reflection records from YALOC-70 provide information on near-surface structures while a wavefront solution to refraction arrivals on the lines MK 23A and MK 23B of Shor (1962) provide information on the basement configuration.

A Bolt PAR 20 in<sup>3</sup> air gun source towed at an average speed of 8 knots was used to generate a continuous seismic reflection profile. Reflections appear on the record to a maximum two-way penetration time of one second in deep water but less where reverberation and reflection multiples interfere with the recorded signal. However, overall record quality is good and sedimentary structures are observable to depths of 1 km. Figure 17 shows tracings from the records made of the major acoustical reflectors along the trackline. The velocity of 2.4 km/sec determined by Shor (1969) from seismic refraction measurements permits calculation of sediment thickness. The straight-line segments beneath the sections indicate the possible upper surface of the basement as suggested by the gravity model of Figure 21.

Folded sediments show clearly on the lower portion of the continental shelf. Sediments dip seaward in the upper portion of

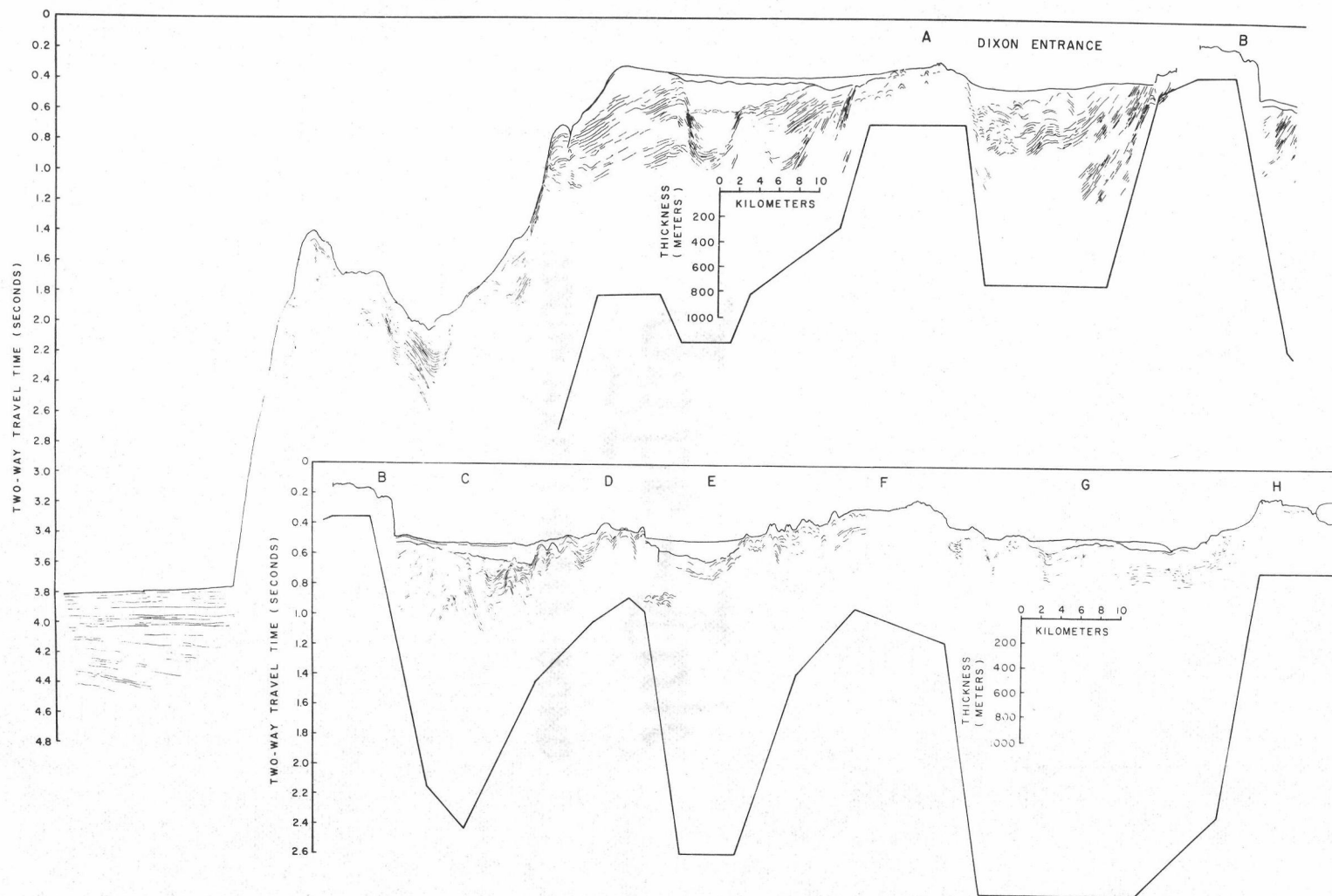


Figure 17. Line drawings of seismic profile records made in Dixon Entrance from the Alaskan Abyssal Plain to Celestial Reef. Thickness is computed from a sediment velocity of 2.4 km/sec. Features A through H are discussed in the text. The lines beneath the section show the upper surface of the basement according to the gravity model of Figure 21.

the shelf. A normal fault appears just east of the shelf break and there is a suggestion of a relic sea channel in the downthrown block. Basement highs appear at A, B, D, F, and H. While these highs may be comprised of highly compacted sediments in their upper layers they are more likely metamorphic or igneous rocks. The termination of dipping layers east of Learmonth Bank (B) suggests the presence of a normal fault. It is probable that the mountains on Prince of Wales Island extend underwater to form the basement high at F. High angle faults or steeply dipping structures mark both sides of the sediment basin at G, associated with the extension of the Clarence Strait trough. The layers west of G, in the trough, show evidence of folding while east of G, the layers show the effects of slumping but not folding. The change suggests a difference in their sedimentary histories.

Dr. George Shor kindly provided seismic refraction seismograms from his lines MK 23A and MK 23B (Figure 15) in Dixon Entrance for re-study. The seismograms were re-read and first arrivals reduced to the sea bottom. Large offsets in the travel-time curve, caused by structures shown in Figure 17, make interpretation by normal methods difficult. Two wave-front diagrams were constructed for the reversed profile using the method of Thornburgh (1930).

Seismic velocities used in the model have a large effect on the

final solution; they are determined from velocities measured by Shor (1962) east of MK 23A from velocities observed along the Bird Lake refraction line of this study, and from the travel-time curves where possible. Sediment velocities measured and used for computation at the eastern end of the line are 2.0 and 3.2 km/sec for the first and second sedimentary layers respectively. At the western end, the velocity determined from first arrivals is 2.4 km/sec. Milne (1964) found that sediment velocities west of MK 23B range from 1.99 to 2.88 km/sec. A velocity of 2.4 km/sec was used for the sediments everywhere except in the basin at the eastern end. A layer west of MK 23B gives an apparent velocity of 5.0 km/sec. Milne (1964) also observed a layer with a velocity of 4.9 km/sec. This layer which appears only at the western end of the profile, has a velocity of 5.0 km/sec in the model. Offsets in the travel-time curve appear at distances where waves from the basement layer arrive making determination of the velocity of the basement layer difficult. Shor (1962) determined the basement velocity as 5.8 km/sec, Milne (1964) determined the velocity as 6.2 km/sec, and from the Bird Lake line the velocity was 5.9 km/sec. Shor (1962) determined an average basement velocity of 5.9 km/sec on several shore lines east of Mk 23A. The basement velocity assumed for the model is 5.9 km/sec. At distances greater than 30 km, the measured apparent velocities on the two lines were 6.96 and 6.65 km/sec. The velocity assumed

for the model is 6.8 km/sec as determined for this layer by Shor (1962).

Initial interpretation of the structure, in terms of plane dipping layers, gave a first approximation to the structure. The wave-front solution was obtained by iterative adjustment of the plane interfaces until the travel times, computed from the wave fronts traveling in both directions, agreed closely with observed values. Figure 18 shows the two wave-front diagrams constructed in this fashion and the observed and computed travel times. Wave fronts are drawn at a time interval of 0.5 second although shorter intervals were used in the presence of thin layers or steep dip. The wave-front method does not give a unique solution in cases of more than two layers without the use of special techniques or where velocities are difficult to determine. The model of Figure 18 assumes that the interface between the 5.9 and 6.8 km/sec layer has slowly varying relief and, on the basis of the reflection profile of Figure 17, that large topographic changes occur in the interface between the 5.9 km/sec layer and the sediments.

The model generated by the wave-front solution indicates two basins containing 1.6 and 2.5 km of sediments respectively. The basins may be bounded on their western margins by high angle faults. The basement rises to the surface immediately west of each basin and to within 1 km of the surface in between. The high velocity 6.8

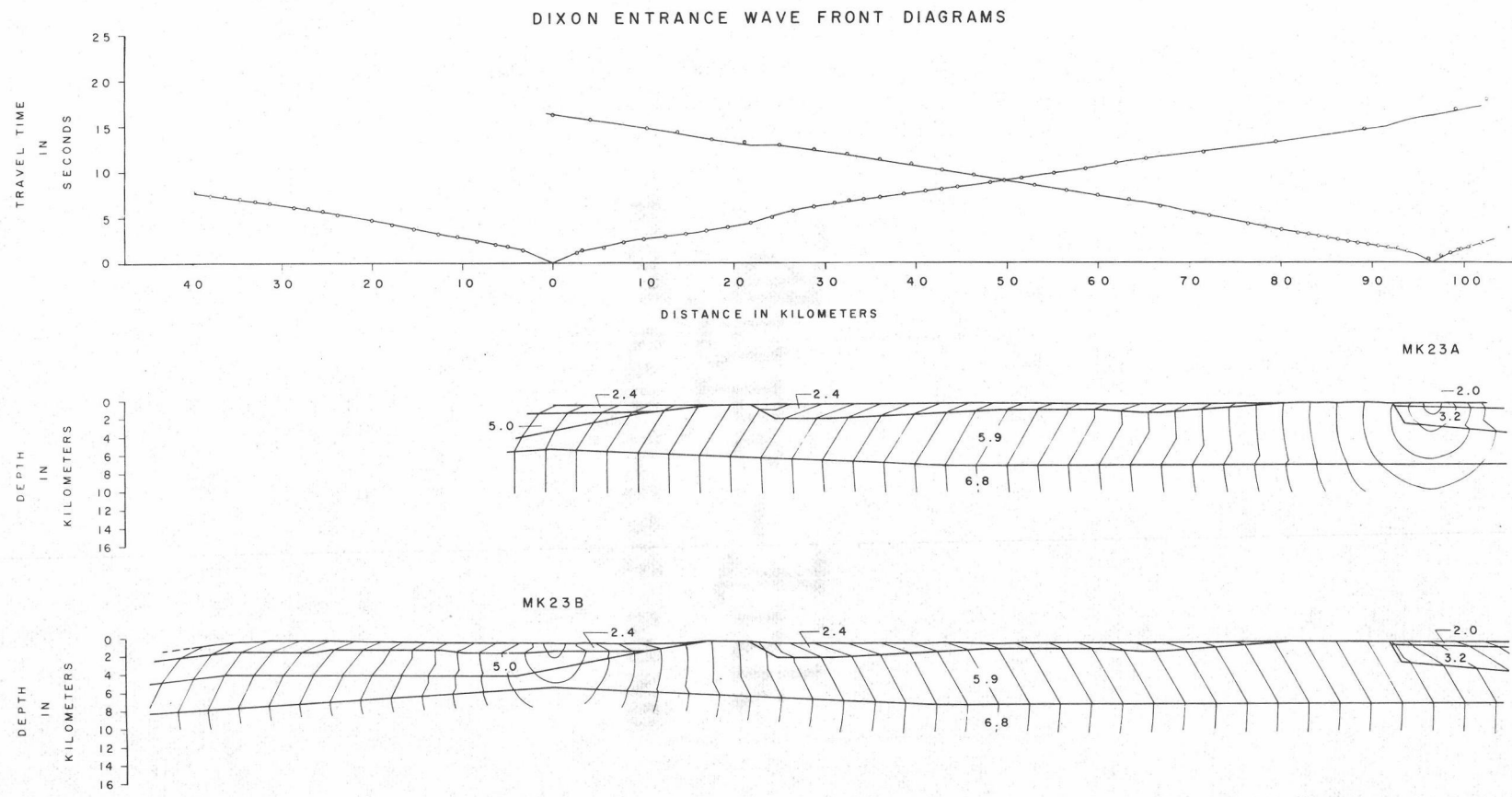


Figure 18. Wave-front solution to reversed seismic refraction profile MK23. Top: expected travel-time curves as calculated from the seismic model superimposed on the observed data; Middle: wave-front solution for waves traveling west; Bottom: wave-front solution for waves traveling east.

km/sec layer lies at 7 km for much of the profile but rises to 5 km beneath the west end of the line before dipping seaward. A wedge of material with a velocity of 5.0 km/sec, present on the western margin, may be due to volcanics or sedimentary rock (Milne, 1964).

### Gravity Crustal Cross Section

Theoretical gravity values, computed from two crustal models, fit gravity profile YA 31 (Figure 13) in Dixon Entrance. The first crustal cross section is an enlargement of the Dixon Entrance crustal and subcrustal cross section presented earlier in Figure 13. Structures deeper than 20 km are identical to Figure 13 in both models.

The wave-front solution of Figure 18, replotted in Figure 19, defines the upper structure in the center of the cross section for Model 1. In the iterative process of fitting the observed gravity, the layer boundaries remained fixed. Densities, on the other hand, were varied as needed from the initial values obtained from the Ludwig, Nafe, and Drake (1971) curve. Figure 20 shows the extent of these variations which are well within the scatter of the original data used to define the curve.

The lines along which gravity and refraction measurements were made coincide at the edge of the continental shelf but diverge to the east at an angle of  $7^\circ$  (Figure 15). This explains, in part, differences between the computed and observed gravity.

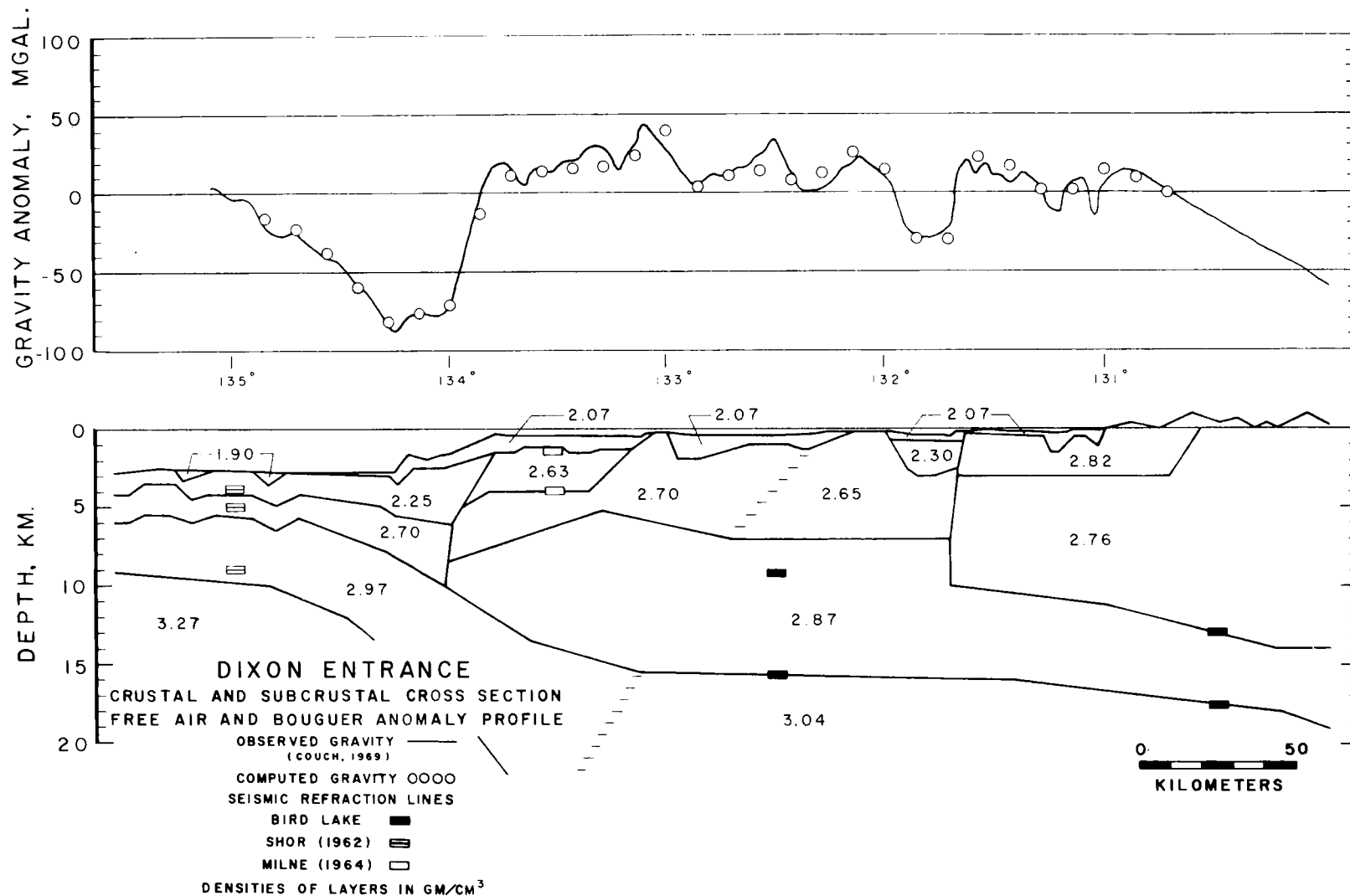


Figure 19. Crustal cross section of Dixon Entrance from seismic and gravity data. Model 1: upper layers determined from the wave front solution of Figure 18.

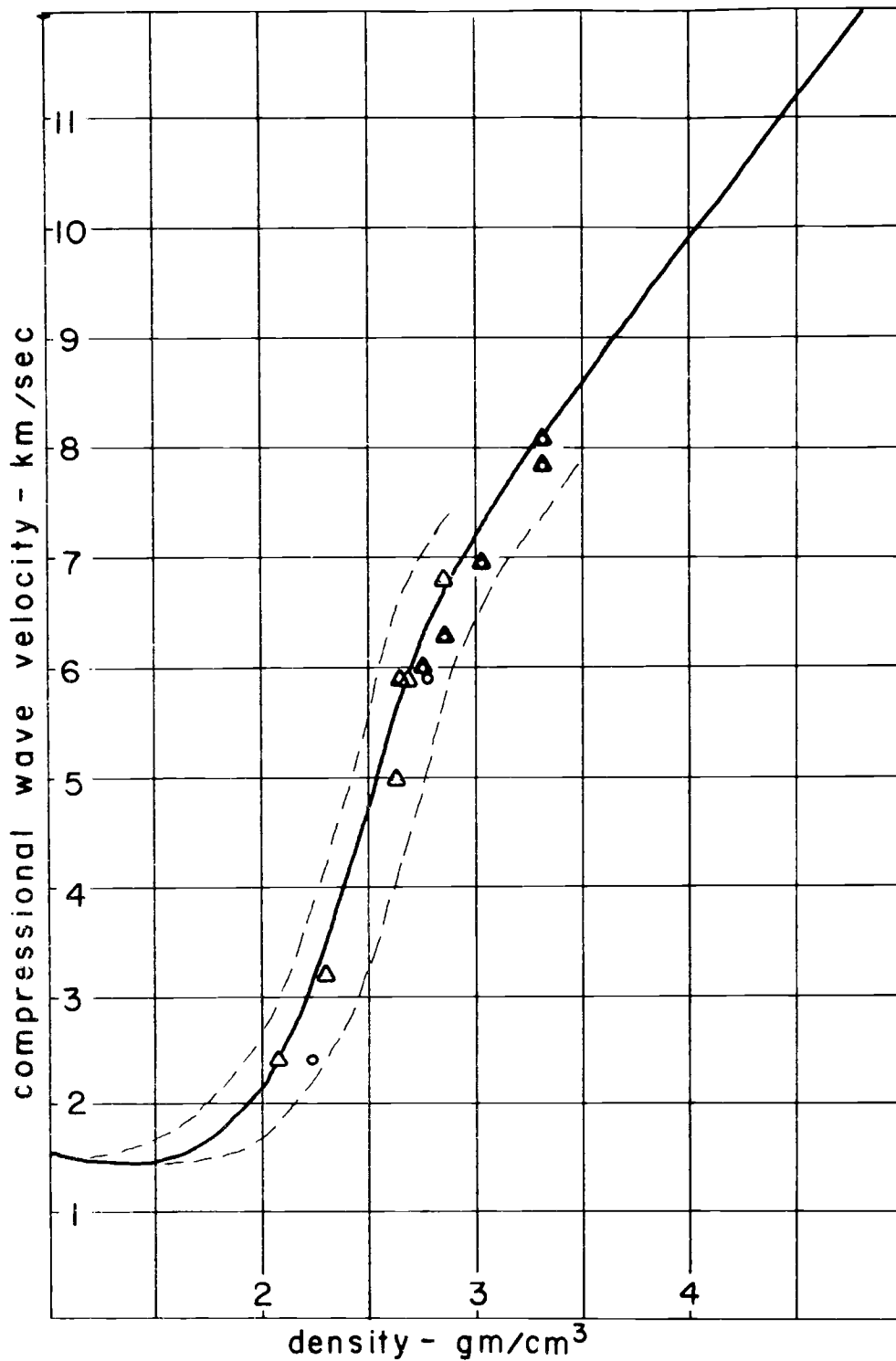


Figure 20. Relation between density and compressional wave velocity used to construct gravity models (from Ludwig, Nafe, and Drake, 1971). Circles indicate densities used in Model 1; triangles indicate densities used in Model 2; dashed lines indicate scatter in the data used to determine the solid line.

The +43 mgl anomaly at 133° W occurs over Learmonth Bank. Near zero gravity values indicate the sedimentary basin to the east of Learmonth Bank. The computed gravity does not agree with a +35 mgl anomaly at 13° 30' W. At this point, the gravity profile is 12 km north of the refraction line and the structure causing the anomaly either diminishes or basalts from Graham Island obscure the structure. The gravity contours at D in Figure 16 support this interpretation.

The -30 mgl anomaly at 131 45' W is probably due to the extension of the Clarence Strait trough which, according to this model, contains sediments 2.6 km thick. The trough may continue south to Hecate Strait where Shouldice (1970), on the basis of drill records, indicates sediment thickness greater than 4.6 km.

Beneath Dixon Entrance, the layer of  $2.87 \text{ gm/cm}^3$  density corresponds to the layer of velocity 6.8 km/sec in Figure 16. This layer extends downward, with no change in density, through the layer of velocity 6.4 km/sec to the layer of velocity 6.96 km/sec of Figure 9. This procedure follows the suggestion made earlier that the layer of velocity 6.8 km/sec is due to the intrusion of the upper crust by high velocity (high density) material from the lower crust or upper mantle near Graham Island.

The upper layer beneath the Coast Mountains has a density of  $2.76 \text{ gm/cm}^3$ . This density, increased from the average value of

2.74 gm/cm<sup>3</sup> found by Hutchison and Roddick (1967) from several thousand measurements of density of plutonic rocks from the western Coast Mountains, is necessary to fit the observed anomaly. A block with high density (2.82 gm/cm<sup>3</sup>) is necessary in order to fit the observed anomaly east of the Clarence Strait trough. This high density may be related to the presence of diorite (2.82 gm/cm<sup>3</sup>, Hutchison and Roddick, 1967) along the mainland coast. An alternative source of the increase in density may be ultrabasic intrusives seen by Taylor and Noble (1960) in southeastern Alaska as far south as Duke Island and thought by Stacey and Stephens (1969) to continue even farther south, possibly to Vancouver Island. On the basis of large gravity anomalies (Couch, 1969; Stacey and Stephens, 1969) and a magnetic anomaly discussed below, this zone of ultramafic intrusions may continue south of Duke Island along the eastern portion of Hecate Strait as far south as Bonilla Island (53° 30' N, 131° 30' W) where pillow lavas are exposed at the surface.

Figure 21 shows Model 2 as an alternative model for the upper crust. Adjustment of the shape of the boundary between sediments and basement rock took place iteratively until the computed gravity agreed with the observed gravity. Two layers comprise the upper crust in this model having velocities of 5.9 and 6.4 km/sec as in Figure 11, determined from the Bird Lake refraction line. It was necessary to increase the density of layers in the cross section in

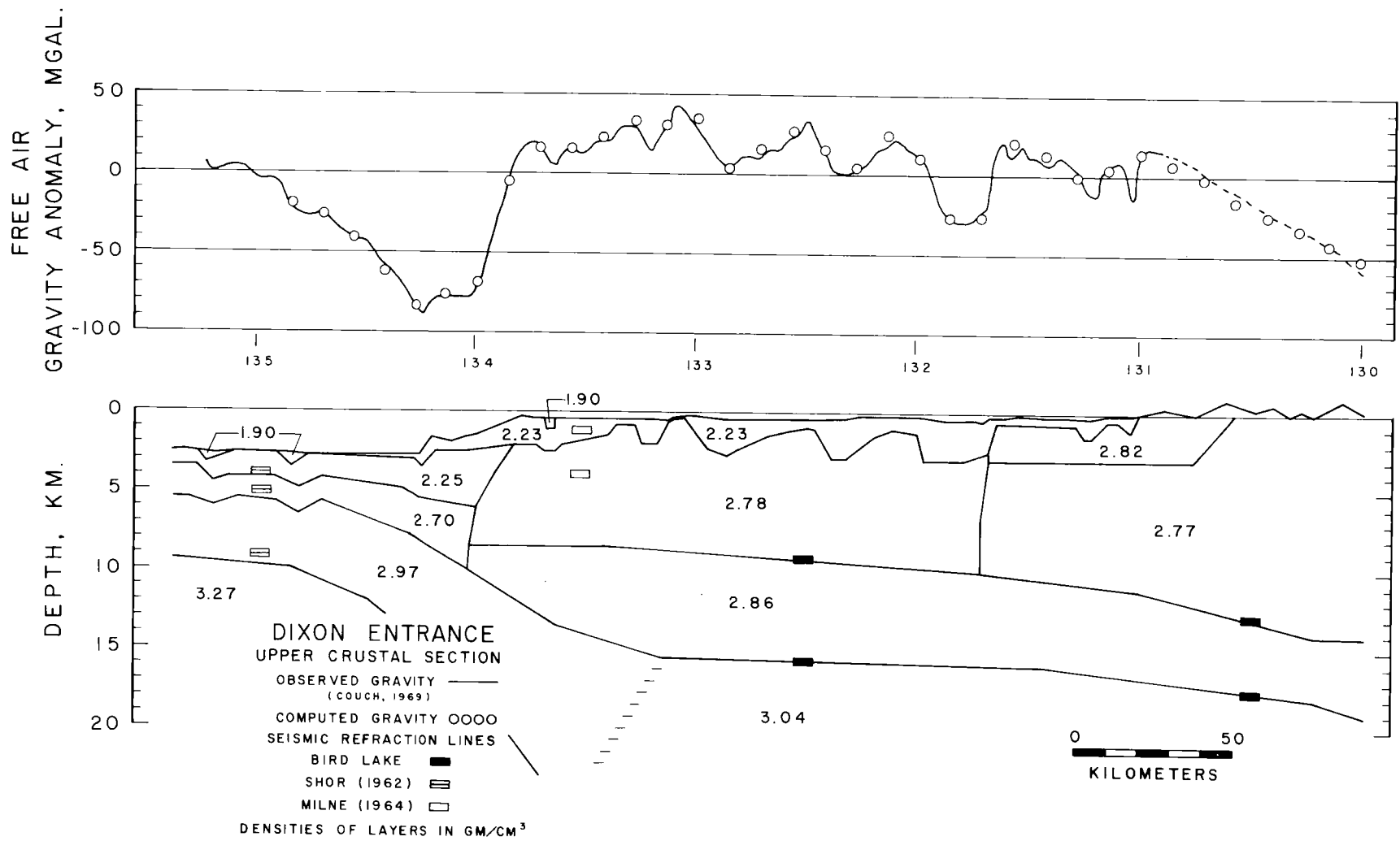


Figure 21. Crustal cross section of Dixon Entrance from seismic and gravity data. Model 2: upper layers determined from iterative fit to observed data.

order to obtain a fit to the observed gravity data. The increase occurred in the sediment layer density (from 2.07 to 2.23 gm/cm<sup>3</sup>) and in the upper basement layer (from 2.65 and 2.70 to 2.78 gm/cm<sup>3</sup>). Figure 20 shows these values in relation to the curve of Ludwig, Nafe, and Drake (1971). This model shows sediment thicknesses of 2.4 and 2.6 km at 133° and 131° 45' respectively (C and G, Figures 16 and 17) and shallow basement at B and F (Figures 16 and 17), very similar to Model 1. In addition, the model brings out a prominent rise in the basement at 132° 30' (D, Figures 16 and 17) which the wave-front solution of Figure 18 only faintly suggests. A broad rise in the basement structure at 133° 35' on the wave-front solution (Figure 18) is narrower and flanked on the east by a basement depression in gravity Model 2 (Figure 21).

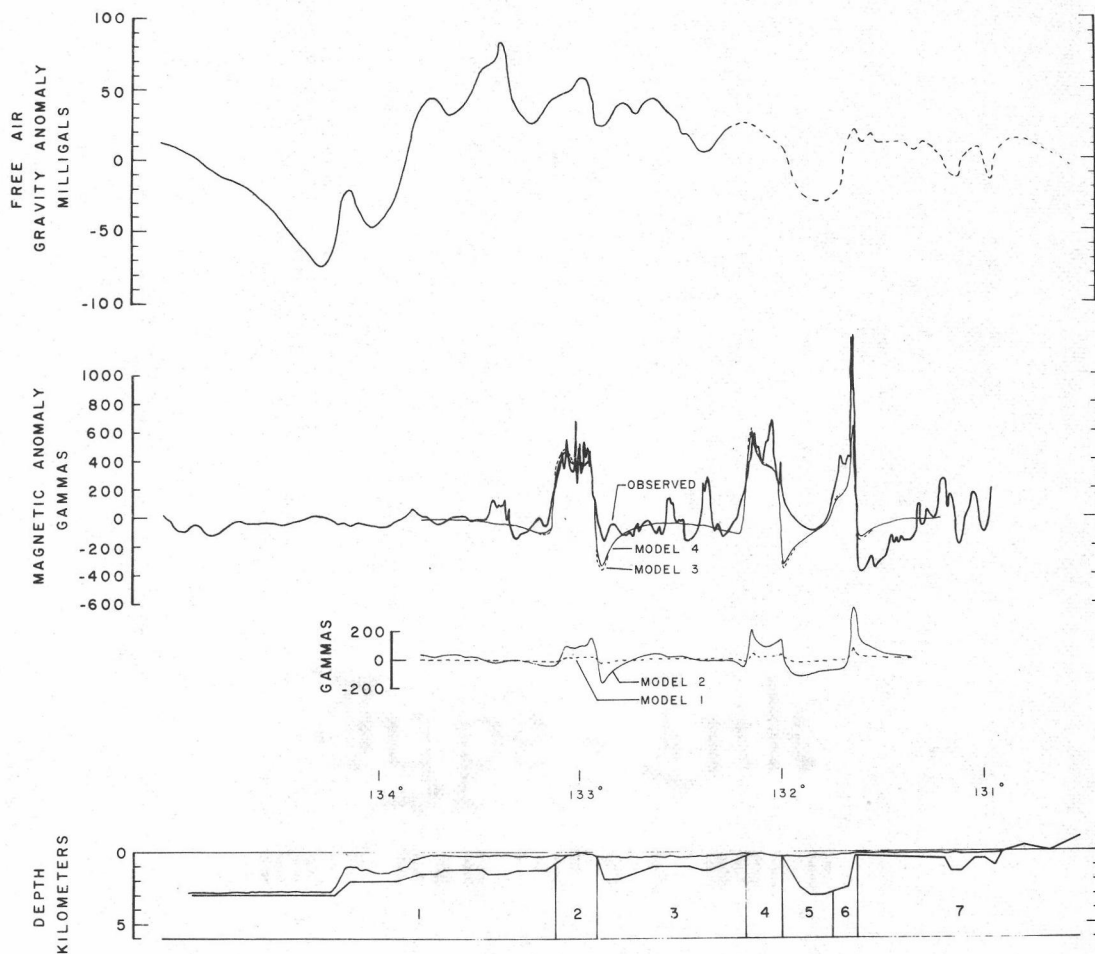
#### Magnetic Measurements and Crustal Cross Section

A Geometrics marine proton precession magnetometer measured the magnetic field along the trackline YALOC-70 in Figure 15. Programs written by Gemperle and Keeling (1970) removed the International Geomagnetic Reference Field (Cain and Cain, 1968; Cain et al., 1968) from the data (digitized at five minute intervals together with maximums and minimums) on a CDC 3300 computer. Figure 22 shows the plotted magnetic anomaly. Magnetic anomalies

exceeding 700 gammas are present between  $133^{\circ} 30' W$  and  $132^{\circ} 40' W$ . Figure 22 also shows the two-dimensional models constructed to estimate the magnetic susceptibility and remanent magnetization necessary to produce these anomalies.

Talwani and Heirtzler (1964) developed a computer program which computes the magnetic effects of two-dimensional magnetized blocks of arbitrary shape given a susceptibility and/or magnetization. The program computes the effect of a two-dimensional flat block which extends to infinity in one horizontal direction. Appropriate combination of these blocks allows the computation of the magnetic effect of any two-dimensional crustal structure which can be approximated by a polygon. Lu (1971) adapted the computer program of Talwani and Heirtzler (1964) to FORTRAN IV for use on a CDC 3300 computer. Theoretical magnetic profiles for four models in Dixon Entrance were computed using this program. Seven blocks make up the model in Figure 22. The upper surface of the blocks is from the wave front solution of Figure 18, the lower surface (arbitrarily assumed to be horizontal) is at a depth of 6 km, and the observed anomalies determine the placement of the vertical boundaries. The sedimentary layers have zero susceptibility and magnetization.

Models 1, 2, and 3 (Figure 22) assume no remanent magnetization. The susceptibility of all blocks in Model 1 is .0004 emu (electromagnetic units), a value commonly observed for granitic rocks.



**DIXON ENTRANCE**  
 YALOC 70 GRAVITY AND MAGNETIC PROFILES  
 AND COMPUTED MAGNETIC PROFILES



<b>MODEL 1</b> ALL BLOCKS $k = 0.0004$ emu $J = 0.0$ emu	<b>MODEL 2</b> ALL BLOCKS $k = 0.002$ emu $J = 0.0$ emu
<b>MODEL 3</b> BLOCKS 1,3,5,7 $k = 0.0004$ emu $J = 0.0$ emu BLOCKS 2,4,6 $k = 0.003$ emu $J = 0.0$ emu	<b>MODEL 4</b> BLOCKS 1,3,5,7 $k = 0.0004$ emu $J = 0.0$ emu BLOCKS 2,4,6 $k = 0.002$ emu $J = 0.0062$ emu

Figure 22. Crustal models developed to fit magnetic anomalies in Dixon Entrance. The gravity profile, taken at the same time as the magnetic profile, is shown for comparison.

For all blocks in Model 2, the susceptibility is .002 emu, a value commonly observed for basaltic rocks. The computed anomaly in Models 1 and 2 is an expression of the relief of the upper surface of the model and in each case is too small to account for the observed anomaly. In Model 3, the blocks are alternately granitic and basaltic material with the basaltic blocks causing the anomalies. Susceptibilities of .0004 emu and .003 emu for the granitic and basaltic blocks respectively give a good fit to the observed data. The susceptibilities in Model 4 are .0004 emu for the granitic blocks and .002 emu for the basaltic blocks; in addition, the basaltic blocks have a remanent magnetization equal to a susceptibility of .001 emu in an axial dipole field of 53,600 gammas. The results of Model 4 are nearly identical to those of Model 3.

The results from the magnetic models suggest that the 700-gamma anomalies observed in Dixon Entrance are due mainly to large contrasts in magnetic susceptibilities of the basement rocks. Computed anomalies, obtained using average susceptibilities for granitic and basaltic rocks, agree with the observed anomalies. If remanent magnetization is present it is not large. Intrusion of high susceptibility rock into low susceptibility rock may be the cause of the anomalies. Alternatively, large susceptibilities associated with highly metamorphosed rocks such as those present on Dall Island and Prince of Wales Island may cause the anomalies.

Haines, Hannaford, and Riddihough (1971), from a high altitude (5 km) aeromagnetic survey of western British Columbia, found a broad positive magnetic anomaly ( $> 200$  gammas) located over Prince of Wales Island which extends southward and coincides with the anomaly at  $132^\circ$  (Figure 22). A second positive anomaly ( $> 400$  gammas) is present on northwestern Graham Island. The two positive anomalies are not connected. The anomalies are two of a series of anomalies which lie between the north-trending, short wavelength, linear anomalies observed in the northeastern Pacific and typical of oceanic areas and long, narrow, northwesterly trending anomalies observed over the Cordilleran zone and the Coast Crystalline belt. The anomalies over the continental margin may be related to structural changes in the transition from oceanic crust to continental crust.

#### Summary

This study of Dixon Entrance, using seismic, gravity, and magnetic methods, maps important structural differences between Graham Island and southeastern Alaska.

The large positive gravity anomaly on northwestern Graham Island coincides with large thicknesses of basalt. The large observed magnetic anomaly and the high velocity layer measured at a depth of 7 km on seismic refraction lines MK23A and MK23B (Shor, 1962) just north of Graham Island suggest that the source of the basalt is

probably deep within the crust. Basalts known to continue under sediments on northeastern Graham Island probably account for the gravity anomaly observed there. The free-air anomaly indicates that the basalt flows extend north of Graham Island 20 to 30 km. A gravity low, indicated by a dashed line through E in Figure 16, extends south from east of Dall Island and terminates north of Graham Island. The shallow acoustical reflector and the positive gravity and magnetic anomalies passing through F in Figure 16 coincide with the Prince of Wales High, a structural lineation mapped by Brew, Loney, and Muffler (1966). High altitude magnetic measurements relate the magnetic anomaly at F to deep structure. Magnetic models, based on surface magnetic measurements, indicate this magnetic body may extend to the surface in the form of basaltic dikes or highly metamorphosed zones.

Seismic reflection measurements indicate that Learmonth Bank is bounded on the east by a fault dipping steeply east. Stacey and Stephens (1969) attribute the 1949 earthquake at  $54.2^{\circ}$  N,  $133.0^{\circ}$  W to movement on the northward extension of the Sandspit fault. The fault-plane solution for this earthquake (Hodgeson and Milne, 1951; Wickens and Milne, 1967) indicates right lateral motion on a fault which strikes  $29^{\circ}$  W and dips  $77^{\circ}$  NE. This information and the linear trend of the gravity contours between Learmonth Bank and Graham Island suggests that the Sandspit fault extends from Graham Island

at least as far north as Learmonth Bank.

Bathymetric contours indicate a broad shelf west of Dall Island, a marked change from the narrow shelf west of Graham Island. Gravity contours suggest that a complex structure is present on the shelf north of the YALOC-70 trackline ( Figure 16).

Negative gravity anomalies in Clarence Strait extend into eastern Hecate Strait. Sediment thicknesses up to 3 km, suggested by model studies, and large magnetic anomalies flanking the gravity low indicate that the Clarence Strait lineament is a major structural feature which separates the Coast Crystalline belt from the Insular Tectonic belt and the Alexander Archipelago.

Structural and geological differences present on opposite sides of Dixon Entrance are attributable to the large quantities of basalt present on Graham Island. Thick layers of basalt probably obscure any structure which extends from the Alexander Archipelago south beneath Graham Island.

## MICROEARTHQUAKE SURVEY OF WESTERN BRITISH COLUMBIA AND SOUTHEASTERN ALASKA

### Introduction

The OSU field party carried out a microearthquake survey along portions of the Inside Passage of British Columbia and southeastern Alaska concurrently with the seismic refraction study described above. Eight stations observed microearthquake activity, most of which occurred at large distances from the stations (S-P times greater than 12 seconds) although five stations recorded nearby microearthquakes.

The possible relationship between faults and microearthquakes requires a more detailed discussion of faults than that given in the description of the geology above. Figure 23 shows major mapped and inferred faults of the region. Observed faults in the region, predominantly normal and probably strike-slip, lie mostly in southeastern Alaska and the Queen Charlotte Islands. Twenhofel and Sainsbury (1958) recognized three lineaments or large zones of many parallel or nearly parallel linear features and faults in southeastern Alaska. These authors named them the Chatham Strait, Clarence Strait, and Coast Range lineaments. They inferred the presence of the Chatham Strait and Clarence Strait lineaments from the straight course of the straits, mapped faults at their landward

extensions, and rocks of different ages on opposite sides of the straits. St. Amand (1957) and Brew, Loney, and Muffler (1966) postulate right-lateral strike-slip movement along Chatham Strait and Twenhofel and Sainsbury (1958) propose vertical movement along Clarence Strait. Twenhofel and Sainsbury (1958) defined the Coast Range lineament as a series of mapped and inferred faults along the southwest border of the Coast Mountains extending from the southeast corner of southwestern Alaska to Lynn Canal where they join or cross the Chatham Strait lineament.

The large-scale faults mapped on the Queen Charlotte Islands (Figure 23) trend northwest-southeast. Earthquakes which occur on the Islands (Figure 2) suggest that at least some of these faults are active. Geologic maps show few if any faults near the vicinity of the mainland coast of British Columbia (e.g. White, 1966; Geological Map of Canada, 1969) possibly because water conceals them. Peacock (1935) suggests that the pattern of linear fiords and narrow longitudinal passages in coastal British Columbia and southeastern Alaska is similar to the pattern of folds, joints, and faults in the bedrock. He also suggests that erosion along such features formed the waterways.

Many investigators (e.g. Gutenberg and Richter, 1954; St. Amand, 1958; Benioff, 1962; Tobin and Sykes, 1968) inferred, on the basis of earthquake epicenters, that the Queen Charlotte Islands

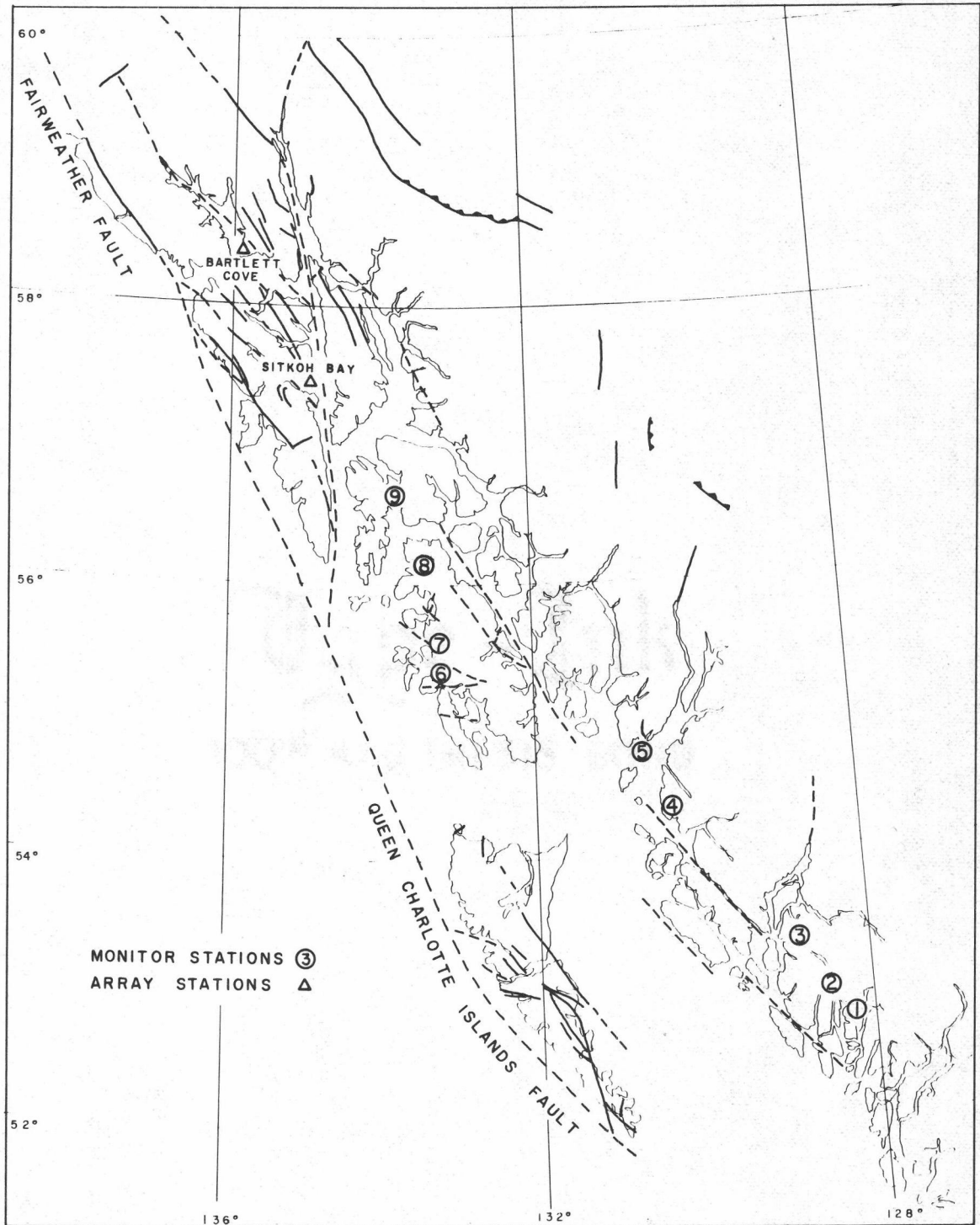


Figure 23. Location of microearthquake recording stations, mapped faults (solid lines), and inferred faults (dashed lines) (after White, 1966; Geological Map of Canada, 1969).

fault lies at the base of the continental slope. Tobin and Sykes (1968) believed that the Queen Charlotte Islands fault continues parallel to the coast as far north as  $60^{\circ}\text{N}$  where it joins the Fairweather fault. St. Amand (1958) suggested that it bifurcates north of the Queen Charlotte Islands and that one branch connects with the Fairweather fault near Cross Sound and the other branch follows Chatham Strait northward until it joins the Denali fault at the northern end of Lynn Canal.

Compared to the large number of earthquake epicenters associated with the Queen Charlotte Islands fault, the number of epicenters located in Inside Passage waters is very small (see Figure 2). The discovery by Milne, Smith, and Rogers (1970) of small earthquakes occurring in eastern southeastern Alaska, a region previously considered to be aseismic, suggests that minor seismic activity also may be present in other portions of the Inside Passage.

#### Field Methods

The unattended OSU instrument package described above recorded microearthquakes in the field program. The goal was to sample microearthquake activity with the unattended instrument wherever a seismic refraction station was attempted. Attempts made to record microearthquakes at the refraction stations were secondary to the purpose of the seismic refraction survey. The

criterion for choosing station locations was to obtain good station spacing on the refraction lines, however, and not to obtain proximity to possible seismic areas.

At each station the seismic system operated for 12 hours except when prevented by instrument failure or schedule limitations. Comparison of chronometer time to WWV radio time broadcasts at the beginning and end of each record gave arrival times accurate to 0.1 second. The attended OSU instrument package recorded micro-earthquakes on magnetic tape at Station 1 using only interval time. Stations 1 through 5 lie in the fiord region of the mainland coast of British Columbia, and Stations 6 through 9 lie on Prince of Wales and Kupreanof Islands in southeastern Alaska. Since the recording stations are distant from major mapped faults and areas of known seismic activity, the survey was made in a seismically quiet region. Figure 23 shows the station locations and Table 5 gives the time periods during which the instruments recorded.

Table 5. Microearthquake survey location, recording interval, and instrument attenuation.

Stn	Latitude degrees	Longitude degrees	Recording interval July, 1970, GMT	Record length (hr, min)	Atten. used (db)
1	51°46.60'	128°12.55'	14; (0700-1200)	(05:00)	
2	53°00.66'	128°30.24'	14; 0220-1437	12:17	-18
3	53°21.79'	128°50.80'	14-15; 2200-1208	14:08	-18
4	54°19.44'	130°22.55'	16; 0600-1609	10:09	-18
5	54°48.96'	130°45.95'	17; 0156-1404	12:08	-12
			17-18; 2255-0340	4:45	-12
6	55°21.83'	133°09.70'	24; 0400-1635	12:35	-12
7	55°34.75'	133°13.80'	26; 0155-1416	12:21	-12
8	56°10.01'	133°24.34'	27; 0125-0707	05:42	-24
9	56°35.16'	133°42.30'	27-28; 2305-0657	07:52	-12

### Data Analysis

Arrival times and S-P times of the events on the records, provided the data for this study. By keeping the recorded noise level at the stations approximately the same on all records, the same criteria could be used to pick events. Table 6 lists 22 separate earthquakes observed during a total of 92 hours of recording time. The S-P times fall into three time intervals: less than five seconds, 12-13 seconds, and more than 20 seconds. Only Station 8 (operated at the lowest gain) recorded no microearthquakes. Station 5 recorded most of the nearby microearthquakes.

### Interpretation

The July, 1970, listing of epicenters (U. S. Department of Commerce, Preliminary Determination of Epicenters, Monthly Listing, July 1970) does not contain any earthquakes listed in Table 5. This is understandable because of the small size of the events and the absence of permanent recording stations along the west coast of northern British Columbia. Examination of the increase in S-P times for Stations 1-4 gives an estimate of the epicenters for the more distant events.

An explanation of P-times and S-times is appropriate at this point. A P-time is the time of arrival of compressional waves from

Table 6. Arrival times and S-P times of events observed in the microearthquake survey.

Station	Date	Arrival time GMT	S-P, sec	Dist km	Event
1	7-14-70	*	24.5	229	(2)
			25.0	235	(3)
			27.2	258	(4)
			4.5	44	5
2	7-14-70	05:06:02.4	4.6	45	1
		09:29:13.0	25.3	238	2
		11:35:21.6	26.7	252	3
		13:07:23.5	26.8	254	4
3	7-15-70	07:12:59.7	34.1	232	6
4	7-16-70	09:56:36.7	38.3	367	7
		13:08:34.5	38.0	364	8
		13:47:30.4	2.5	22	9
		15:34:04.6	39.5	390	10
5	7-17-70	05:19:59.7	0.0	0	11
		05:20:03.3	0.0	0	12
		05:28:04.1	3.0	24	13
		08:00:09.1	0.0	0	14
	7-18-70	01:54:25.9	0.0	0	15
		02:23:58.5	35.0	342	16
6	7-24-70	16:15:51.2	12.5	101	17
7	7-26-70	03:27:57.5	12.6	102	18
8	7-27-70	no events			
9	7-28-70	00:13:21.2	2.1	16	19
		00:50:44.8	13.4	110	20
		03:13:48.1	37.1	364	21
		03:44:47.2	12.4	100	22

\* Only interval time was obtained at Station 1; events in parentheses are correlated to events 2, 3, and 4 at Station 2 on the basis of S-P time and their sequence in time.

an earthquake; an S-time is the time of arrival of shear waves from an earthquake. The following expression relates P-velocity to S-velocity:

$$V_p = \sqrt{\frac{2-2\sigma}{1-2\sigma}} V_s$$

where  $\sigma$  is Poisson's ratio. If Poisson's ratio is 0.25, an approximate value suggested by the Ludwig, Nafe, and Drake (1971) curves for crustal velocities, then the relation between P- and S-velocities is simply

$$V_p = \sqrt{3} V_s$$

Large amplitude differences, usually observed between the P-wave and S-wave, simplify the measurement of the S-P time. The crustal layering, determined by means such as seismic refraction, and the S-P time give the epicentral distance (see Appendix 2).

Assuming that the epicenters for events 2, 3, 4, 6, 7, 8, and 10 all lie in the same region, the epicentral distance increases from 230 km for event 2 at Station 1 to 390 km for event 10 at Station 4. The increase in distance suggests that the sources are to the south of the recording stations. The striking of arcs from Stations 1 and 2 for events 2, 3, and 4 resulted in two groups of two-station epicenter locations. One group of epicenters located in this fashion lies in the Coast Mountains midway between Prince George and Prince Rupert. The other group is west of Queen Charlotte Sound at 51°N, 130°W

near the site of a magnitude  $M=6$  earthquake which occurred only three weeks earlier on June 24, 1970 (U. S. Department of Commerce, Preliminary Determination of Epicenters, Monthly Listing, June, 1970), near the southern end of the Queen Charlotte Islands fault. The increasing S-P times observed at the northern stations and the high seismicity west of the British Columbia coastline suggest that the majority of the distant earthquakes observed in this survey are attributable to activity along the Queen Charlotte Islands fault.

Events observed at Stations 5, 7, and 9 with S-P times of 12-13 seconds ( $\sim 100$  km) may originate offshore in the Queen Charlotte Islands fault zone west of the recording stations. An alternate origin is in eastern southeastern Alaska, an area from which Milne, Smith, and Rogers (1970) observed events.

Five of the nine stations observed microearthquakes with S-P times less than 5 seconds; four of these stations are on the mainland coast of British Columbia. Boucher and Fitch (1969) indicated that it is rare for the number of events recorded on a given day to vary more than a factor of 2 from the mean in a reasonably active area which suggests that the above observations are indicative of the seismicity of the area.

If the area in the vicinity of the mainland coast is reasonably active, as the occurrence of microearthquakes recorded at widely spaced stations suggests, then a microearthquake rate for the region

is of the order of several events per day. Station 5 is anomalous in this respect since five microearthquakes occurred in 17 hours; however three of the microearthquakes occurred during a ten-minute period. This location is the only one which recorded events with zero S-P times. Stresses caused by the interaction of several linear, possibly fault-controlled, geographical features in the vicinity of the station may be responsible for the observed microearthquakes.

The level of seismicity in the Inside Passage may be due to secondary effects of the seismically active but distant Queen Charlotte Islands fault or alternatively, may be due to background seismicity associated with long-term adjustments to tectonic processes such as intrusion or localized isostatic adjustment at the heads of fiords due to ice removal (e.g. Couch, 1969). This study shows, however, that microearthquakes do occur at a low rate in the relatively aseismic region of the Inside Passage.

MICROEARTHQUAKE MEASUREMENTS AT TWO  
TEMPORARY ARRAYS IN  
SOUTHEASTERN ALASKA

Introduction

Time remaining at the end of the seismic refraction experiment permitted OSU personnel to record microearthquakes at two temporary arrays located at Bartlett Cove and Sitkoh Bay in northern southeastern Alaska during four days in July and August, 1970. Arrival time differences across the array and the geometry of the array permitted the determination of six microearthquake epicenters.

Movement along the Chatham Strait fault is the subject of considerable controversy. St. Amand (1957) proposed that this line of faulting is a continuation of the Denali fault system of south-central Alaska and suggested approximately 240 km of right-lateral movement may have occurred on the Denali fault. On the basis of apparent displacement of major geologic features, Lathram (1964) concluded that 195 km of right-lateral movement had taken place. Brew, Loney, and Muffler (1966) presented a paleogeographic analysis which suggests 85 km right-lateral separation of pre-Tertiary strata along Chatham Strait. Loney, Brew, and Lanphere (1967) report the possibility of several kilometers of vertical movement on the Chatham Strait fault from radiometric ages of uplifted plutons. Gemperle and

Couch (1970) conclude that a component of normal faulting is present from reflection profiles in Chatham Strait.

The available seismic evidence does not suggest contemporary movement along the fault or along faults which join it from Chichagof and Baranof Islands. Gutenberg and Richter (1954) listed no earthquake epicenters along these faults. Tobin and Sykes (1968) relocate one epicenter near the convergence of the Fairweather fault, Peril Strait fault and Chichagof-Sitka-Patterson Bay fault, but the epicentral uncertainty does not allow assignment to a particular fault. Sykes (Tobin and Sykes, 1968) operated a high-gain seismograph in the vicinity of Sitka and reported microearthquakes offshore but none apparently related to the Chichagof-Sitka fault.

Tobin and Sykes (1968) suggested that the Denali fault is, or at one time was, a transform fault connecting the known spreading centers in the northeastern Pacific to the eastern end of the Aleutian Island trench. During the past 60 years, however, epicenters associated with this fault lie in the region west of  $144^{\circ}\text{W}$  (Gutenberg and Richter, 1954; Tobin and Sykes, 1966). The most active major fault in southeastern Alaska at the present time is the Fairweather fault (Tobin and Sykes, 1968). Hamilton and Meyers (1966) identify a possible northern extension of this fault which intersects the Denali fault near  $63^{\circ}\text{N}$ ,  $143^{\circ}\text{W}$ . The line of epicenters of major earthquakes, which extends northward along the trace of the Fairweather

fault from Cross Sound (Tobin and Sykes, 1965), suggests that the Fairweather fault takes up the greatest part of the motion along the Queen Charlotte Islands fault and that very little, if any motion, occurs on the Denali fault east of  $143^{\circ}$  W. or on its extension into Chatham Strait.

Boucher and Fitch (1969), however, show that the Denali fault is active microseismically (2-10 microearthquakes per day) along its entire length from Mt. McKinley National Park in southern Alaska to the head of Lynn Canal in southeastern Alaska. They interpret the difference between the high seismicity determined from microearthquakes and the low seismicity determined from large earthquakes in terms of either aftershock activity from a large earthquake in the unrecorded past or to background seismicity associated with a creep phenomenon. In order to determine if this type of movement continues southward along the Chatham Strait fault (the extension of the Denali fault), OSU personnel placed arrays at two locations west of Chatham Strait.

#### Field Methods

Two arrays recorded during a week at the end of July and beginning of August, 1970. Figure 24 shows the location of the stations, one established on the eastern side of Sitkoh Bay, just west of Chatham Strait, and the other located in southern Glacier

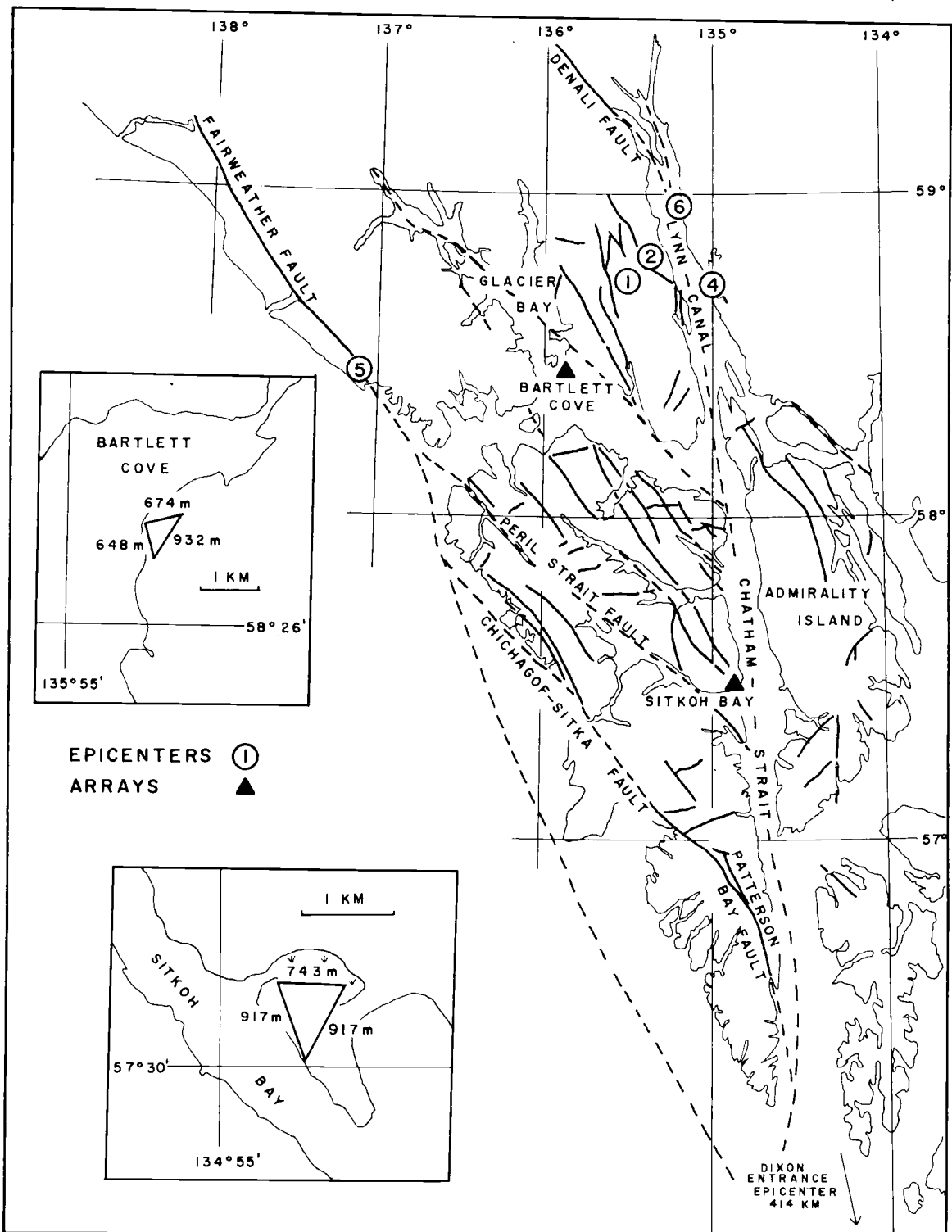


Figure 24. Positions and geometry of the recording arrays, epicenter locations, mapped faults (solid lines), and inferred faults (dashed lines) (after Brew, Loney, and Muffler, 1966).

Bay at Bartlett Cove. The tripartite arrays were approximately one kilometer in dimension, and incorporated four seismometers, three vertical and one horizontal. Figure 24 shows the location and geometry of the arrays. The OSU seismic recording system described above recorded the seismic signals from all four geophones together with time signals on magnetic tape. Simultaneously, a single-channel recorder monitored one geophone. WWV standard time broadcasts provided hourly time checks of the crystal-controlled clock. The arrays were surveyed using a steel tape, a staff compass, and an Abney level. Seismometer separation and azimuthal angles between array legs from the survey data were calculated with a computer program written in FORTRAN IV for use on a CDC 3300 computer (Appendix 1).

### Data Analysis

This section describes the analysis of microearthquake arrivals observed during 27 hours of recording at Sitkoh Bay and during 54 hours of recording at Glacier Bay. The first step in the analysis was to play back the magnetic tapes in the laboratory and record the arrivals on a four-channel hot-wire visual recorder operated at a paper speed of 50 mm/sec. Measurements were made from these records of arrival time differences at the three vertical seismometers and the S-P time from the trace of the horizontal seismometer.

An assumed crustal velocity model permitted the calculation of the azimuth from the array to the epicenter and, in addition, the apparent velocity of the wave assuming that the wave arrives as a plane wave front. It was difficult to correlate the first motion with sufficient accuracy across the traces, due to minor differences in wave character from one trace to the next. A method of visual correlation determined the time differences by comparing the first few cycles of each trace. The resolution of time differences attainable is limited by the low frequency of the waves recorded and the method used to determine time differences. An estimation of the uncertainty in reading time differences is  $\pm 4$  milliseconds which results in an estimated uncertainty in azimuth of  $20^\circ$  and in velocity of 8%.

The geometry of the array, together with the arrival time differences, permits the computation of the azimuth and apparent velocity of the wave. The calculation of the epicentral distance and focal depth is done using classical ray theory and a Poisson's ratio of 0.25 in a crustal model where the velocity is known as a function of depth. Stauder and Ryall (1967) derived a method of locating hypocenters using a small array. The program EPIARRAY, written in FORTRAN IV for use on a CDC 3300 computer, uses this method. Appendix 2 gives the theory and program listing for this method.

The crustal model used for the hypocenter determinations is

the velocity structure determined from the Bird Lake refraction line given in Table 3. Two changes were made to this model in the upper layer. Modification of the crustal section at the Sitkoh Bay array includes an upper layer of velocity 5.6 km/sec to correspond to a 2.7 km thick layer of similar velocity determined from the refraction study by Hales and Asada (1966) north of Skagway. The structural model for Bartlett Cove includes 50 meters of glacial till at 1.75 km/sec to better approximate conditions under the array. Table 7 gives the parameters for the two models.

Table 7. Crustal models used in the computation of hypocenters.

	Layer thickness, km	P-wave velocity, km/sec
Sitkoh Bay	2.70	5.60
	6.60	5.90
	6.50	6.30
	10.20	6.96
		7.87
Bartlett Cove	.05	1.75
	2.70	5.60
	6.60	5.90
	6.50	6.30
	10.20	6.96
	7.87	

(Poisson's ratio assumed to be 0.25)

### Interpretation

Table 8 lists and Figure 24 shows the epicenter solutions of the array data. The most striking observation is the low seismicity in the region near each array. This suggests that the locations of both arrays were in seismically quiet areas. No epicenters lie in Chatham Strait, although the Sitkoh Bay array lies only 2 km from it. Two epicenters appear in the St. Elias Mountains, east of Glacier Bay, two are in northern Lynn Canal, one is 30 km north of Cross Sound, and one is 30 km west of Dixon Entrance. Instrument magnification was approximately 800,000 except for an eight-hour period at Bartlett Cove when it was approximately 200,000 during a period of large microseisms. Examination of short period microfilmed records from the permanent Sitka, Alaska, seismic station, operated by the U. S. Coast and Geodetic Survey, for the time periods during which the arrays were in operation shows no indication of the earthquakes listed in Table 8 nor of any others except for a magnitude  $M=7$  teleseism from Colombia, South America (which was also recorded by the Sitkoh Bay array). There appears to be no instrumental reason, except for low gain, for the lack of recorded arrivals on the Sitka records.

The lack of epicenters in Chatham Strait suggests that seismic activity along the Chatham Strait fault is very low. The low observed

seismicity agrees with the observations of Tobin and Sykes (1968) who noted that there were no epicenters located in Chatham Strait during the past 60 years. The high microearthquake activity noted by Boucher and Fitch (1969) along the Denali fault does not appear to be present in Chatham Strait near Sitkoh Bay.

Table 8. Epicenter solutions obtained from array data.

Number	Date	P-wave arrival time, GMT	S-P time sec	P-wave apparent vel, km/sec	Dist, km	Azi, deg	Depth km
1	7-31-70	02:11:16.0	16.9	9.0	145	345	92
2	7-31-70	02:12:06.5	16.8	6.9	151	349	15
3	7-31-70	10:46:06.0	40.1	7.7	414	168	25
4	8-03-70	03:02:31.0	7.3	6.9	60	59	15
5	8-03-70	03:37:23.1	8.4	7.3	72	271	25
6	8-03-70	05:29:41.5	9.2	9.6	70	36	58

The epicenter west of Dixon Entrance falls among a cluster of epicenters associated with the Queen Charlotte Islands fault (see Figure 2). The location of this earthquake is more uncertain than the others because of its large epicentral distance.

Only one epicenter lies in the vicinity of the Fairweather fault near the epicenter of the magnitude  $M=7.9$  earthquake of July 10, 1958. The low value of seismicity indicates that the aftershock activity from the 1958 earthquake has dropped below the level that could be recorded at the two arrays. The data of Utsu (1962) indicates that the aftershock activity immediately following the earthquake of

1958 was relatively low compared to its large magnitude. Ward and Bjornsson (1971) note an exponential decrease in observed microearthquake activity away from arrays due to geometrical spreading and attenuation. For microearthquakes in Iceland, they observe that the average number of microearthquakes per day drops from 20 at an epicentral distance of 3 km to 2 microearthquakes per day at 15 km. If this decrease with distance of observed microearthquakes is true in southeastern Alaska, then low microearthquake rates should be observed for areas at large distances from the recording array. Since the Bartlett Cove array is nearly 60 km from the Fairweather fault, and since Utsu's (1962) data suggests the aftershocks originate from a small epicentral area, the observed rate of one microearthquake in 54 hours may be an accurate indication of seismicity of the fault. If the array were moved closer to the fault zone, an exponential increase in the number of observed microearthquakes would be expected.

On the basis of the number of observed microearthquakes, the northern Lynn Canal area is the site of moderate seismic activity. These epicenters may be related to activity on the Denali fault noted by Boucher and Fitch (1969) in the vicinity of Haines. The presence of epicenters in Lynn Canal implies that the Denali fault may extend beneath it. The lack of epicenters to the south indicates that the fault in Chatham Strait may not be active. Motion along the extension

of the Denali fault may be responsible for the fault pattern mapped on northern Admiralty Island.

The hypocenter depths given in Table 8 include two deep earthquakes (59 and 92 km). Since most earthquakes in this region occur at normal depths (33 km) the presence of deep earthquakes requires an explanation. The explanation that they are due to observational errors from a misread time difference fails because the records, when interpreted several times, gave the same results. It is unlikely that a crustal inhomogeneity under the array is an explanation since one deep earthquake was registered at each array. The use of uncalibrated arrays (calibrated, for example, by an explosion) is a possible but unlikely explanation since hypocenters from nearly opposite directions lie at normal depths. It is concluded that the depths are accurate and that they indicate seismic activity at greater than normal depth. This is not the first report of a hypocenter greater than normal in this region since a shock occurred at  $58.8^{\circ}$  N,  $135.9^{\circ}$  W at a depth of 109 km on January 17, 1961 (U. S. Coast and Geodetic Survey, United States Earthquakes, 1961). The 1961 earthquake epicenter location lies slightly to the northwest of the deep microearthquakes (1 and 6) observed at the arrays. Earthquakes with foci deeper than normal occur in the vicinity of  $61.5^{\circ}$  N and  $141^{\circ}$  W and may be related to the intersection of the Fairweather fault and the eastern extension of the Aleutian trench. The anomalous

deep hypocenters northeast of Glacier Bay do not seem to have a similar explanation.

## SUMMARY AND CONCLUSIONS

Interpretation of two unreversed seismic refraction lines in southeastern Alaska and western British Columbia indicates that the earth's crust thickens from 26 km on the continental margin north of Dixon Entrance to 30 km on the mainland coast south of Dixon Entrance. The crust on the margin north of Dixon Entrance consists of a layer 9 km thick with a velocity of 5.90 km/sec, a layer 7 km thick with a velocity of 6.30 km/sec, and a layer 10 km thick with a velocity of 6.96 km/sec overlying the M discontinuity with a velocity of 7.86 km/sec. The crust on the mainland coast south of Dixon Entrance consists of a layer 13 km thick with a velocity of 6.03 km/sec, a layer 5 km thick with a velocity of 6.41 km/sec, and a layer 12 km thick with a velocity of 6.70 km/sec overlying the M discontinuity with a velocity of 8.11 km/sec. The measurements agree with previous estimates of crustal thickness by Couch (1969) from gravity measurements. From amplitude measurements, a computed value of  $Q = 260$  indicates greater than average attenuation in the uppermost mantle of the continental margin.

Gravity models, constrained by the seismic measurements, suggest that the crust has uniform thickness between the continental shelf and the Coast Mountains. A map compiled from Bouguer gravity measurements of others indicates a region of near-zero anomalies

(associated with uniform crustal thickness) which extends along the continental margin of British Columbia and southeastern Alaska as far north as  $58^{\circ}$  N. The relatively thin crust and step-like transition inferred from this study is apparently characteristic of the continental margin of western North America (Couch, 1969).

A seismic profiler record in Dixon Entrance shows folded sediments in the upper layers and basement highs, some of which are bounded by faults dipping at an angle of approximately  $70^{\circ}$ . These features are evidence that the region has experienced both compressional and tensional stresses normal to the coast. The tensional features may be due to the northwest-southeast tension in the Pacific plate west of British Columbia proposed by Dehlinger *et al.* (1971). The compressional features may be a result of underthrusting of the North American plate by the Pacific plate during the Mesozoic (Couch, 1969) or to local intrusions and uplift.

Gravity models indicate the presence of sedimentary rock nearly three kilometers thick in troughs east of Learmonth Bank and west of Celestial Reef. These troughs lie northwest-southeast, parallel to the coast, and are aligned with structural lows present in southeastern Alaska. Linear gravity anomalies, coincident with structural highs and lows from mapped geology, extend southeastward from southeastern Alaska but decrease in magnitude and disappear midway across Dixon Entrance. Thick layers of basalt present on

Graham Island may extend northward and obscure these features.

A steep gravity gradient correlates with observed faulting on the eastern margin of Learmonth Bank. On the basis of gravity anomalies which extend in a southerly direction, the fault may be an extension of the Sandspit fault on Graham Island.

A magnetic model indicates that structural highs present at Learmonth Bank and on both sides of the extension of Clarence Strait are responsible for large observed magnetic anomalies. The distinguishing magnetic feature of the basement highs is their large susceptibility suggestive of basic intrusives or highly metamorphosed rock. The observed magnetic anomalies may be near-surface expressions of deep crustal structure associated with the transition zone between oceanic crust and continental crust.

A microearthquake survey indicates a microearthquake seismicity of several events per day along the mainland coast of British Columbia. The activity may be due to secondary effects of seismic activity on the Queen Charlotte Islands fault zone or to local uplift from isostatic adjustment to ice removal. Observed microearthquakes which originate at large distances from the Inside Passage probably occur in the Queen Charlotte Islands fracture zone.

Two temporary arrays recorded microearthquakes in northern southeastern Alaska. A crustal structure based on the seismic refraction measurements permitted location of the epicenters. No

epicenters lie in Chatham Strait along the Chatham Strait fault even though one array recorded only 2 km from it. Epicenters lie in the southern St. Elias mountains (at greater than normal depths) and on the Fairweather fault, as might be expected from historic earthquakes. Other epicenters lie in northern Lynn Canal along the possible extension of the Dehali fault. Since no epicenters lie in southern Lynn Canal on Chatham Strait, movement along the Denali fault may be taken up elsewhere in northern southeastern Alaska, perhaps on northern Admiralty Island.

## BIBLIOGRAPHY

- Adachi, R. 1954. On a proof of fundamental formula concerning refraction method of geophysical prospecting. *Kumamoto Journal of Science* 2:18-25.
- Asada, T. 1957. Observations of near-by microearthquakes with ultrasensitive seismometers. *Journal of the Physics of the Earth* 5:83-113.
- Banks, Ernest Robey. 1969. Isostatic and Bouguer gravity anomalies along the Inside Passage of Alaska and British Columbia. Master's thesis. Corvallis, Oregon State University. 56 numb. leaves.
- Benioff, H. 1962. Movements on major transcurrent faults. In: *Continental drift*, ed. by S. K. Runcorn, New York. Academic Press. p. 103-134.
- Berry, M. J. and G. F. West. 1966. Reflected and head wave amplitudes in a medium of several layers. In: *The earth beneath the continents*, ed. by John S. Steinhart and T. Jefferson Smith. Washington D.C. American Geophysical Union. p. 464-481.
- Bomford, G. 1962. *Geodesy*. London, Clarendon Press. 561 p.
- Boucher, Gary and Thomas J. Fitch. 1969. Microearthquake seismicity of the Denali fault. *Journal of Geophysical Research* 74:6638-6648.
- Brew, David A., Robert A. Loney and L. J. Patrick Muffler. 1966. Tectonic history of southeastern Alaska. In: *A symposium on the tectonic history and mineral deposits of the western Cordillera of British Columbia and neighboring parts of the United States*. Vancouver, 1964. Montreal. p. 149-170. (Canadian Institute of Mining and Metallurgy. Special Volume no. 8.)
- Brown, A. Sutherland. 1966. Tectonic history of the insular belt of British Columbia. In: *A symposium on the tectonic history and mineral deposits of the western Cordillera of British Columbia and neighboring parts of the United States*. Vancouver, 1964. Montreal. p. 83-100. (Canadian Institute of Mining and Metallurgy. Special Volume no. 8.)

- Cain, Joseph C. and Shirley J. Cain. 1968. Derivation of the International Geomagnetic Reference Field (IGRF(10/68)). Goddard Space Flight Center Publ. no. X-612-68-501. 11 p.
- Cain, Joseph C., Shirley Hendricks, Walter E. Daniels and Duane C. Jensen. 1968. Computation of the main geomagnetic field from spherical harmonic expansion. National Space Flight Data Center Publ. no. 68-11. 46 p.
- Chiburis, Edward Frank. 1965. Crustal structures in the Pacific Northwest states from phase-velocity dispersion of seismic surface waves. Ph.D. thesis. Corvallis, Oregon State University. 170 numb. leaves.
- Couch, Richard William, 1969. Gravity and structures of the crust and subcrust in the northeast Pacific Ocean west of Washington and British Columbia. Ph.D. thesis. Corvallis, Oregon State University. 179 numb. leaves.
- Dehlinger, Peter, R. W. Couch, D. A. McManus, and Michael Gemperle. 1971 Northeast Pacific structure. In: The Sea, Volume 4, Part II, ed. by Arthur E. Maxwell, New York, Wiley. p. 133-189.
- Dehlinger, P., M. Gemperle, R. W. Couch and D. W. Hood. 1966. Free-air gravity anomalies along the Inside Passage of British Columbia and Alaska. Journal of Geophysical Research 71: 6011-6015.
- Dietz, R. S. 1961. Continent and ocean basin evolution by spreading of the sea floor. Nature 190:854-857.
- Gemperle, Michael and Richard W. Couch. 1970. Geophysical investigations of the continental margin off southeast Alaska. (Abstract) EOS, Transactions, American Geophysical Union 51:316.
- Gemperle, M. and K. Keeling. 1970. Geophysical data reduction and plotting computer programs. Technical Report no. 180. Reference 70-10, Department of Oceanography, Oregon State University. 56 p.
- Geological Map of Canada. 1969. Geological Survey of Canada. Department of Energy, Mines and Resources. Map 1250A.

- Grant, F. S. and G. F. West. 1965. Interpretation theory in applied geophysics. New York, McGraw-Hill. 584 p.
- Gutenberg, B. and C. F. Richter. 1954. Seismicity of the earth, 2nd ed. Princeton, N. J., Princeton University Press. 310 p.
- Haines, G. V., W. Hannaford and R. P. Riddihough. 1971. Magnetic anomalies over British Columbia and the adjacent Pacific Ocean. Canadian Journal of Earth Sciences 8:387-391.
- Hales, A. L. and T. Asada. 1966. Crustal structure in coastal Alaska. In: The earth beneath the continents, ed. by John S. Steinhardt and T. Jefferson Smith. Washington, D. C. American Geophysical Union. p. 420-432.
- Hamilton, W. and W. B. Meyers. 1966. Cenozoic tectonics of the western United States. Reviews of Geophysics 4:509-549.
- Heelan, P. A. 1953. On the theory of head waves. Geophysics 18: 871-893.
- Heiskanen, W. A. 1938. Catalogue of the isostatically reduced gravity stations. Helsinki (International Association of Geodesy. Isostatic Institute. Publication no. 5). 139 p.
- Heiskanen, W. A. and F. A. Vening Meinez. 1958. The earth and its gravity field. New York, McGraw-Hill. 470 p.
- Hess, H. H. 1962. History of the ocean basins. In: Petrologic studies: a volume in honor of A. F. Buddington. New York. Geological Society of America p. 599-620.
- Hodgson, J. H. and W. G. Milne. 1951. Direction of faulting in certain earthquakes of the North Pacific. Bulletin of the Seismological Society of America 41:221-242.
- Hron, F. 1970. Criteria for selection of phases in synthetic seismogram calculations. (Abstract) EOS, Transactions, American Geophysical Union 51:776.
- Hron, F. 1971. Department of Physics, University of Alberta. Personal communication. Edmonton, Canada. May 12.
- Hutchison, W. W. and J. A. Roddick. 1967. Specific gravity of plutonic rocks in the northern Coast Mountains. (Abstract) Geological Society of America. Cordilleran Section, Santa Barbara, California. Special Paper no. 115. p. 333.

- Johnson, Stephen H. and Richard W. Couch. 1970. Crustal structure in the North Cascade Mountains of Washington and British Columbia from seismic refraction measurements. *Bulletin of the Seismological Society of America* 60:1259-1269.
- Kanasewich, E. R. and F. Hron. 1970. Synthetic seismograms for crustal studies using generalized ray theory. (Abstract) *EOS, Transactions, American Geophysical Union* 51:775.
- Knopoff, L. 1956. The seismic pulse in materials possessing solid friction, I, plane waves. *Bulletin of the Seismological Society of America* 46:175-184.
- Lathram, E. H. 1964. Apparent right-lateral separation on Chatham Strait fault, southeastern Alaska. *Bulletin of the Geological Society of America* 75:249-252.
- Lehner, Francis E. and Frank Press. 1966. A mobile seismograph array. *Bulletin of the Seismological Society of America* 56: 889-897.
- LePichon, Xavier. 1968. Sea floor spreading and continental drift. *Journal of Geophysical Research* 73:3661-3697.
- Loney, R. A., D. A. Brew and M. A. Lanphere. 1967. Post-Paleozoic radiometric ages and their relevance to fault movements, northern southeastern Alaska. *Bulletin of the Geological Society of America* 78:511-526.
- Lu, Richard Shih-Ming. 1971. Magnetic and gravity interpretation of YALOC-69 data from the Cocos Plate area. Master's thesis. Corvallis, Oregon State University. 105 numb. leaves.
- Ludwig, William J., John E. Nafe and Charles L. Drake. 1971. Seismic refraction. In: *The Sea, Volume 4 Part I*, ed. by Arthur E. Maxwell. New York, Wiley. p. 53-84.
- McManus, D. A. 1967. Physiography of Cobb and Gorda rises, northeast Pacific Ocean. *Bulletin of the Geological Society of America* 78:527-546.
- Milne, A. R. 1964. Two seismic refraction measurements: North Pacific basin and Dixon Entrance. *Bulletin of the Seismological Society of America* 54:41-50.
- Milne, W. G. 1954a. Canadian west coast earthquakes, 1952. *Publications of the Dominion Observatory*. Vol. 16, no. 9. Ottawa. Vol. 16, no. 9. p. 14-28.

- Milne, W. G. 1954b. Canadian west coast earthquakes. 1953. Publications of the Dominion Observatory, Ottawa. Vol. 16, no. 13. p. 30-40.
- Milne, W. G. 1956a. Canadian west coast earthquakes, 1954. Publications of the Dominion Observatory, Ottawa. Vol. 18, no. 3. p. 42-55.
- Milne, W. G. 1956b. Seismic activity in Canada, west of the 113th meridian 1841-1951. Publications of The Dominion Observatory, Ottawa. Vol. 18, No. 7. p. 119-146.
- Milne, W. G. and F. Lombardo. 1952. Canadian west coast earthquakes, 1951. Publications of the Dominion Observatory, Ottawa. Vol. 16, no. 3. p. 81-89.
- Milne, W. G. and K. A. Lucas. 1961. Seismic activity in western Canada 1955-1959 inclusive. Publications of the Dominion Observatory, Ottawa. Vol. 26. no. 1. p. 3-23.
- Milne, W. G., W. E. T. Smith and G. C. Rogers. 1970. Canadian seismicity and microearthquake research in Canada. Canadian Journal of Earth Sciences 7:591-601.
- ✓ Mooney, Harold M., Campbell Craddock, Paul R. Farnham, Stephen H. Johnson, and Gary Volz. 1970. Refraction seismic investigations of the northern midcontinent high. Journal of Geophysical Research 75:5056-5086.
- Morgan, W. Jason. 1968. Rises, trenches, great faults, and crustal blocks. Journal of Geophysical Research 73:1959-1982.
- Murphy, Leonard M. 1950. United States Earthquakes, 1947. U. S. Coast and Geodetic Survey Publication 730. 62 p.
- Murphy, Leonard M. and William K. Cloud. 1953. United States earthquakes, 1951. U. S. Coast and Geodetic Survey Publication no. 762. 50 p.
- Murphy, Leonard M. and Franklin P. Ulrich. 1951a. United States earthquakes, 1948. U. S. Coast and Geodetic Survey Publication no. 746. 50 p.

- Murphy, Leonard M. and Franklin P. Ulrich. 1951b. United States earthquakes, 1949. U. S. Coast and Geodetic Survey Publication no. 748. 63 p.
- Murphy, Leonard M. and Franklin P. Ulrich. 1952. United States earthquakes, 1950. U. S. Coast and Geodetic Survey Publication no. 755. 47 p.
- Oliver, Jack, Alan Ryall, James N. Burne and David B. Slemmons. 1966. Microearthquake activity recorded by portable seismographs of high sensitivity. *Bulletin of the Seismological Society of America* 56:899-924.
- Peacock, M. A. 1935. Fiord-land of British Columbia. *Bulletin of the Geological Society of America* 46:633-696.
- Preliminary determination of epicenters, monthly listings; June, July, August, 1970. National Ocean Survey, Rockville, Md. U. S. Department of Commerce.
- Raff, A. D. and R. G. Mason. 1961. Magnetic survey off the west coast of North America, 40° N. latitude to 50° N. latitude. *Bulletin of The Geological Society of America* 72:1267-1270.
- Richter, Charles F. 1958. *Elementary Seismology*. San Francisco, W. H. Freeman. 768 p.
- Roddick, J. A. 1966. Coast crystalline belt of British Columbia. In: *A symposium on the tectonic history and mineral deposits of the western Cordillera of British Columbia and neighboring parts of the United States*. Vancouver, 1964. Montreal. p. 73-82. (Canadian Institute on Mining and Metallurgy. Special Volume no. 8.)
- Roller, J. C. 1965. Crustal structure in the eastern Colorado plateaus province - seismic refraction measurements. *Bulletin of the Seismological Society of America* 55:107-120.
- Rothe, J. P. 1969. *The seismicity of the earth 1953-1965*. Paris, United Nations Educational Scientific and Cultural Organization. 336 p.
- Ryall, Alan and David J. Stuart. 1963. Travel times and amplitudes from nuclear explosions, Nevada test site to Ordway, Colorado. *Journal of Geophysical Research* 68:5821-5835.

- St. Amand, Pierre, 1957. Geological and geophysical synthesis of the tectonics of portions of British Columbia, the Yukon Territory, and Alaska. *Bulletin of the Geological Society of America* 68:1343-1370.
- Shor, George G., Jr. 1962. Seismic refraction studies off the coast of Alaska: 1956-1957. *Bulletin of the Seismological Society of America*. 50:37-57.
- Shouldice, David H. 1970. Geology of the western Canadian continental shelf. (Abstract) *Bulletin of the American Association of Petroleum Geologists* 54:5.
- Stacey, R. 1967. Geophysicist, Dominion Observatory of Canada, Gravity Division. Personal communication to R. W. Couch. Ottawa, Canada. April 14.
- Stacey, R. A. and L. E. Stephens. 1969. An interpretation of gravity measurements on the west coast of Canada. *Canadian Journal of Earth Sciences* 6:463-474.
- Stacey, R. A., L. E. Stephens, R. V. Cooper and B. G. Brule. 1969. Gravity measurements in British Columbia with map, no. 88 - British Columbia coastal area. Gravity Map Series of the Dominion Observatory, Ottawa. 11 p.
- Stauder, W. 1959. A mechanism study: The earthquake of October 24, 1927. *Pure and Applied Geophysics* 44:135-144.
- Stauder, W. 1960. The Alaska earthquake of July 10, 1958: seismic studies. *Bulletin of the Seismological Society of America* 50: 293-322.
- Stauder, William and Alan Ryall. 1967. Spacial distribution and source mechanism of microearthquakes in central Nevada. *Bulletin of the Seismological Society of America* 57:1317-1345.
- Talwani, M. and J. R. Heirtzler. 1964. Computation of magnetic anomalies caused by two-dimensional structures of arbitrary shape. In: *Computers in the mineral industries*, ed. by G. A. Parks *et al.*, 1963. Stanford. p. 464-480. (Stanford University Publications, Geological Sciences. Vol. 9, no. 1)

- Tatel, H. E. and M. A. Tuve. 1955. Seismic exploration of a continental crust. In: Crust of the earth, ed. by A. Polder-vaart, New York. Geological Society of America. Special Paper 62. p. 35-50.
- Tatel, H. E. and M. A. Tuve. 1956. The earth's crust: seismic studies. In: Carnegie Institution of Washington Year Book 55, Washington, D. C. p. 81-85.
- Taylor, H. P. and J. A. Noble. 1960. Origin of the ultramafic complexes in southeastern Alaska. In: International Geologic Congress. Report of the Twenty-first Session Norden, Part 13. Copenhagen. Det Berlingske Bogtrykkeri. p. 175-187.
- Thiel, E., W. E. Bonini, N. Ostenso and G. P. Woollard. 1958. Gravity measurements in Alaska. 77 numb. leaves. (University of Wisconsin. Geophysics Research Center. Reference no. 58-54 on Air Force Cambridge Research Center Contract AF19 (604) - 2157).
- Thornburgh, H. R. 1930. Wave-front diagrams in seismic interpretation. Bulletin of the American Association of Petroleum Geologists 14:185-200.
- Tobin, D. G. and L. R. Sykes. 1966. Relationship of hypocenters of earthquakes to the geology of Alaska. Journal of Geophysical Research 71:1659-1667.
- Tobin, Don G. and Lynn R. Sykes. 1968. Seismicity and tectonics of the northeast Pacific Ocean. Journal of Geophysical Research 73:3821-3845.
- Tocher, D. 1960. The Alaska earthquake of July 10, 1958: movement on the Fairweather fault and field investigation of southern epicentral region. Bulletin of the Seismological Society of America 50:267-292.
- Twenhofel, William S. and C. L. Sainsbury. 1958. Fault patterns in southeastern Alaska. Bulletin of the Geological Society of America 60:1431-1442.
- U. S. Coast and Geodetic Survey. 1955-1962. United States Earthquakes, 1955 through 1962 (Annual serial). Washington, D.C., U. S. Department of Commerce.

- U. S. Department of Commerce. Preliminary determination of epicenter (PDE) cards. 1963-1970. Issued periodically by the U. S. Coast and Geodetic Survey and the National Ocean Survey. Rockville, Md.
- Utsu, Tokiyi. 1962. On the nature of three Alaskan aftershock sequences of 1957 and 1958. *Bulletin of the Seismological Society of America* 52:279-297.
- Ward, Peter L. and Sveinbjorn Bjornsson. 1971. Microearthquakes, swarms, and the geothermal areas of Iceland. *Journal of Geophysical Research* 76:3953-3982.
- Werth, Glenn C., Roland Herbst and Donald L. Springer. 1962. Amplitudes of seismic arrivals from the M discontinuity. *Journal of Geophysical Research* 67:1587-1610.
- White, William H. 1966. Summary of tectonic history. In: A symposium of the tectonic history and mineral deposits of the western Cordillera of British Columbia and neighboring parts of the United States. Vancouver, 1964. Montreal. p. 83-100. (Canadian Institute of Mining and Metallurgy. Special Volume no. 8.)
- White, W. R. H. and J. C. Savage. 1965. A seismic refraction and gravity study of the earth's crust in British Columbia. *Bulletin of the Seismological Society of America* 55:463-486.
- Wickers, A. J. and J. H. Hodgeson. 1967. Computer re-evaluation of earthquake mechanism solutions, 1922-1961. *Publications of the Dominion Observatory*, vol. 33, No. 1.
- Willmore, P. L. 1959. The application of the Maxwell impedance bridge to the calibration of electromagnetic seismographs. *Bulletin of the Seismological Society of America* 49:99-114.
- Wilson, J. Tuzo. 1965a. A new class of faults and their bearing on continental drift. *Nature* 207:343-347.
- Wilson, J. Tuzo. 1965b. Transform faults, oceanic ridges, and magnetic anomalies southwest of Vancouver Island. *Science* 150:482-485.
- Woollard, G. P., N. A. Ostenso, E. Thiel and W. E. Bonini. 1960. Gravity anomalies, crustal structure, and geology in Alaska. *Journal of Geophysical Research* 65:1021-1037.

Worzel, J. L. 1965. Pendulum gravity measurements at sea, 1936-1959. New York, Wiley, 422 p.

Wright, J. K., E. W. Carpenter and R. A. Saville. 1962. Some studies of the P waves from underground nuclear explosions. *Journal of Geophysical Research* 67:1155-1160.

## APPENDICES

## APPENDIX 1

REDUCTION OF SURVEY DATA TO OBTAIN  
ARRAY DIMENSIONS

The computer program, SURVEY, computes distances and elevations in meters and azimuths in degrees between two or more points or geophones in an array from survey data obtained with a compass, a measuring tape, and a level. The program computes N-S, E-W, and vertical components of each line segment making up a traverse between a reference location and a geophone given the length, the orientation, and the angle with the vertical of each segment. The computer sums and stores the components of the line segments necessary to reach a surveyed point from a common reference point. Once all the surveyed points are inserted, the program computes distances and azimuth from each point to the other points. Written in FORTRAN IV, the program ran on a CDC 3300 computer. The program parameters are:

Input cards

- 1) General control
  - N Number of surveyed points or geophone locations
  - IDEG, IMIN Declination, in degrees and minutes, of the magnetic field. This is zero if the declination was set into the compass before making the reading

TITLE            Survey identification  
 FORMAT(I1, X, I2, X, I2, X, 6A8)

- 2)    Reference point information  
       REF            Latitude, longitude, elevation, and other  
                       information about the reference point.  
                       The contents of this card appears in  
                       entirety on the printout

FORMAT(9A8)

- 3)    First card of each leg of the survey  
       GN            Geophone number  
       CH            Number of the channel which is recording  
                       the geophone output

FORMAT(I3, X, I2)

- 4)    Line segments from survey  
       DI            Length of the line segment in feet  
       A1            North (N) or south (S) compass direction  
       DEG, MIN      Orientation of line segment in degrees  
                       and minutes  
       A2            East (E) or west (W) compass direction  
       ABN           Level reading in per cent rise

FORMAT(F6. 1, X, A1, I2, X, I2, A1, X, F5. 1)

Follow card 4 with one end-of-file (EOF) card at the end of each leg of the array and repeat from card 3 until all legs are surveyed. Follow the final leg with two EOF cards and repeat from card 1 for different arrays. Follow the final leg of the last array with three EOF cards.

#### Output (High speed line printer)

- 1)    Survey identification  
       TITLE            Survey identification  
       N                Number of survey points or geophones  
 FORMAT(1H1, 24HSURVEY DATA ON ARRAY AT 6A8, 21  
 HNUMBER OF GEOPHONES= , I1)

- 2)    Declination information  
       IDEG, IMIN      Declination correction applied to data  
                       output  
 FORMAT(1H , 51 HAZIMUTH ANGLES CORRECTED FOR  
 MAGNETIC DECLINATION= , I2, X, I2, 1HE)

- 3) Reference information  
 REF Information about reference position  
 FORMAT(1H , 24HREFERENCE POSITION DATA=, 9A8///)
- 4) Input and computed information  
 D Distance of each line segment in feet  
 DIM Distance of each line segment in meters  
 A1 N or S, compass direction  
 DEG, MIN Orientation of line segment  
 A2 E or W, compass direction  
 ABN Level reading  
 ALAT North component in meters  
 ADEP East component in meters  
 ELE Elevation change in meters  
 FORMAT(1H , F6. 1, X, F6. 2, 2X, A1, I2, X, I2, A1, 2X, F5. 1, 3X,  
 F8. 2, 4X, F6. 2)
- 5) Summary of a surveyed position  
 GN Geophone number  
 CH Channel number  
 FORMAT (1 HO, 16H GEOPHONE NUMBER, I3, 2X, 15H CHANNEL  
 NUMBER , I2)  
 S1 Sum of north components  
 S2 Sum of east components  
 DIST Distance to reference position  
 FORMAT(1H , 26HTOTAL OF NORTH COMPONENTS=, F8. 2,  
 7HMETERS/1 H , 26HTOTAL OF EAST COMPONENTS=,  
 F8. 2, 7H Meters /1H, 26HDISTANCE TO REFERENCE=,  
 F8. 2, 7H METERS)  
  
 THETA Azimuth from reference position  
 THETB Azimuth to reference position  
 SEL Elevation with respect to reference  
 position  
 FORMAT(1H, 26HAZIMUTH TO REFERENCE= , F8. 2, 8H  
 DEGREES/1H , 26HAZIMUTH TO REFERENCE= ,  
 F8. 2, 8H DEGREES/ 1H , 26H ELEVATION WRT  
 REFERENCE= , F8. 2, 7H METERS///)
- 6) Summary of a surveyed array  
 I Geophone number  
 J Geophone number  
 TH1 Azimuth from geophone I to geophone J  
 DIS Distance between geophones I and J  
 TH2 Azimuth from geophone J to geophone I  
 FORMAT(1H , 3X, I2, X, I2, X, F6. 2, 2X, F7. 2, 4X, F6. 2)

The program listing is:

```

PROGRAM SURVEY
C CARD 1= N IS NUMBER OF GEOPHONES, IDEG,IMIN IS DECLINATION OF MAGN
C FIELD (=00 IF INCLUDED IN ORIG SURVEY) TITLE IS ARRAY IDENTIFICAT.
C CARD 2= INFO ON SURVEY REFERENCE POINT SEE COMMENT AFTER CARD 99
C CARD 3= START SURVEY, SO GIVE GEOP NO. AND RECORDING CHANNEL NO.
C CARD 4= SURVEY INFO. DI=MEASURED LENGTH IN FEET. A1,DEG,MIN,A2=
C FORWARD DIRECTION. ARN=ABNEY READING IN RISE/100 FEET (PER CENT)
C REPEAT CARD 4 UNTIL REACH DESIRED GEOPHONE
C END SURVEY OF A GEOPHONE. FOLLOW CARDS (S) 4 WITH ONE EOF CARD (73-74)
C AND REPEAT FROM CARD 3
C END SURVEY OF THIS ENTIRE ARRAY. FOLLOW CARDS 4 WITH TWO EOF CARDS AND
C REPEAT FROM CARD 1
C END SURVEY OF ALL ARRAYS. FOLLOW CARD(S) 4 WITH THREE EOF CARDS AND
C LOGOFF
      DIMENSION TITLE(6),LOC(6),ALA(4,50),ADE(4,50),SLA(4),SDE(4),REF(9)
      INTEGER A1,A2,GN,CH,DEG
      REAL LOC
      P=7.14159265
      R=P/180.
      RAD=180./P
100 READ 101,N,IDEG,IMIN,TITLE
101 FORMAT (I1,X,I2,X,I2,X,6A8)
      IF (EOF(60)) CALL EXIT
      DECL= IDEG+IMIN/60.
      WRITE (61,99) TITLE,N
      99 FORMAT (1H1,24HSURVEY DATA ON ARRAY AT ,5A8,21HNUMBER OF GEOPHONES
      1= ,I1)
      WRITE (61,104) IDEG,IMIN
104 FORMAT (1H ,51HAZIMUTH ANGLES CORRECTED FOR MAGNETIC DECLINATION=
      1,I2,X,I2,1HF)
C REF SHOULD CONTAIN LAT, LONG, ELEVATION AND OTHER INFO ABOUT REF PT
      READ 105, REF
105 FORMAT (9A8)
      WRITE (61,106) REF
106 FORMAT (1H ,24HREFERENCE POSITION DATA=, 9A8///)
107 READ 108,GN,CH
108 FORMAT (I3,X,I2)
C EOF HERE SAYS OUTPUT OF STATION DATA
      IF (EOF(60)) GO TO 200
      I=04
      J=0
      SEL=SLA(I)=SDE(I)=0.0
      WRITE (61,110)
110 FORMAT (1H ,61HHORIZ DIST IN ANGLE ABNEY NORTH COMP EAST COM
      1? RISE IN)
      WRITE (61,112)
112 FORMAT (1H ,61HFEET METERS READING PERCENT IN METERS IN METER
      1S METERS/)
115 READ 116,DI,A1,DEG,MIN,A2,ARN
116 FORMAT(F6.1,X,A1,I2,X,I2,A1,X,F5.1)
C EOF HERE SAYS END OF TRAVERSE MAKES SUMS
      IF (EOF(60)) GO TO 150
      J=J+1
      ANG=DEG+ MIN/60.
      THET=ATANF(ARN*.71)
      D=DI*COSE(THET)
      DIM=D*.3048006
      ADEP=DIM*SINF(ANG*R)
      ALAT=DIM*COSE(ANG*R)
      IF (A2.EQ.1HW) ADEP=-ADEP

```

```

IF (A1.EQ.1HS) ALAT=-ALAT
FLF=DIM*ARN*.71
SFL=SFL+ELE
SLA(I)=SLA(I)+ALAT
SDF(I)=SDF(I)+ADEP
ALA(I,J)=SLA(I)
ADF(I,J)=SDF(I)
FLFM=FLF*.3048006
WRITE(61,120) 0,DTM,A1,DEG, MIN,A2,ARN,ALAT,ADEP,FLF
120 FORMAT(1H ,F6.1,X,F6.2,2X,A1,I2,X,I2,A1,2X,F5.1,3X,F8.2,3X,F8.2,
14X,F6.2)
GO TO 115
150 WRITE(61,160)GN,CH
150 FORMAT(1H0,16HGEOPHONE NUMBER ,I3,2X,15HCHANNEL NUMBER ,I2)
S1=SLA(I)
S2=SDF(I)
DIST=SQRT(S1*S1+S2*S2)
WRITE(61,165)S1,S2,DIST
155 FORMAT(1H ,26HTOTAL OF NORTH COMPONENTS=,F8.2,7H METERS/
11H ,26HTOTAL OF EAST COMPONENTS=,F8.2,7H METERS/
11H ,26HDISTANCE TO REFERENCE=,F8.2,7H METERS)
IF (DIST.EQ.0.) GO TO 166
THETA=ASINF(SDF(I)/DIST)
164 IF (S1.GE.0.) GO TO 167
THETA=P-THETA
GO TO 168
167 IF (THETA.LT.0.) THETA=2.*P+THETA
168 THETA=THETA*RAD
THETA=THETA+DECL
IF (THETA.LT.0.) THETA=THETA+360.
IF (THETA.GE.360.) THETA=THETA-360.
THETA=THETA+180.
IF (THETA.GE.180.) THETA=THETA-180.
GO TO 169
166 THETA=0.
THETA=0.
169 WRITE(61,170)THETA,THETA,SEL
170 FORMAT(1H ,26HAZIMUTH FROM REFERENCE =,F8.2,8H DEGREES/1H ,26HAZ
11MUTH TO REFERENCE =,F8.2,8H DEGREES/1H ,26HELEVATION WRT REF
11ERENCE =,F8.2,7H METERS///)
GO TO 107
200 WRITE(61,205)
205 FORMAT(1H ,35HSUMMARY AZI TO DIST IN M AZI FROM)
DO 250 I=7,10
DO 250 J=7,10
IF (I.EQ.J) GO TO 250
DELLA=SLA(I)-SLA(J)
DELDE=SDF(I)-SDF(J)
DIS=SQRT(DELLA*DELLA+DELDE*DELDE)
TH1=ASINF((-DELDE)/DIS)
IF (SLA(J).GE.SLA(I)) GO TO 210
TH1=P-TH1
GO TO 211
210 IF (TH1.LT.0.) TH1=2.*P+TH1
211 TH1=TH1*RAD
TH1=TH1+DECL
IF (TH1.LT.0.) TH1=TH1+360.
IF (TH1.GE.360.) TH1=TH1-360.
TH2=TH1+180.
IF (TH1.GE.180.) TH2=TH1-180.
WRITE(61,240)I,J,TH1,DIS,TH2
240 FORMAT(1H ,3X,I?,X,I2,X,F6.2,2X,F7.2,4X,F6.2)
250 CONTINUE
GO TO 100
END

```

## APPENDIX 2

## HYPOCENTER LOCATION FROM SEISMIC ARRAY DATA

Array geometry and arrival time differences permit the computation of the direction of propagation of a plane wave front observed at an array. Stauder and Ryall (1967) derive for the direction of propagation,  $\theta$ , of a ray and the apparent velocity,  $\bar{V}$ , of the wave in Figure 25

$$\theta = \tan^{-1} \left( \frac{\left( \frac{D_{13} \Delta t_{12}}{D_{12} \Delta t_{13}} \right) \cos Az_{13} - \cos Az_{12}}{\sin Az_{12} - \left( \frac{D_{13} \Delta t_{12}}{D_{12} \Delta t_{13}} \right) \sin Az_{13}} \right)$$

$$\bar{V} = \frac{D_{12}}{\Delta t_{12}} \cos(\theta - Az_{12}) = \frac{D_{13}}{\Delta t_{12}} \cos(\theta - Az_{13})$$

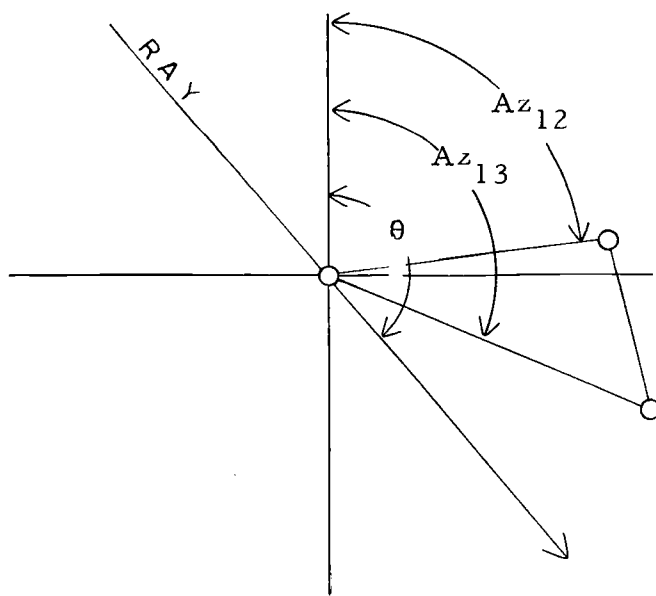


Figure 25. Diagram illustrating equation parameters for the direction of approach of a ray and the geometry of a tripartite array.

They also obtain equations describing a least squares technique if four, instead of three, geophones form the array. The two greater time differences from each of the four triangles determine values of  $\theta$  and  $\bar{V}$  which best fit all the arrival times. If the subscript  $i$  refers to quantities of one leg of a triangle and  $t_i$  is the corresponding arrival time difference of the wave front, then they write the error equation from the expression for  $\bar{V}$  above as:

$$\frac{\Delta t_i}{D_i} - \frac{1}{\bar{V}} (\cos \theta \cos Az_i + \sin \theta \sin Az_i) = E_i$$

Making the definitions

$$\theta = \tan^{-1} (X/Y)$$

$$\bar{V} = (X^2 + Y^2)^{-1/2}$$

then the error equation is

$$\frac{\Delta t_i}{D_i} - X \cos Az_i - Y \sin Az_i = E_i$$

Solving for values of  $X$  and  $Y$  which make  $E_i^2$  a minimum, they obtain:

$$\sum_i \cos^2 Az_i X + \sum_i \sin Az_i \cos Az_i Y = \sum_i \frac{\Delta t_i}{D_i} \cos Az_i$$

$$\sum_i \cos Az_i \sin Az_i X + \sum_i \sin^2 Az_i Y = \sum_i \frac{\Delta t_i}{D_i} \sin Az_i$$

The values of  $\theta$  and  $\bar{V}$  permit the calculation of the hypocenter

using the quantities defined in Figure 26, the difference between times of arrival of P- and S- waves (S-P) and the equations

$$\sin \phi_i = V_i / V$$

$$d_i = z_i / \cos \phi_i$$

$$d_n = \left\{ (S-P) - \sum_{i=1}^{n-1} .732 d_i / V_i \cdot V_n / .732 \right.$$

$$R = \sum_{i=1}^{n-1} z_i \tan \phi_i + d_n \sin \phi_n$$

$$Z = \sum_{i=1}^{n-1} z_i + d_n \cos \phi_n$$

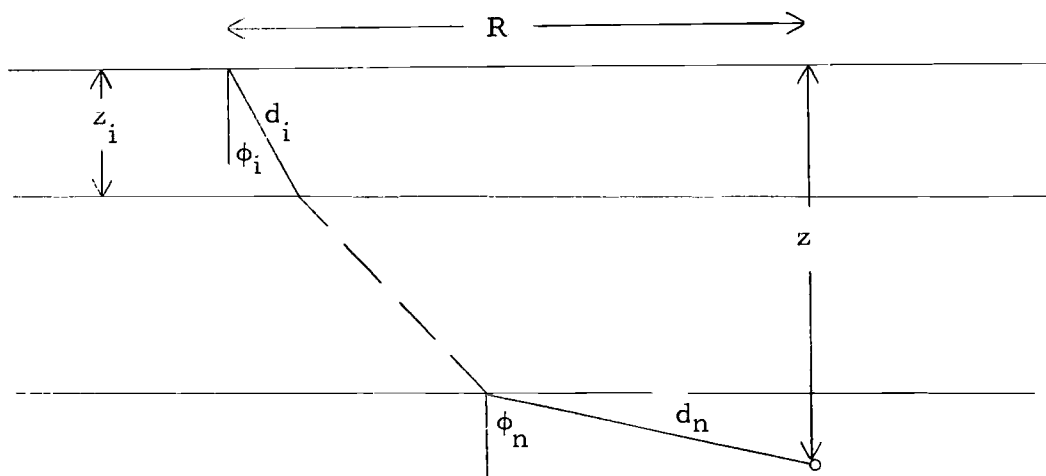


Figure 26. Straight line ray paths assumed and quantities used to calculate hypocenters.

The computer program, EPIARRAY, solves the equations given above and computes hypocenters given the array geometry, arrival times at three or four geophones, S-P time, and a crustal structure. Written in FORTRAN IV, the program ran on a CDC 3300 computer. The program parameters are:

Input cards

- 1) General control
 

NG	Number of geophones
L	Number of crustal layers
TITLE	Array identification

 FORMAT(2I1, 8A8)
  
- 2) Layer velocities
 

V(I)	Layer velocities
------	------------------

 FORMAT(9F8.2)
  
- 3) Layer thicknesses
 

TH(I)	Layer thicknesses
-------	-------------------

 FORMAT(9F8.2)
  
- 4) Array geometry
 

I	Azimuth and distance from this geophone number
J	Azimuth and distance to this geophone number
ANG	Azimuth in degrees
DIS	Distance in kilometers

 FORMAT(I2, X, I2, X, F6.2, X, F6.2)
  
- 5) Arrival time data
 

DATE	Day, month, and year
TIME	Hour, minute and second of first arrival
T(I)	Time of arrival at Ith geophone in seconds later than TIME
A(I)	Sense of motion at Ith geophone; if no arrival, leave blank
SMP	Difference, in seconds, of time of arrival of P- and S-waves

 FORMAT(I6, X, I6, F6.4, A1, F6.4, A1, F6.4, A1, F6.4, A1, F7.3)

Output (High speed line printer)

- 1) Identification
  - TITLE Identification of array
  - FORMAT(1H , 8A8, //)
  
- 2) Crustal model
  - I Layer number
  - V(I) Layer velocity
  - TH(I) Layer thickness
  - FORMAT(1H , 2X, I1, 3X, F6. 2, 4X, F6. 2)
  
- 3) Array geometry
  - I Azimuth and distance from this geophone number
  - J Azimuth and distance to this geophone number
  - ANG Azimuth in degrees
  - DIS Distance in kilometers
  - FORMAT(1H , 3X, I2, X, I2, 3X, F7. 2, 4X, F7. 5)
  
- 4) Individual array solutions
  - KL, KM, KN Geophone numbers used in triade solution
  - THETD Azimuth to epicenter
  - KL, KM Geophones on one leg of triade
  - VB1 Apparent velocity between geophones KL and KM
  - KL, KN Geophones on second leg of triade
  - VB2 Apparent velocity between geophones KL and KN
  - FORMAT(1H , 'FOR TRIADE=', 3I2, 'AZIMUTH TO EPICENTER= ', F8. 3, 'APP VEL ', 2I2, 2X, F7. 3, 2X, 'APP VEL ', 2I2, 2X, F7. 3)
  
- 5) Least squares solution
  - DATE Day, month, and year
  - TIME Hour, minute, and second of first arrival
  - T(I) Time of arrival at Ith geophone in seconds later than TIME
  - A(I) Sense of motion at Ith geophone
  - SMP S-P time
  - VB Apparent velocity
  - SDV Standard deviation of the velocity
  - THETLS Azimuth to the epicenter

SDT	Standard deviation of the azimuth
AN(J)	Incident angle of the ray at the Jth layer
SR	Epicentral distance in kilometers
SX	Eastward component of SR
SY	Northward component of SR
SZ	Depth of the earthquake

FORMAT(1H , I6, X, I6, F6. 3, A1, F6. 3, A1, F6. 3, A1, F6. 3, A1,  
F7. 3, F6. 2, F6. 2, F7. 2, F6. 1, 6 F5. 1, F7. 2, ///)

The program listing is:

```

PROGRAM EPIARRAY
  DIMENSION T(10),A(10),N(10),TT(4),AA(4),NN(4),DT(4),JI(4),JJ(4),
  1 TITLE(8),V(9),TH(9),AN(6),LE(4),SNP(4),AZ(10,10),D(10,10)
  INTEGER DATE,TIME,A,AA
C PROGRAM COMPUTES EPICENTER FROM ARRIVAL TIME DIFFERENCES AT 3- OR 4-
C DECTOR ARRAY USING GIVEN EARTH MODEL AND SIMPLE RAY THEORY
C CARD 1= NG IS NUMBER OF GEOPHONES, L IS NUMBER OF CRUSTAL LAYERS
C TITLE IS FOR IDENTIFICATION CARD 2 GIVES L LAYER VELOCITIES
C CARD 3 GIVES L-1 LAYER THICKNESSES NEXT 12 CARDS GIVE ARRAYINFO=
C ANG AND DIS ARE AZIMUTHAL ANGLE IN DEGREES AND DISTANCE FROM GEOPHONE
C I TO GEOPHONE J NEXT CARD(S) GIVE ARRIVAL INFO= DATE IS
C DAYMONTHYEAR, TIME IS HOURMINUTESECOND,T(I) AND A(I) ARE ARRIVAL TIME
C AND SENSE OF FIRST MOTION AT GEOPHONE I. IF NO ARRIVAL ON A GEOPHONE
C LEAVE A(I) BLANK, SMP IS S MINUS P TIME.END ARRIVAL TIME DATA WITH
C ONE EOF CARD AND REPEAT FROM CARD 1 FOR DIFFERENT ARRAYS IF DESIRED
C END LAST ARRAY DATA WITH TWO EOF CARDS
  P=3.14159265
  RAD=P/180.
  R=180./P
  3 READ(60,1) NG,L,TITLE
  IF(EOF(60))CALL EXIT
  1 FORMAT(2I1,8A8)
  READ(60,2) (V(I),I=1,L)
  2 FORMAT(9F8.2)
  L1=L-1
  READ (60,2) (TH(I),I=1,L1)
  WRITE (61,12) TITLE
  12 FORMAT (1H ,8A8,/)
  WRITE (61,13)
  13 FORMAT (1H ,#LAYER VELOCITY THICKNESS#)
  WRITE (61,14) (I,V(I),TH(I),I=1,L1)
  14 FORMAT (1H ,2X,I1,3X,F6.2,4X,F6.2)
  WRITE (61,15) L,V(L)
  15 FORMAT (1H ,2X,I1,3X,F6.2,/)
  WRITE(61,16)
  16 FORMAT (1H ,#ARRAY INFO AZI TO DIST IN KM#)
  DO 7 K=1,12
  READ (60,5) I,J,ANG,DIS
  5 FORMAT (I2,X,I2,X,F6.2,X,F6.2)
  WRITE (61,17) I,J,ANG,DIS
  17 FORMAT (1H ,3X,I2,X,I2,3X,F7.2,4X,F7.5)
  AZ(I,J)=ANG*RAD
  7 D(I,J)=DIS
  WRITE (61,18)
  18 FORMAT (1H-)
  777 READ(60,8) DATE,TIME,T(7),A(7),T(8),A(8),T(9),A(9),T(10),A(10),
  1 SMP
  8 FORMAT(I6,X,I6,F6.4,A1,F6.4,A1,F6.4,A1,F6.4,A1,F7.3)
  IF(EOF(60)) GO TO 3
  STS=0.$ST=0.$SV=0.$SVS=0.$SZ=0.$SR=0.0$SD1=0.0$SD2=0.0$SD3=0.0
  SD4=0.0$SX1=0.0$SX2=0.0$SX3=0.0$SX4=0.0$SY1=0.0$SY2=0.0$SY3=0.0
  SY4=0.0$AN(1)=0.0$AN(2)=0.0$AN(3)=0.0$AN(4)=0.0$SDV=0.0$SDT=0.0
  THETLS=0.0$AN(5)=0.0$AN(6)=0.0
  DO 9 I=7,10
  9 N(I)=I
C RELOCATES DATA TO BE USED IN SEQUENCING
  DO 10 I=1,4
  TT(I)=T(I+6)
  AA(I)=A(I+6)
  10 NN(I)=N(I+6)

```

```

C  ARRANGES TIMES, CHANNEL NUMBER ANO FIRST MOTION IN DECREASING ORDER
  DO 20 I=1,3
    <=I+1
    DO 20 J=K,4
      IF(TT(I).GE.TT(J).AND.AA(I).NE.1H ) GO TO 20
      TE=TT(I)
      TT(I)=TT(J)
      TT(J)=TE
      NE=NN(I)
      NN(I)=NN(J)
      NN(J)=NE
      JE=AA(I)
      AA(I)=AA(J)
      AA(J)=JE
20  CONTINUE
    LO=0
21  LO=LO+1
    IF(LO.NE.1) GO TO 110
    IA=1$IB=2$IC=1$ID=3$IE=1
    GO TO 130
110 IF(LO.NE.2) GO TO 115
    IA=1$IB=2$IC=1$ID=4$IE=2
    GO TO 130
115 IF(LO.NE.3) GO TO 120
    IA=1$IB=3$IC=2$ID=4$IE=1
    GO TO 130
120 IA=2$IB=3$IC=1$ID=4$IE=1
130 NU=0
    NA=NN(IA)
    NB=NN(IB)
    ND=NN(ID)
C  COMPUTE AND SORT TIME DIFFERENCES AND PUT LARGEST FIRST
  DO 50 I=IA,IB,IC
    DO 50 J=IB,IO,IE
      IF(I.EQ.J) GO TO 50
      NI=NN(I)
      NJ=NN(J)
      NU=NU+1
      DT(NU)=T(NI)-T(NJ)
      JI(NU)=NN(I)
      JJ(NU)=NN(J)
50  CONTINUE
    DO 70 I=1,2
      II=I+1
      DO 70 J=II,3
        IF(DT(I).GE.DT(J)) GO TO 70
        TEM=DT(I)
        DT(I)=DT(J)
        DT(J)=TEM
        JE=JI(I)
        JI(I)=JI(J)
        JI(J)=JE
        JM=JJ(I)
        JJ(I)=JJ(J)
        JJ(J)=JM
70  CONTINUE
    IF(JI(1).EQ.JI(2)) GO TO 135
    IF (JJ(1).EQ.JJ(2)) GO TO 140
    IF (JJ(1).EQ.JI(2)) GO TO 145
    KL=JI(1)$KM=JI(2)$KN=JJ(1)

```

```

      GO TO 200
135  KL=JI(1)$KM=JJ(2)$KN=JJ(1)
      GO TO 200
140  <L=JJ(1)$KM=JI(2)$KN=JI(1)
      GO TO 200
145  KL=JJ(1)$KM=JJ(2)$KN=JI(1)
C   COMPUTE ARRIVAL DIRECTION AND APPARENT VELOCITY FOR EACH TRIADE
200  D12=D(KL,KM)
      D13=D(KL,KN)
      T12=ABSF(T(KL)-T(KM))
      T13=ABSF(T(KL)-T(KN))
      RAT=D13*T12/D12/T13
      IF(T(KL).LT.T(KM)) GO TO 142
      AZ12=AZ(KM,KL)
      GO TO 143
142  AZ12=AZ(KL,KM)
143  IF(T(KL).LT.T(KN)) GO TO 144
      AZ13=AZ(KN,KL)
      GO TO 148
144  AZ13=AZ(KL,KN)
148  CF12=COSF(AZ12)
      CF13=COSF(AZ13)
      SF12=SINF(AZ12)
      SF13=SINF(AZ13)
      H=RAT*CF13-CF12
      B=SF12-PAT*SF13
      THET=ATANF(H/B)
      IF(AZ(ND,NB)-AZ(NB,NA)) 150,150,155
150  AZL=AZ(NB,NA)*R
      AZS=AZ(ND,NB)*R
      GO TO 160
155  AZL=AZ(ND,NB)*R
      AZS=AZ(NB,NA)*R
160  IF((AZL-AZS).GT.180.) GO TO 170
      IF(AZL.GT.90.) GO TO 162
      A1=AZL+270.
      GO TO 164
162  A1=AZL-90.
164  IF(AZS.GT.270.) GO TO 166
      A2=AZS+90.
      GO TO 180
166  A2=AZS-270.
      GO TO 180
170  IF(AZL.GT.270.) GO TO 172
      A2=AZL+90.
      GO TO 174
172  A2=AZL-270.
174  IF(AZS.GT.90.) GO TO 176
      A1=AZS+270.
      GO TO 180
176  A1=AZS-90.
180  THETO=THET*R
      IF((A2-A1).LT.0.) GO TO 190
      IF(THETO.GT.0.) GO TO 186
      DO 185 K=1,4
      THETO=THETO+90.
      IF(THETO.LT.A2.AND.THETO.GT.A1.OR.THETO.GT.360.) GO TO 199
185  CONTINUE
186  DO 187 K=1,4
      IF(THETO.LT.A2.AND.THETO.GT.A1.OR.THETO.GT.360.) GO TO 199

```

```

197 THETD=THETD+90.
190 IF(THETD.GT.0.) GO TO 195
    DO 193 K=1,4
    THETD=THETD+90.
    IF(THETD.GT.A1.OR.THETD.LT.A2.OR.THETD.GT.360.) GO TO 199
193 CONTINUE
195 DO 197 K=1,4
    IF(THETD.GT.A1.OR.THETD.LT.A2.OR.THETD.GT.360.) GO TO 199
197 THETD=THETD+90.
199 THET=THETD*RAD
    IF(THETD.LT.180.) GO TO 230
    THETD=THETD-180.
    GO TO 240
230 THETD=THETD+180.
C THET IS AZIMUTH FROM EPICENTER IN RADIANS
C THETD IS AZIMUTH TO EPICENTER IN DEGREES
240 CONTINUE
    VB1=D12*COSF(THET-AZ12)/T12
    VB2=D13*COSF(THET-AZ13)/T13
    VB1=ABSF(VB1)
    VB2=ABSF(VB2)
    VB=(VB1+VB2)/2.
    WRITE (61,201) KL,KM,KN,THETD,KL,KM,VB1,KN,VB2
201 FORMAT(1H ,#FOR TRIADE= #,3I2,# AZIMUTH TO EPICENTER= #,F8.3,# APP
    1 VEL #,2I2,2X,F7.3,2X,# APP VEL #,2I2,2X,F7.3)
    THET=THETD*RAD
C SUM ELEMENTS FOR STD DEV FOR THETA AND VB
    ST=ST+THETD
    TS=THETD*THETD
    STS=STS+TS
    SV=SV+VB1
    VS=VB1*VB1
    SVS=SVS+VS
C SUM ELEMENTS FOR LEAST SQUARE DETERMINATION OF THETA AND VELOCITY
    SD1=SD1+CF12**2+CF13**2
    SD2=SD2+SF12*CF12+SF13*CF13
    SD3=SD2
    SD4=SD4+SF12**2+SF13**2
    SX1=SX1+T12*CF12/D12+T13*CF13/D13
    SX2=SD2
    SX3=SX3+T12*SF12/D12+T13*SF13/D13
    SX4=SD4
    SY1=SD1
    SY2=SX1
    SY3=SD2
    SY4=SX3
    C=L0
    CC=L0-1
    IF(AA(4).NE.1H ) GO TO 205
    IF(L0-2) 203,204,206
203 STO=KL$KL=KN$KN=STO
    L0=L0+1
    GO TO 200
204 STO=KL$KL=KM$KM=STO
    L0=L0+1
    GO TO 200
205 IF(L0.LT.4) GO TO 21
206 SDT=SQRTF((C*STS-ST*ST)/(C*CC))
    SDV=SQRTF((C*SVS-SV*SV)/(C*CC))
    DET=SD1*SD4-SD2*SD3

```

```

X=(SX1*SX4-SX2*SX3)/DET
Y=(SY1*SY4-SY2*SY3)/DET
VB=1./SQRTF(X*X+Y*Y)
THETA=ATANF(Y/X)
THETLS=THETA*R
IF(THETD.GT.90..AND.THETD.LT.180..AND.THETA.LT.0.) THETLS=THETLS+1
130.
IF(THETD.GT.180..AND.THETD.LT.270..AND.THETA.GT.0.) THETLS=THETLS+
1180.
IF(THETD.GT.270..AND.THETA.LT.0.) THETLS=360.+THETLS
C COMPUTE EPICENTER
THET=THETLS*RAD
I=1
IF(V(1).GT.VB) GO TO 314
AN(1)=ASINF(V(1)/VB)
AM=AN(1)
LE(1)=TH(1)/COSF(AM)
Z=LE(1)*COSF(AM)
Q=LE(1)*SINF(AM)
SNP(1)=.732*LE(1)/V(1)
IF(SMP.GT.SNP(1)) GO TO 300
LE(1)=SMP*V(1)/.732
SZ=LE(1)*COSF(AM)
SR=LE(1)*SINF(AM)
GO TO 310
300 SPA=SZ=SR=0.
302 I=I+1
SZ=SZ+Z
SR=SR+Q
IF(V(I).GT.VB) GO TO 314
AN(I)=ASINF(V(I)/VB)
AM=AN(I)
IF(I.EQ.L) GO TO 315
LE(I)=TH(I)/COSF(AM)
Z=LE(I)*COSF(AM)
Q=LE(I)*SINF(AM)
SNP(I)=.732 *LE(I)/V(I)
SPA=SPA+SNP(I-1)
SP=SPA+SNP(I)
IF (SMP.GT.SP) GO TO 302
LE(I)=(SMP-SPA)*V(I)/.732
GO TO 316
314 AM=P/2.
315 LE(I)=(SMP-SP )*V(I)/.732
316 Z=LE(I)*COSF(AM)
Q=LE(I)*SINF(AM)
SZ=SZ+Z
SR=SR+Q
310 SX=SR*SINF(THET)
SY=SR*COSF(THET)
GO 320 I=1,6
320 AN(I)=AN(I)*R
WRITE(61,350)
350 FORMAT(1H0, # DATE TIME CH7 CH8 CH9 CH10 S-F VEL
1 ERR THET ERR I1 I2 I3 I4 I5 I6 R X
1Y Z#)
WRITE(61,360) DATE,TIME,T(7),A(7),T(8),A(8),T(9),A(9),T(10),A(10),
1SMP,VB,SDV,THETLS,SDT,AN(1),AN(2),AN(3),AN(4),AN(5),AN(6),SR,SX,
1SY,SZ
360 FORMAT(1H ,I6,X,I6,F6.3,A1,F6.3,A1,F6.3,A1,F6.3,A1,F7.3,F6.2,F6.2,
1 F7.2,F6.1,6F5.1,F7.2,3F7.2,///)
GO TO 777
END

```